

SEXUAL DIMORPHISM IN WHITE SOUTH AFRICAN CRANIA

Candice Small



Original published work submitted to the Faculty of Health Sciences, University of the Witwatersrand, Johannesburg, in fulfilment of the requirements for the degree of Doctor of Philosophy.
Johannesburg, 2016

DECLARATION

I, Candice Small, declare that this thesis is my own, unaided work. It is being submitted for the degree of Doctor of Philosophy (PhD) at the University of the Witwatersrand, Johannesburg. It has not been submitted before for any degree or examination in any other University.

.....

Candice Small

.....day of....., 2016.

DEDICATED TO

Ma and Ded – for your endless love and support

Goggie – for all your sacrifices

My kids – for keeping me sane

Presentations arising from this thesis:

2015 AESOP 3D imaging in a South African context workshop (University of Pretoria): Oral presentation

Title: Assessing sexual dimorphism and allometry within a white South African sample using geometric morphometrics.

2014 International Association of Forensic Sciences (Seoul, South Korea): Oral presentation and session chair

Title: Assessing sexual dimorphism and allometry within a white South African sample using geometric morphometrics.

2013 International Association of Craniofacial Investigators (Kruger National Park): Oral presentation

Title: Assessing the effects of tooth loss in adult crania using geometric morphometrics.

Interfaculty Symposium (University of the Witwatersrand): Poster presentation

Title: Assessing the effects of tooth loss in adult crania using geometric morphometrics.

Publications arising from this thesis:

Small C, Brits D, Hemingway J. Assessing the effects of tooth loss in adult crania using geometric morphometrics. *Int J Legal Med.* 2015;130(1):233–43.

ABSTRACT

Sexual dimorphism is one of four critical factors assessed by forensic anthropologists when compiling biological profiles. The current study used geometric morphometric methods to analyse various aspects of sexual dimorphism in white South African crania to significantly contribute to current forensic standards for this underrepresented population.

As edentulous crania are a major contributing factor to the low number of publications on white South African populations, the question arose as to how tooth loss affects cranial structures and the accuracy of sex and ancestry estimation. Two hundred and twenty nine crania were digitised using landmarks and sliding semilandmarks, both globally and for a number of cranial subsets. Although a number of effects were identified when the skull was analysed globally, only the maxillary alveolar ridges were significantly affected when subsets were analysed individually. As both upper facial height and palate shape were significantly altered by tooth loss, the effects of tooth loss on cranial structures and sex and ancestry estimations were investigated.

Next, to parse out the mechanisms by which sexual dimorphism causes morphological variation, overall sexual dimorphism, common allometry and non-allometric sexual dimorphism were individually assessed. Global and subset data were studied and the effects of sexual dimorphism and allometry were found to be universal, with significant differences being observed between the sexes both globally and regionally. A significant non-allometric component was, however, only found to contribute to the shape of the zygomatic bone.

Finally, the accuracy of 17 widely used traditional cranial measurements was compared to all possible interlandmark distances (ILDs) attainable from 45 fixed landmarks. Discriminant functions derived using the ILDs compared well to those of previous work on white South Africans, thus demonstrating the similarity between traditional and 3-D methods. Finally, custom discriminant functions were created for a number of cranial subsets and for the cranium in its entirety. The subsets achieved sexing accuracies ranging between 71.8% and 83.7%, with the nasomaxilla proving most accurate. The overall cranial function attained a cross-validated sexing accuracy of 88.2%. These functions are critical for sex estimation not only for intact crania, but also for the innumerable fragmentary cranial remains recovered regularly in South Africa.

ACKNOWLEDGEMENTS

I would like to extend my sincere gratitude and appreciation to the following individuals, without whom this thesis would not have been possible:

- Dr Desiré Brits for all the knowledge she instilled in me. Also, for being there through all the hard times both academically and personally. I could not have asked for a better supervisor, mentor and friend.
- Professor Lynne Schepartz whose input and support are invaluable. You truly are an inspiration.
- Mr Jason Hemingway for many, many, many hours of wading through statistics. I now feel a little less daunted by the “stats monster”.
- Our Heads of school Professor Thomas Daly, and more recently, Professor Maryna Steyn for allowing me access to the Raymond A. Dart Collection of Human Skeletons.
- Mr Brendon Billings and Mr Diago Shangase for their assistance in the Raymond A. Dart Collection of Human Skeletons.
- Drs Tea Jashashvili and Anna Oetlé for crucial statistical input.
- Ms Andrea Kolkenbeck-Ruh for assistance with the final draft and putting up with my moaning.
- My parents and my fiancé, Tony, for all their help with the thesis, and all the years of financial and emotional support. This thesis never would have been possible without your love, guidance and true selflessness. I am blessed.
- The financial assistance of the National Research Foundation (NRF) towards this research is hereby acknowledged (Grant UID: 79474). Opinions expressed and conclusions arrived at are those of the author and are not necessarily to be attributed to the NRF.

TABLE OF CONTENTS

TITLE PAGE	i
DECLARATION	ii
DEDICATED TO	iii
Presentations arising from this thesis:	iv
Publications arising from this thesis:	iv
ABSTRACT	v
ACKNOWLEDGEMENTS	vi
TABLE OF CONTENTS	vii
NOMENCLATURE	xii
LIST OF FIGURES	xiii
LIST OF TABLES	xvi

CHAPTER ONE: INTRODUCTION AND CHAPTER OUTLINE

1.1 INTRODUCTION	2
1.2 CHAPTER OUTLINE	3
1.2.1 Chapter Two: Literature Review	3
1.2.2 Chapter Three: Assessing the effects of tooth loss on the crania of white South Africans using geometric morphometrics	3
1.2.3 Chapter Four: Morphological variation in white South African crania: sexual dimorphism and allometry	4
1.2.4 Chapter Five: Traditional cranial measurements versus 3-D-derived interlandmark distances for sex estimation in white South Africans	5
1.2.5 Chapter Six: Discussion and Conclusion	6

CHAPTER TWO: LITERATURE REVIEW

2. INTRODUCTION	8
2.1 FORENSIC ANTHROPOLOGY IN SOUTH AFRICA	8
2.2 SEXUAL DIMORPHISM	9
2.3 SEX ESTIMATION	12
2.3.1 Morphological/ Quantitative Methods	12
2.3.2 Metric/ Quantitative Analyses	13
2.3.3 Geometric Morphometrics	14
2.3.3.1 Semilandmark methods in geometric morphometrics	16
2.4 TOOTH LOSS	16

CHAPTER THREE: ASSESSING THE EFFECTS OF TOOTH LOSS ON THE CRANIA OF WHITE SOUTH AFRICANS USING GEOMETRIC MORPHOMETRICS

3.1 INTRODUCTION	20
3.2 MATERIALS AND METHODS	21
3.2.1 Materials	21
3.2.2 Data Collection Procedure	22
3.2.2.1 Zygomatics	24
3.2.2.2 Orbits	24
3.2.2.3 Nasal aperture	25
3.2.2.4 Maxilla	25
3.2.2.5 Basicranium	26
3.2.2.6 Dental scoring	26
3.2.3 Data Resampling and Reworking	26
3.2.4 Statistical Analyses	27
3.2.4.1 Repeatability	27
3.2.4.2 Preliminary analyses	28
3.2.4.3 Analysis of tooth loss	29
3.3 RESULTS	30
3.3.1 Repeatability	30
3.3.2 Global Analyses	31
3.3.3 Individual Curve Analyses	33
3.4 DISCUSSION	33
3.4.1 Repeatability	33
3.4.2 Global Observations	34
3.4.3 Individual Curve Observations	36
3.5 CONCLUSIONS	38

CHAPTER FOUR: MORPHOLOGICAL VARIATION IN WHITE SOUTH AFRICAN CRANIA: SEXUAL DIMORPHISM AND ALLOMETRY

4.1 INTRODUCTION	51
4.2 MATERIALS AND METHODS	54
4.2.1 Materials	54
4.2.2 Data Collection Procedure	54
4.2.3 Data Resampling and Reworking	55
4.2.4 Statistical Analyses	55
4.2.4.1 Preliminary analyses	55

4.2.4.2 Analysis of overall sexual dimorphism	56
4.2.4.3 Analysis of allometry	57
4.2.4.4 Analysis of non-allometric sexual dimorphism	58
4.3 RESULTS	58
4.3.1 Preliminary Analyses	58
4.3.2 Global Analyses	58
4.3.2.1 Overall sexual dimorphism	58
4.3.2.2 Common allometry	60
4.3.2.3 Non-allometric sexual dimorphism	61
4.3.3 Subset Analyses	61
4.3.3.1 Basicranium - Sexual dimorphism	62
4.3.3.2 Basicranium - Common allometry	62
4.3.3.3 Maxilla - Sexual dimorphism	63
4.3.3.4 Maxilla - Common allometry	63
4.3.3.5 Zygomatics - Sexual dimorphism	64
4.3.3.6 Zygomatics - Common allometry	64
4.3.3.7 Zygomatics - Non-allometric sexual dimorphism	65
4.3.3.8 Orbits - Sexual dimorphism	65
4.3.3.9 Orbits - Allometry	65
4.3.3.10 Nasal aperture - Sexual dimorphism	66
4.3.3.11 Nasal aperture - Allometry	66
4.4 DISCUSSION	67
4.4.1 General Findings	67
4.4.2 Detailed Observations	69
4.4.2.1 Sexual dimorphism	69
4.4.2.2 Allometry	75
4.4.2.3 Non-allometric sexual dimorphism	78
4.5 CONCLUSIONS	79
TRADITIONAL CRANIAL MEASUREMENTS VERSUS 3-D INTERLANDMARK DISTANCES FOR SEX ESTIMATION IN WHITE SOUTH AFRICAN	
5.1 INTRODUCTION	94
5.2 MATERIALS AND METHODS	96
5.2.1 Materials	96
5.2.2 Data Collection Procedure	97
5.2.3 Statistical Analyses	97
5.2.3.1 Preliminary analyses	97
5.2.3.2 Sample interlandmark distances	98
	ix

5.2.3.3 Published interlandmark distances	98
5.2.3.4 Validation of 3-D derived interlandmark distances	99
5.2.3.5 Cranial subsection landmark selection	99
5.2.3.6 Discriminant analyses and discriminant functions	99
5.2.3.7 Top cranial interlandmark distances and cranial discriminant functions	101
5.2.3.8 Validation of discriminant functions	101
5.3 RESULTS	102
5.3.1 Three-dimensional Interlandmark Distance Validation	102
5.3.2 Traditional Interlandmark Distances and most accurate 3-D Derived Interlandmark Distances	103
5.3.3 Individual Subset Discriminant Analyses	104
5.3.3.1 Basicranium	104
Univariate Statistics and Direct Discriminant Analyses	104
Stepwise Discriminant Analyses	105
Discriminant Function Accuracies	105
5.3.3.2 Basipalate	106
Univariate Statistics and Direct Discriminant Analyses	106
Stepwise Discriminant Analyses	106
Discriminant Accuracies	107
5.3.3.3 Zygomatics	107
Univariate Statistics and Direct Discriminant Analyses	107
Stepwise Discriminant Analyses	107
Discriminant Accuracies	108
5.3.3.4 Orbit	108
Univariate Statistics and Direct Discriminant Analyses	108
Stepwise Discriminant Analyses	108
Discriminant Accuracies	109
5.3.3.5 Nasomaxilla	109
Univariate Statistics and Direct Discriminant Analyses	109
Stepwise Discriminant Analyses	110
Discriminant Accuracies	110
5.3.4 Cranial Interlandmark Distances and Discriminant Functions	110
5.3.4.1 Direct discriminant analyses	110
5.3.4.2 Stepwise discriminant analyses	111
5.3.4.3 Discriminant accuracies	111
5.4 DISCUSSION	112
5.4.1 Three-dimensional interlandmark distance validation	113

5.4.2 Traditional Interlandmark Distances and most accurate 3-D Derived Interlandmark Distances	114
5.4.3 Global Cranial and Individual Subset Discriminant Analyses	116
5.4.3.1 Basicranium and basipalate	117
5.4.3.2 Orbit	117
5.4.3.3 Zygomatics and nasomaxilla	118
5.4.3.4 Global cranial function	118
5.5 CONCLUSIONS	119
CHAPTER SIX: OVERALL DISCUSSION AND CONCLUSIONS	
6.1 INTRODUCTION	141
6.2 CHAPTER TWO: Assessing the effects of tooth loss on the crania of white South Africans using geometric morphometric	141
6.3 CHAPTER FOUR: Morphological variation in white South African crania: sexual dimorphism and allometry	142
6.4 CHAPTER FIVE: Traditional cranial measurements versus 3-D derived interlandmark distances for sex estimation in white South Africans.	144
6.5 LIMITATIONS AND FUTURE RESEARCH	146
6.6 CONCLUSIONS	147
REFERENCES	150
APPENDIX A	167
Ethical Consent Form	167
APPENDIX B	167
Turn-It-In Digital Receipt	167
APPENDIX C	167
Assessing the effects of tooth loss in adult crania using geometric morphometrics Int J Legal Med. 2015; 130(1):233-43.	167

NOMENCLATURE

SxD: Sexual Dimorphism

3-D: Three-dimensional

2-D: Two-dimensional

GMM: Geometric Morphometrics

PPS: Partial Least Squares

PCA: Principal Components Analysis

PC: Principal Component

GPA: Generalised Procrustes Superimposition

PLS: 2-Block Partial Least Squares

CA: Common Allometry

NASXD: Non-allometric Sexual Dimorphism

ILD: Interlandmark Distance

LDA: Linear Discriminant Analysis

LR: Logistic Regression

LIST OF FIGURES

FIGURE		Page
Figure 3.1.	Illustration of the landmarks and curves used in this study: a) Inferior view; b) Lateral view; c) Anterior view. Abbreviation and number index correspond to curve numbers in Table 3.2.	40
Figure 3.2.	Histograms of the results of the tests measuring intra-observer repeatability. A) Frequency of the Procrustes distances between all possible paired observations in the sample (blue) and between the repeated observations (red). B) Relative effect of measurement error after accounting for the influence of allometry in the sample (blue) and between repeated observations (red).	41
Figure 3.3.	Lateral (left) and anterior (right) wireframe illustrations of observer error. Ellipses depict the degree of error produced at each landmark. Larger ellipse = greater amount of measurement error. More elliptically shaped ellipses = higher degree of directional error.	42
Figure 3.4.	Results of the 2-Block partial least squares (PLS) analyses showing the first four vectors. Closed circles indicate female specimens, Open circles represent male specimens. The specimens that are all clustering along a straight line represent those that are completely edentulous.	43
Figure 3.5.	Anterior, inferior and lateral side by side representations (left) and vector diagrams (right) illustrating the changes in skull morphology associated with dental loss. Green areas are equivalent; Red indicates a large increase; and Blue shows a large decrease. The gradation of colours between red and blue (from yellow to turquoise) indicate morphologies that lie between the two extremes. In the vector diagrams on the right, arrows indicate the change in a structure of a completely edentulous individual (red), to a completely dentate individual (blue). The size of the arrows in the figure represents the relative magnitude of the structural change.	44
Figure 3.6.	Anterior, inferior and lateral coloured representations (left) and vector diagrams (right) of the structural changes in the morphology of the maxilla associated with tooth loss. In the side by side illustrations, green areas are equivalent, red indicates a large increase, and blue shows a large decrease. The gradation of colours between red and	45

blue (from yellow to turquoise) indicate morphologies that lie between the two extremes. In the vector diagrams on the right, arrows indicate the change in a structure from edentulous (red), to dentate, (blue). The size of the arrows in the figure represents the relative amount of structural change.

- Figure 4.1.** Scatter plots of the distribution of male (blue) versus female (red) data points along PC1 vs. PC2 (A), PC2 vs. PC3 (B) and PC3 vs. PC4,(C) as well as a histogram of the percentage of the variance accounted for by each principal component (D). 80
- Figure 4.2.** Plot of the cumulative contribution of the first 100 principal components for sex discrimination accuracy. The broken line represents the plateau in predictive accuracy at which the number of principal components needed for the regression analysis was chosen. 81
- Figure 4.3.** Surface scan deformations displaying the relative differences in cranial shape between males and females from anterior (a), inferior (b), and lateral (c) views. In the images, spectra from light blue to dark blue indicate areas that are relatively smaller than areas coloured in spectra of red, from pale to dark red. Note that regions of the neurocranium, and much of the posterior basicranium, were void of landmarks and thus the differences observed here are an artefact of the methods and landmark locations. 82
- Figure 4.4.** Surface scan deformations displaying the relative differences in cranial shape between small and large individuals from anterior (a), inferior (b), and lateral (c) views. In the images, spectra from light blue to dark blue indicate areas that are relatively smaller than areas coloured in spectra of red, from pale to dark red. 83
- Figure 4.5.** Surface scan deformation images of the effects of non-allometric sexual dimorphism on female cranial form shape anterior in (a), inferior (b), and lateral (c) views. Non-allometric sexual dimorphism is also directly compared to sexual dimorphism to demonstrate the similarities and differences between the results. In the images, spectra from light blue to dark blue indicate areas that are relatively smaller than areas coloured in spectra of red, from pale to dark red. 84

Figure 4.6.	Surface scan deformations of the effects of non-allometric sexual dimorphism on male cranial shape from anterior in (a), inferior (b), and lateral (c) views. Non-allometric sexual dimorphism is also directly compared to sexual dimorphism to demonstrate the similarities and differences between the results. In the images, spectra from light blue to dark blue indicate areas in which more variation is seen, coloured in spectra of red, from pale to dark red.	85
Figure 4.7.	Vector diagrams and wireframe images of the differences between male (blue) and female (red) basicrania on the left, and allometric difference between large (green) and small (purple) basicrania on the right. Images displaying variation in common allometry were scaled by a factor of two to aid visualisation	86
Figure 4.8.	Vector diagrams and wireframe images of the differences between male (blue) and female (red) maxillae on the left, and allometric difference between large (green) and small (purple) maxillary dental arcades on the right. Images displaying variation in common allometry were scaled by a factor of two to aid visualisation.	87
Figure 4.9.	Vector diagrams and wireframe images of the differences between male (blue) and female (red) zygomatic bones on the left, and allometric difference between large (green) and small (purple) zygomatic bones on the right. Images displaying variation in common allometry were scaled by a factor of four to aid visualisation.	88
Figure 4.10.	Vector diagrams and wireframe images of the differences between male (blue) and female (red) zygomatic bones before removing the effect of size (left), and after removing the effect of size (right). No scaling was necessary.	89
Figure 4.11.	Anterior, inferior and lateral wireframe images of the morphological changes in the orbits associated with sexual dimorphism (left) and allometry (right). In the images, red indicates female, blue male, while purple indicates small individuals and green large individuals.	90
Figure 4.12.	Anterior, inferior and lateral wireframe images of the morphological changes in the nasal aperture associated with sexual dimorphism (left) and allometry (right). In the images red = female, blue = male, purple = small and green = large.	91

LIST OF TABLES

TABLE	Page
Table 3.1. Age distribution of sample by decade and dental state, SD =standard deviation (n= 229).	46
Table 3.2. Landmark number, definitions and abbreviations for all fixed landmarks used in this study	47
Table 3.3. Subset breakdown and description of curves and semilandmarks. Curve numbers correspond to those in Figure. 3.1.	49
Table 4.1. Age distribution of sample by decade and dental state. SD= standard deviation (n= 227).	92
Table 5.1. Comparison of the sex estimation accuracies of the discriminant functions derived by Steyn and İşcan (S&I, 1998) (1) with the functions derived by the current investigation (Current) using 3-D derived interlandmark distances.	120
Table 5.2. Comparison of the accuracy of traditional cranial interlandmark distances with the most accurate interlandmark distances derived in the current investigation. Both logistic regression (LR) and direct discriminant function accuracies (LDA) are listed. Isp = ipsilateral; Cntr = contralateral.	121
Table 5.3. Individual ILD sex estimation accuracies achieved by logistic regression (LR) and linear discriminant analyses (LDA), as well as univariate statistics including means, standard deviations (SD), Wilks' lambda and F-ratios for basicranial landmarks.	123
Table 5.4. Direct discriminant analysis function coefficients, group centroids and sectioning points for all basicranial interlandmark distances that achieved discrimination accuracies of 70.0% or above.	123

Table 5.5.	Stepwise discriminant analysis results for the best basicranial interlandmark distances including coefficients, centroids and sectioning points.	124
Table 5.6.	Comparison of sex estimation accuracies achieved using original and cross-validated basicranial discriminant functions (derived by both direct and stepwise procedures).	124
Table 5.7.	Individual ILD sex estimation accuracies achieved by logistic regression (LR) and linear discriminant analyses (LDA), as well as univariate statistics including means, standard deviations (SD), Wilks' lambda and F-ratios for basipalate landmarks.	125
Table 5.8.	Direct discriminant analysis function coefficients, group centroids and sectioning points for all basipalate interlandmark distances that achieved discrimination accuracies of 70.0% or above.	126
Table 5.9.	Stepwise discriminant analysis results for the best basipalate interlandmark distances including coefficients, centroids and sectioning points.	127
Table 5.10.	Comparison of sex estimation accuracies achieved using original and cross-validated basipalate discriminant functions (derived by both direct and stepwise procedures).	127
Table 5.11.	Individual ILD sex estimation accuracies achieved by logistic regression (LR) and linear discriminant analyses (LDA), as well as univariate statistics including means, standard deviations (SD), Wilks' lambda and F-ratios for zygomatic landmarks.	128
Table 5.12.	Direct discriminant analysis function coefficients, group centroids and sectioning points for all zygomatic interlandmark distances that achieved discrimination accuracies of 70.0% or above.	130
Table 5.13.	Stepwise discriminant analysis results for the best zygomatic interlandmark distances including coefficients, centroids and sectioning points.	131

Table 5.14.	Comparison of sex estimation accuracies achieved using original and cross-validated zygomatic discriminant functions (derived by both direct and stepwise procedures).	131
Table 5.15.	Individual ILD sex estimation accuracies achieved by logistic regression (LR) and linear discriminant analyses (LDA) as well as univariate statistics including means, standard deviations (SD), Wilks' lambda and F-ratios for orbital landmarks.	132
Table 5.16.	Direct discriminant analysis function coefficients, group centroids and sectioning points for all orbital interlandmark distances that achieved discrimination accuracies of 70.0% or above.	132
Table 5.17.	Stepwise discriminant analysis results for the best orbital interlandmark distances including coefficients, centroids and sectioning points.	133
Table 5.18.	Comparison of sex estimation accuracies achieved using original and cross-validated orbital discriminant functions (derived by both direct and stepwise procedures).	133
Table 5.19.	Individual ILD sex estimation accuracies achieved by logistic regression (LR) and linear discriminant analyses (LDA), as well as univariate statistics including means, standard deviations (SD), Wilks' lambda and F-ratios for nasomaxillary landmarks.	134
Table 5.20.	Direct discriminant analysis function coefficients, group centroids and sectioning points for all nasomaxillary interlandmark distances that achieved discrimination accuracies of 70.0% or above.	135
Table 5.21.	Stepwise discriminant analysis results for the best nasomaxillary interlandmark distances including coefficients, centroids and sectioning points.	136
Table 5.22.	Comparison of sex estimation accuracies achieved using original and cross-validated nasomaxillary discriminant functions (derived by both direct and stepwise procedures).	136

Table 5.23.	Individual ILD sex estimation accuracies achieved by logistic regression (LR) and linear discriminant analyses (LDA), as well as univariate statistics including means, standard deviations (SD), Wilks' lambda and F-ratios for all cranial landmarks.	137
Table 5.24.	Direct discriminant analysis function coefficients, group centroids and sectioning points for all cranial interlandmark distances that achieved discrimination accuracies of 70.0% or above.	138
Table 5.25.	Stepwise discriminant analysis results for the best cranial interlandmark distances including coefficients, centroids and sectioning points for variables X1 to X7 as per equation in Section 5.3.4.3.	139
Table 5.26.	Comparison of sex estimation accuracies achieved using original and cross-validated cranial discriminant functions (derived by both direct and stepwise procedures).	139

CHAPTER ONE

Introduction and Chapter Outline

1.1 INTRODUCTION

The field of forensic anthropology is rapidly expanding in South Africa with new publications each year not only by South African researchers, but also by international scholars (1–6). Forensics is of immense importance due to the high rates of violent crime and the correspondingly high number of unidentified sets of remains (7). Anthropologists employ a wide array of skeletal elements and have developed population-specific standards for the estimation of sex, ancestry, age, stature and post-mortem interval (8–10). Sex is one of four critical factors assessed by forensic anthropologists when compiling biological profiles to reduce the number of possible matches (6). Numerous skeletal components have been assessed for sexual dimorphism (SxD). After the pelvis, the skull is one of the most accurate and often best preserved elements (11).

The Raymond A. Dart Collection of Human Skeletons (Dart Collection) and the Pretoria Bone Collection are the most frequent sources of reference material for these investigations, yet each has one major drawback: the paucity of fully dentate white South African crania (12,13). As population standards have been exclusively derived from fully or near fully dentate specimens, there is a correspondingly low number of publications investigating the morphology of this population (1). Additionally, few studies have aimed at validating previously published standards derived for white South Africans and even fewer apply contemporary, three-dimensional (3-D) landmark-based methods. This void in the research prompted the investigation of morphological and metric aspects of SxD in white South African crania. Additionally, the effects of tooth loss are of concern, not only because this has stunted research on this population, but also because it can hinder positive victim identification.

The global aims of this work were:

1. To elucidate the ante-mortem effects that tooth loss has on cranial form and thus, on the estimation of sex, and to develop a means of mitigating these effects.
2. To produce much needed insights into the morphological sex differences in white crania by exploring overall dimorphism and its allometric and non-allometric components.

3. To investigate the validity of commonly used traditional cranial measurements using 3-D interlandmark distances, and to tailor them for white South Africans.

The following objectives were outlined:

1. To investigate tooth loss in white South African crania using geometric morphometric methods (GMM), on both the entire cranium (globally) and on various cranial subsets (regionally).
2. To subject 3-D data to GMM in order to visually demonstrate the variations that exist between the sexes and to parse out the contributions of both allometry and non-allometric SxD to this variation.
3. To scrutinise the sex estimation accuracy of traditional measures of the skull by comparing them to all possible measures derived from 3-D data. The most accurate measures were then used to create new standards for both intact and fragmentary remains.

1.2 CHAPTER OUTLINE

In order to adequately elucidate the intricacies of SxD in the crania of white South Africans the remainder of this thesis was subdivided into five main chapters, briefly surmised below.

1.2.1 Chapter Two: Literature Review

This chapter highlights some of the critical studies in forensic anthropology that centre around the estimation of sex from numerous skeletal elements, with emphasis on the skull. It also introduces the role of forensic anthropology in South Africa and briefly introduces the concept of GMM.

1.2.2 Chapter Three: Assessing the effects of tooth loss on the crania of white South Africans using geometric morphometrics

Numerous studies aimed to derive population-specific forensic standards for South African populations to increase the accuracy of biological profiles. However, a disproportionate number of these studies focused on the remains of black individuals. This is because cranial metric standards are exclusively derived from dentate

individuals, rendering the vast majority of white specimens unusable due to significant tooth loss. Furthermore, increasing life expectancies have led to the question of how aging and tooth loss affect bony landmarks of the face. Hence, this study analysed the effects of tooth loss on white South African crania using geometric morphometric techniques. A secondary aim was to explore the use of GMM to mitigate the effect of tooth loss from the 3-D dataset. The purpose of this was to approximate pre-tooth loss cranial morphology, and hence, allow for the use of the entire cranial collection rather than selected, fully dentate crania and thus vastly increase sample size. Two hundred and twenty nine (229) dry cranial specimens of white individuals (111 males and 118 females aged between 18 and 95 years) were randomly selected from the Dart Collection housed at the University of the Witwatersrand. Both fixed landmarks and sliding semilandmarks were digitised on the viscerocranium and basicranium. Following this, curve data were acquired from the face, basicranium, the maxillary alveolar ridges, the zygomatics, the nasal aperture and the orbits. GMM techniques were applied to determine the effects of tooth loss on the skull as a whole as well as its effects on the above mentioned curves. Although a number of effects were seen when the skull was analysed in its entirety, only the maxillary alveolar ridges proved to be significantly affected when curves were analysed individually. As both upper facial height and palate shape were significantly altered, several traditional osteometric measurements and qualitative traits may be affected. Upper facial height and palate shape are useful during the assessment and estimation of race and sex and hence this study demonstrates the importance of considering dental state.

1.2.3 Chapter Four: Morphological variation in white South African crania: sexual dimorphism and allometry

Geometric morphometric methods (GMM) continue to garner popularity and are becoming increasingly commonplace in forensic studies. Despite being applied in a series of publications investigating the crania of black South Africans, there is no work that examines SxD in white crania as a whole. Additionally, no attempts have been made to clarify the allometric or non-allometric components of SxD, yet they are critically important for truly comprehending its complexity. Thus, this study used GMM methods not only to assess the morphological consequences of SxD, but also its allometric and non-allometric components. A sample of 227 white South African crania (114 males and 113 females aged between 19 and 95 years) were analysed both

globally, in terms of the entire skull, and regionally in terms of the basicranium, alveoli, zygomatic arches, nasal aperture and orbits. The effects of SxD and allometry proved to be universal, with significant differences globally and in every structure analysed regionally. A significant non-allometric component was however only found to contribute to the shape of the zygomatics. In conclusion, we demonstrated not only the unique ability of GMM to detect the subtle nuances of both sex and size differences, but also its ability to elucidate both allometric and non-allometric components of SxD. These results are significant as they broaden current knowledge about the population under investigation and may help improve anthropological standards in future.

1.2.4 Chapter Five: Traditional cranial measurements versus 3-D-derived interlandmark distances for sex estimation in white South Africans

Current biological profiles depend heavily on the use of discriminant functions derived using linear discriminant analyses. The traditional cranial measurements most commonly taken when applying these functions have been in use for over half a decade, yet no attempts have been made to determine whether they are truly the most accurate measurements. The final component of this thesis aimed to test the accuracy of traditional metric measures by comparing them with all possible 3-D-derived ILDs attainable from 45 digitised landmarks, following the reintroduction of size. Subsequently, the measures deemed most accurate were used to create novel, more accurate discriminant functions for the cranium as a whole as well as for the basicranium, zygomatics, and orbits. Two new subsets, namely the nasomaxilla (comprising of both nasal and maxillary landmarks) and the basipalate (comprising of both basicranium and palate landmarks) were also created and subjected to the same analyses. Only three of the seventeen commonly measured traditional ILDs were on par with the top ILDs derived from 3-D data. The discriminant functions derived from the top 3-D ILDs in this investigation demonstrate accuracies ranging from 71.8% to 83.7% when applied to subset data. The nasomaxilla function achieved the highest accuracies and the orbit function had the poorest performance. All subset discriminant functions are useful for forensic analyses of sex from fragmentary remains. Finally, the function derived for the cranium in its entirety had a cross-validated accuracy of 88.2%. These results outperform those of Steyn and İşcan (1), which are the present gold standard for sex estimation in white South Africans. This demonstrates the advantage

of using newer methods such as GMM to support the current, more traditional metric and morphological methods.

1.2.5 Chapter Six: Discussion and Conclusion

In this final chapter the important findings of each study are highlighted and summarised. Future directions and limitations of the research are also discussed.

CHAPTER TWO

Literature Review

2. INTRODUCTION

In this chapter, forensic anthropology and the issues relating to sex estimation in South Africa, the underlying intricacies of SxD that contribute to sex differences between crania, and the methods of sex estimation employed when establishing a biological profile are discussed. Finally, the effects and consequences of tooth loss in white South African crania for sex estimation and forensic applications are explored.

2.1 FORENSIC ANTHROPOLOGY IN SOUTH AFRICA

South Africa has a high number of impoverished residents, with 32.3% of the population believed to live below the lower-bound poverty line as of 2011. In 2012, over 24% of the population was unemployed (Statistics South Africa, 2014). As a result, the crime rate is extremely high. The country has the second highest rate of murder in Africa and the twelfth highest amount per capita in the world.

(<http://www.crimestatssa.com/toptenbyprovince.php?ShowProvince=Gauteng>).

Victims may be maimed and mutilated; in some cases they are killed for use in traditional medicine (*muti*) (15). Bodies are often found buried in shallow graves in the veldt, which facilitates skeletisation and fragmentation from exposure and scavenger activity (7). Due to these circumstances, traditional assessment of demographics by forensic pathologists is difficult as dental records seldom exist and DNA analyses are costly and time-consuming (10). Forensic anthropologists are approached to aid in identifying victims (7).

Forensic anthropology is a relatively new discipline that focuses on identifying skeletonised human remains using techniques coined by anthropologists in a medico-legal setting (6,8,16,17). Bidmos et al. (6) consider the true progenitor of forensic anthropology in South Africa to be Phillip Tobias, with his pioneering works on race. South Africa's first skeletal collections were established in the early 20th century and housed at the University of Cape Town and Stellenbosch. During the 1920's and 1930's, Raymond Dart of the University of the Witwatersrand also started a skeletal collection, the now known as the Raymond A. Dart Collection of Human Skeletons (18). The Dart is now the largest collection of cadaver-derived skeletal material in southern Africa, and comprises a number of diverse groups including various African Bantu language speaking tribes, white South Africans of European descent, Khoisan individuals, Coloured individuals of mixed ancestry and a limited number of Asians (13). Pioneering studies on the cranial variation of black South Africans were

conducted by de Villiers (19) and Rightmire (20). These studies laid the groundwork for subsequent research that constitutes the basis of current forensic anthropology in the country. Forensic anthropology is an increasingly popular area of investigation as three of the country's top universities (Cape Town, Pretoria, and Witwatersrand) now offer training in the discipline (6)

One of the most important tasks facing forensic anthropologists is the development of a biological profile, used to help identify skeletal remains (6,8,16). A biological profile includes the estimation of sex, racial affinity and age as well as individualising factors such as stature, osteopathology, handedness and trauma (8,10,21). Sex estimation is a crucial task facing anthropologists as its establishment helps eliminate 50% of the population and, therefore, it is often the first step when compiling a biological profile (7). Before the measurement of sex differences can be reviewed, a thorough understanding of the mechanism by which these differences come about is imperative. Thus, the following section explains SxD, its posited causes and some factors that modify its expression.

2.2 SEXUAL DIMORPHISM (SxD)

Variations between the human sexes are evident, even to the untrained eye. Human females are generally about 92% the size of their male counterparts (9). The relative gracility of females is also evident when compared to males (8). Numerous studies have investigated the possible causes of this variation in robusticity, especially in the cranium, and attribute it to three influences: 1) Genetic drift, a neutral microevolutionary process resulting in random gene frequencies which is important as robusticity, especially in vault and temporal bones, is thought to have a large genetic component; 2) Climate, by which thermoregulatory adaptations shape morphology (such an increase in brachycephalisation in response to cold); and 3) Biomechanics, relating to the differential use of the masticatory complex (22,23).

Compared to other hominoids, humans have relatively low levels of dimorphism (24). Schaefer et al. (25) found that humans have intermediate cranial sexual size dimorphism between *Pongo pygmaeus* and *Gorilla gorilla* at the highest end of the spectrum, and *Pan paniscus* and *Pan troglodytes* at the lowest end. González et al. (26) analysed the craniofacial patterning of modern and Pleistocene/early Holocene skulls and investigated allometric and non-allometric shape variation. They

demonstrated significant allometry and found that the removal of allometric effects resulted in similar feature patterning between the sexes. A reduction in glabellar and zygomatic variation was also recorded once the allometric effect was mitigated. Bastir and Rosas (27) analysed allometric and non-allometric differences in the airways. They demonstrated that allometry accounts for 2% of the overall variation between the sexes. The non-allometric component accounted for the characteristically tall, narrow nasal aperture and narrow choanae in males (27).

Overall sexual dimorphism has both an allometric and non-allometric component. Allometry is the effect that size has on shape, or the scaling effect. It is considered on three levels, consisting of the static, ontogenetic and evolutionary dimensions (28). The variation that remains once the effect of allometry has been mitigated is the non-allometric component of SxD. Understanding the role of allometry in the expression of SxD is critical, especially when using geometric morphometric methods where size is removed, but the allometric effect remains (29). This allometric effect can modify the expression of SxD either synergistically or antagonistically.

Rosas and Bastir (30) analysed SxD and allometry in a Portuguese sample using GMM and determined that both sex and size significantly affect shape. The lower face and cranial proportions were most significantly affected by allometry in their study. Gunz et al. (31) deconstructed cranial dimorphism into allometric and non-allometric components. Using sliding semilandmark methods, they found the most differences in the parietals, zygomatics, nasal aperture and orbits.

For over a century sexual selection has been considered the major driving force behind dimorphism, following Darwin's arguments in *On the Origins of Species* and *The Descent of Man* (32). He proposed that characteristics favouring a male's ability to outcompete others for mates, such as increased size and strength, result in the propagation of those features. Future generations of males will become increasing larger and stronger thereby differentiating them from their female counterparts. Darwin also considered whether dimorphism could be influenced by ecological factors (32).

Since Darwin's time, the complex nature of SxD and its causes have been extensively researched. SxD is widely considered to be the result of three main factors: 1) sexual selection, 2) niche dimorphism or ecological causation and 3) food competition between the sexes. Shine (33) reviewed published accounts of ecological causes of dimorphism in most animal taxa. Shine concluded that the ubiquity of

ecological influences across species suggests that environmental factors have a greater influence on the expression of dimorphism than previously thought.

Additional modifiers of SxD have been proposed. Rice (34) investigated the role of sex chromosomes in dimorphism using mathematical models. He demonstrated that X-linked genes not only influence biological sex but also code for dimorphic traits and thus have a significant role in the evolution of SxD. Ruff (35) demonstrated how long bone diaphyseal bending strength as well as thickness is sexually dimorphic and population-specific. He postulated that division in labour, in this case involving a greater amount of running in males, leads to larger tibial measures below the knee, anteroposteriorly, while in females, increases in the mediolateral bending-loading in the proximal femur were attributed to wider pelvises. In terms of population differences, he found that subsistence strategies influenced SxD in that hunter-gatherers display the greatest dimorphism, followed by agricultural societies, and industrial societies being least dimorphic. This was likely as a result of differences in physical exertion (35).

Nutritional stresses and the aging process are extrinsic modifiers of SxD (36–38). Stini (38) demonstrated that an increase in nutritional stresses results in a decrease in SxD and that boys are more affected by this than girls. Suazo and colleagues (36) tested the effect of nutritional stresses on the expression of SxD and showed a decrease in the accuracy of sex estimation in males, but an increase in accuracy in females indicating a reduction in dimorphism. This decrease in dimorphism may result from reduced muscle action on the cranial bones resulting in reduced muscle markings and hence an increase in gracility.

The effects of aging on SxD have also been investigated, with some contradictory results. Walker (39) asserted that females over 45 years of age tend to develop features that may lead to their misclassification as male. By his account, the supraorbital area becomes more robust in postmenopausal females. Supraorbital robusticity in males also increases with age, however, the onset is apparently at a much younger age. These age-related cranial modifications may account for sex biases in archaeological populations. More recently, Nikita (37) used GMM to analyse the effect of aging on cranial SxD and sex estimation. This study did not corroborate Walker's findings. To the contrary, Nikita showed that apparent age changes in shape were not significant in either sex. A statistically significant cranial size increase was, however, observed for males with increasing age, presumably due to periosteal bone

deposition, although the size increase was negligible in females. These findings further illustrate the complexities of human SxD.

2.3 SEX ESTIMATION

Due to its importance in evolutionary research and its ability to withstand fragmentation and diagenesis, the skull is one of the best studied skeletal elements (8,11). Additionally, recent studies show that the skull is the most frequently recovered skeletal element in South African forensic contexts. This section reviews the advantages and disadvantages of commonly used sex estimation methods, with reference to cranial research.

2.3.1 Morphological/ Quantitative Methods

In modern forensic anthropology, morphological examinations involve the visual assessment of cranial landmarks that are not pathological, generally not visible on the body surface and are difficult to assess metrically (6,18,40). Some commonly employed morphological sex-specific features of male crania include greater overall robusticity, larger mastoids and external occipital protuberances, more protrusive glabellae, squared orbits, taller and narrower nasal apertures, broad “U”-shaped palates, and more protrusive mental eminences (6,40–43). Morphological methods are simple to use, time efficient, cost effective, and can be applied to fragmentary specimens. However, they are highly subjective, cannot readily be subjected to rigorous multivariate statistical testing, can be difficult to reproduce due to subjectivity and often ill-defined methodology, and require a highly skilled observer (6,40–43).

The problem of subjectivity in morphological assessments has been reduced by using ordinal scoring systems (18,42,44). These are used for classifying discrete bony features (e.g. yes/no or absent/present) and for continuums of expressions (e.g. progressive closure of the cranial sutures, scored on a scale of one to five) (18,44). Walker’s (42) morphological system is commonly employed in forensic investigations as it is quick and easy to apply. Based on characteristics first detailed by Buikstra and Ubelaker (45), Walker employed linear discriminant analyses and an ordinal scoring system and was able to correctly assign sex in 90% of specimens. His methodology was tested in a South African context by Krüger and colleagues (46) on a sample of 245 black and white South Africans. The authors demonstrated similar accuracies to those found by Walker for white males (94.0%-97.0%), but very low accuracies in their female counterparts (31.0%-62.0%). This result highlighted the need for population-

specific standards for this unique population. After developing those, the female accuracies rose to 83.0%-94.0%. In a separate study, L'Abbé and associates (47) assessed a different set of morphological features in black, white and coloured South Africans. In this investigation, also implementing ordinal scoring, they demonstrated that only inter-orbital breadth was significantly influenced by sex alone, whilst nasal bone contour, nasal breadth, and interorbital breadth were influenced by the interaction of sex and ancestry.

2.3.2 Metric/ Quantitative Analyses

Metric analyses involve taking measurements between various anatomical landmarks (6). Most metric studies employ linear discriminant analyses to create discriminant functions that use predetermined measurements to estimate sex (48,49). Logistic regression, an alternative to discriminant analyses, has been gaining favour of late because it is less constrained by assumptions such as normality (50). This subject will be discussed in greater detail in Chapter Five.

A number of studies have analysed metric variation between the sexes in a South African context (1,4,20,51,52). Using basic univariate statistics, de Villiers (19) investigated SxD in black South African crania and found that the glabellar prominence, superior orbital margin, inferior margin of the nasal aperture, supramastoid crest and the mastoid process were particularly dimorphic. Loth and Henneberg (53) found the morphology of the mandibular ramus flexure in South Africans to be extremely dimorphic. Their study achieved sexing accuracies of between 91% and 99%, depending on the dental state of the mandible investigated. Such levels are as accurate as using the pelvis. In one of the few analyses conducted on white South Africans, İşcan and Steyn (1) measured 12 cranial and 5 mandibular dimensions and achieved sexing accuracies of between 80% (bizygomatic breadth alone) and 86% (all cranial dimensions). More recently, Dayal et al. (54) were able to achieve accuracies ranging between 80% and 85% using 14 cranial and 6 mandibular measurements of black South Africans. The effects of applying FORDISC 3.0 to metric dimensions collected from South African crania were investigated by L'Abbé et al. (52). They found sex classification errors were more common than ancestry errors, highlighting that unique sex characteristics are present in this population. Their conclusions provide further substantiation of the need for more detailed analyses of SxD in white South Africans.

Advantages of metric analyses are that they are less subjective than morphological assessments, can be readily tested using multivariate statistics, and are easily reproducible, given that landmarks and procedures are well-defined and can be implemented by less experienced observers (6). The disadvantages are that they are more time consuming to perform than morphological assessments, require specialised equipment that can be expensive, and can be difficult to apply if observed regional differences cannot be quantified through measurement (6,42).

2.3.3 Geometric Morphometrics

Geometric morphometrics (GMM) is a relatively new technique for analysing morphological characteristics by metric means and thereby eliminating some of the problems associated with traditional techniques mentioned above (6,55,56). Rohlf and Marcus (57) coined the term *Geometric Morphometrics* and believed that the method would revolutionise morphometrics. Indeed, GMM has gained considerable favour in recent years due to the fact that it retains all the geometric information throughout data collection, whereas traditional metric analyses tends to collapse structures into a number of landmarks, measurements and angles (55,58). The technique involves the analysis of two-dimensional (2-D) or three-dimensional (3-D) Cartesian coordinates of homologous landmarks captured across all specimens of interest. After the coordinates are digitised they are superimposed using either generalised or partial Procrustes superimposition (56,58,59). In the first step in the process, known as translation, all configurations are moved to the origin of the coordinate system. Following translation, size is mitigated such that shape can be assessed independent of the bias introduced by overt size differences. During this “scaling” step a scaling factor, known as centroid size, is retained such that size can be evaluated or even reintroduced at a later stage, should it be of interest. The scaling step can also be skipped in a process called Procrustes size preservation, which is particularly useful in forensic investigations as 3-D landmarks can be analysed using traditional morphometric techniques (60). Finally, the configurations are rotated using a least squares procedures to minimise the sum of squared distances between corresponding landmarks (61).

Recently, GMM has gained considerable interest amongst anthropologists, and has been applied to numerous skeletal elements including the skull (62–65), mandible (58,65,66), pelvis (67) and scapula (55,68). Of these, the cranium has garnered the

most attention due to the high accuracies reported for both sex and ancestry estimation.

Several examples of GMM applications to forensic anthropological sex estimation provide evidence of the success of the methodology. Franklin et al. (3) studied SxD in Black South Africans by collecting 96 landmarks from 332 skulls and utilising the generalised Procrustes superimposition technique. Using principal components analysis, they found that lateral projection of the zygomatic bones, forehead contour, frontal profile, face shape, length of the midbasal region, and curve of the supramastoid crest were the most dimorphic features. Pretorius et al. (69) conducted a study on SxD in the same population using thin plate splines, canonical variants analyses, and relative warp plots. They focused specifically on the shape of the greater sciatic notch, flexure of the mandibular ramus, and the shape of the orbits. The shape of the greater sciatic notch was the most dimorphic feature (93.1% accuracy in black males) and the orbits provided a better estimate of sex than did mandibular ramus flexure (73.3% versus 69.6% in black males, respectively) They also demonstrated that canonical variants analyses provided clearer results than thin plate splines for the population in question.

Similarly impressive results have been obtained for populations from other world regions. Bigoni and colleagues (63) studied a central European population from Bohemia in a similar fashion as the above mentioned studies, but they also included 39 semilandmarks along the midsagittal curve. They noted that there were no significant differences in this population in the cranium as a whole or in the basicranium, but they achieved outstanding accuracies of 100% using the shape of the nasal aperture, orbits and palate, and 99% using the midsagittal curve. Green and Curnoe (64) used GMM to demonstrate differences between the sexes in a Southeast Asian population. They found that facial breadth, particularly across the zygomatic and postorbital regions, and cranial vault breadth are especially dimorphic, and also that significant size differences are present. Using this knowledge they conducted discriminant analyses and were able to achieve 86.8% accurate sex estimation. These findings are very important, as previous studies have demonstrated size but not shape differences in this population. Ji et al. (62) focused on the orbits of a Chinese population. They identified significant sex differences in all orbital parameters except orbital height, and also found the orbits to be symmetrical. They did not determine sexing accuracies, however.

2.3.3.1 Semilandmark methods in geometric morphometrics

Geometric morphometrics (GMM) is based on capturing shape differences from the coordinates of homologous landmarks. It therefore faces the same limitations as traditional morphometrics when landmarks are damaged or missing, or too few are available to adequately capture shape via curves or outlines (58). To solve this, Bookstein (70) suggested the use of semilandmarks that are slid a certain distance along a curve until they attain positions that are similar to the reference structure (58,59). In this way, homologous points on curves can be compared (59). When semilandmarks slide, they do so to remove tangential variation. This can be done in two ways, either by minimising bending energy when semilandmarks are slid (in a parallel direction relative to the curve) allowing the landmark to align to the reference form, or by using the minimum Procrustes distance method that estimates the direction tangential to the curve and removes the component of the difference along the tangent whereby removing the difference in semilandmark position between the reference form and target specimen. Perez et al. (59) investigated the effectiveness of these two techniques by analysing the shape of the orbits, nasal aperture, maxilla, zygomatics and frontal bone. They concluded that the minimum Procrustes distance method was more accurate because the bending energy method resulted in larger intra- and interpopulation differences. This was believed to be due to differences in the placing of semilandmarks along the curves. Another interesting observation made in this study was that the difference between the two methods became more noticeable if an increased number of semilandmarks were used, suggesting that the number of semilandmarks should be limited as much as possible.

One of the most important advantages of GMM is that it overcomes observer subjectivity as shape is analysed statistically (63). Furthermore, GMM allows shape to be analysed independent of size. Morphological variation, as expressed through GMM, can be graphically depicted in intuitive images, and GMM can detect subtle variations that traditional metric and morphological methods cannot (3,58,63,69,71). Disadvantages of GMM are that technical equipment and an in-depth understanding of the statistical nuances of the technique are required. Data collection can also be time consuming (3,58,69).

2.4 TOOTH LOSS

In South Africa, most cranial research depends on samples derived from one of three skeletal collections, namely the Pretoria Bone Collection, the Raymond A. Dart Collection of Human Skeletons and the Kirsten Skeletal Collection. Despite the tremendous scientific value of these collections, they share a major limitation: the majority of the white crania are completely toothless (edentulous) because the collections are primarily comprised of elderly body donors. The lack of dentate specimens has directly contributed to the low number of publications relating to biological variation in white South Africans, as edentulous specimens must be excluded from many basic variation studies.

Tooth loss is attributed to numerous intrinsic and extrinsic factors. Intrinsic factors such as dietary status, hormonal shifts and the aging process result in weakening of the periodontal ligaments, residual alveolar ridge resorption, tooth loosening and eventual loss (72,73). Extrinsic factors, such as smoking and poor oral hygiene, also contribute to tooth loss (74). Edentulism has effects on the dentoalveolar complex and more remotely located structures of the facial skeleton. Haraldson (75) reported that tooth loss results in a decrease in the forces exerted on the alveolar margin of the maxilla. This in turn leads to a decrease in microfracture formation and hence, a decrease in bone deposition. A superior and posterior shift in the maxilla (76,77) is associated with a decrease in all facial dimensions, but specifically upper facial height (78–80). Tallgren (81) demonstrated that the loss of residual ridge height continues even 25 years after teeth are extracted. Mardinger et al. (82) found an increase in the size of the nasopalatine canal following tooth loss. In terms of muscular changes, edentulous individuals have greater reductions in masseter and medial pterygoid cross-sectional areas when compared with dentate subjects (83). This reduction in muscle mass explains the five to six-fold reduction in bite force demonstrated by Haraldson (84) and the reduction in cortical thickness of all facial bones reported by Dechow et al. (85).

Facial changes related to tooth loss have been qualitatively described in detail, yet little is known about the quantitative effect that edentulism has on the cranium as a whole and also on the accuracy of sex and ancestry estimation. Chapter 3 deals specifically with this question.

This review focused on SxD and its importance for understanding cranial variation and the need to expand the knowledge base regarding SxD as it applies to modern forensic anthropology practice. The value of GMM and the advantages of using this method for

evaluating SxD were considered. Finally, this chapter emphasised the gap in the literature regarding analyses of white South African crania due the high frequencies of edentulous individuals in study collections derived from cadaveric material.

The end-goal of this research is to assess sexual dimorphism in white South Africans and improve current methods of discriminating males from females. However, current skeletal collections are composed of individuals who have donated their remains for research purposes and are thus generally of advanced age. Tooth loss is, thus, commonplace among these individuals. Tooth loss is known to affect skeletal morphology, and its significant effect on cranial variation has led studies to exclude individuals with missing teeth. Therefore, the broad aims of this research are to 1) Assess the effects that tooth loss has on cranial morphology and mitigate these effects, thus increasing the sample size of white South African crania available for study; 2) Use the large sample of white crania available after controlling for tooth loss to assess sexual dimorphism, the relative contribution of allometry to this dimorphism and the degree to which sexual dimorphism influences cranial morphology in the absence of allometric effects; and 3) To improve sex estimation accuracy by creating new discriminant functions using this large dataset and 3-D methods.

CHAPTER THREE

Assessing the effects of tooth loss on the
crania of white South Africans using
geometric morphometrics

3.1 INTRODUCTION

In South Africa, high rates of interpersonal violence and murder ignited an interest in forensic anthropology as the number of unidentified skeletonised remains continues to climb (7). Many forensic investigators set out to derive population-specific standards in order to increase the accuracy of biological profiles and to aid in the identification of individuals (7,66,86). Most studies were conducted on black individuals using traditional morphometrics and none investigated the effects of tooth loss on the craniofacial structures. Unfortunately, information pertaining to edentulism in South Africa is scarce. Van Wyk et al. (87) noted that the most recent survey that included edentulism was published in 1989. This study, by Du Plessis et al. showed that 12.6% of South Africans between the ages of 35 and 44 across all population groups were completely edentulous. The incidence of edentulism was found to be highest in the Coloured population (51.6%), and females displayed greater levels in all populations (87).

Despite being of primarily Dutch descent, white South Africans have been isolated from their European ancestors for hundreds of years. Admixture and possibly adaptations to the local environment shaped this population into a unique entity worthy of specific population standards (1). Furthermore, as the life expectancy of South Africans is likely to reach 76 years by 2100 (88), there will inevitably be an increased number of skeletonised remains with varying degrees of tooth loss needing assessment by forensic anthropologists.

Once teeth are lost due to factors such as poor dental health, periodontal disease, poor diet, bone disease and smoking (72,73), significant microscopic and macroscopic changes to the maxilla occur. The process of aging also increases the risk of tooth loss as bone becomes more porous and the number of active osteoblasts versus osteoclasts diminishes. This, together with other histological changes, causes bone loss to double between the ages of 60 and 80 years (89). It has been shown that 12 months post-extraction, alveolar ridge height decreases by up to 44% (73). There is up to 500% reduction in masticatory force, resulting in further resorption of the underlying bone in these inactive areas (80,85). Heath (90) evaluated the effects of edentulism on British individuals between the ages of 20 and 84 years and found that although edentulous

subjects displayed significant alveolar resorption and a decrease in total facial height, these changes did not extend to the upper face. Facial height decreases were also demonstrated by Tallgren (78), Bartlett et al. (79), Crothers (91) and Sviekata et al. (80), in conjunction with supero-posterior movement of the maxilla (76,77). While Heath (90) found no significant changes to the basicranium or the hard palate, Pietrokofski and Massler (92) demonstrated that the maxillary buccal plate resorbed faster than the palatal plate resulting in a reduced arch length. Edentulous individuals display thinner cortical bone in all regions of the face, but similar or greater elastic moduli (a measure of the force required to produce non-permanent structural change) and density in the zygomatics and cranial vault (85).

As numerous standard skull measurements are used for the estimation of sex and ancestry, it may be important to factor in the structural changes associated with the loss of teeth to optimise the accuracy of biological assessments (45). The lack of anthropological research regarding tooth loss, as well as the high number of unidentified skeletons found in South Africa, warrant a study that focuses particularly on the effect of tooth loss on craniofacial structures. Furthermore, the relative paucity of research on white South African skulls using GMM further supports the need for such research.

Hence the aim of this research was to use GMM methods to analyse the effects of tooth loss on white South African crania on global and regional anatomical scales by employing semilandmarks to identify fine-scale changes to the basicranium, maxilla, zygomatic bones, nasal aperture and orbits.

3.2 MATERIALS AND METHODS

3.2.1 Materials

A total of 229 crania were selected by filtering out desired accession numbers from a catalogue of specimens housed in the Dart Collection. Those consisted of 118 males and 111 females (Table 3.1) of European descent (white). Most of the white individuals in the Dart Collection are from body donations and represent persons who are of Dutch, German, French, British, and Portuguese descent (13,67). The first Dutch

immigrants took up residence in South Africa in 1652. Thereafter, an additional influx of Europeans occurred between the 17th and 19th centuries and included French Huguenots, Germans and British settlers, respectively (5). Three hundred years of isolation, facilitated by admixture and genetic drift, have made this population of individuals distinct from their European ancestors. In fact, the prevalence of rare genetic disorders including Huntington's chorea, hypercholesterolemia, Fanconi anaemia and schizophrenia have made this population a textbook example of the founder effect (93,94). A number of forensic publications have assessed white South African specimens from the Dart Collection and Pretoria Bone Collection, and have deemed the sample to be homogenous and significantly different from white Europeans and Americans (95). The ages ranged between 18 – 95 years to ensure that the skulls had an adult configuration and to include a broad spectrum of adult skull morphologies. All of the selected individuals were born between the late 19th to 20th centuries. Crania displaying varying degrees of dental loss were incorporated in the study, including completely edentulous individuals, so that the structural changes resulting from tooth loss could be evaluated. Additionally, edentulous skulls were included because such a large proportion of the cranial material representing white individuals are edentulous. The sample included a total of 160 edentulous skulls. When teeth were lost, and if the individual wore dentures prior to death, was not known. Skulls exhibiting any other signs of damage, pathology or obvious orthodontic rehabilitation were excluded.

3.2.2 Data Collection Procedure

Prior to data collection, fixed landmarks on each cranium were marked with pencil. This was done to ensure accurate data capturing as sutures are often completely obliterated in older individuals, making landmarks hard to identify once crania are fixed to the work surface. Specimens with missing landmarks were excluded. A complete list of the cranial landmarks is provided in Table 3.2. Strips of dental clay were secured along the cut surface of the neurocranium which allowed each cranium to be fixed to the work surface in an inverted position, with the viscerocranium directed anteriorly. This ensured that all landmarks could be digitised at a single sitting, avoiding the additional error of

fitting separate sets together. Crania that still possessed a vault were oriented in a similar manner, only using a ring of clay to securely fix them to the work surface.

Using a Microscribe® 3-DX digitiser (Immersion Corp., San Jose, CA) interfaced to a personal computer, cranial landmarks were digitised in a fixed sequence by touching the tip the stylus to each landmark and stepping on a foot pedal to mark their exact location. The x, y, and z coordinates of each landmark, calculated using optical angle encoders at each of the microscibe joints, were recorded in an *MS Excel* spreadsheet in millimetres with up to four decimal places.

Curve data were captured by tracing the surface of each curve with the tip of the stylus as a continuous stream of points (semilandmarks) registered at 0.5mm intervals between the fixed landmarks recorded earlier. Semilandmarks are points that are used to define outlines and curves that have an insufficient number of homologous landmarks to adequately define their shape (31,60). Gunz et al. (60) define semilandmarks as “deficient” as they are not discrete landmarks, nor are they homologous. To overcome this, semilandmarks are treated as missing data and estimated simultaneously. This minimises total bending energy (31). The cranium was subdivided by region to allow for finer scale resolution of differences between these regions, which may have been obscured by larger variation across the cranium as a whole. The rationale for grouping landmarks into the chosen subsets was, firstly, to maintain continuity with both traditional (1) and geometric morphometric based publications (72). Additionally, intuitive, anatomical groupings of landmarks were used to make the regions easy to recognise, thus increasing repeatability, and maintaining the geometric integrity of the regions. Finally, recent studies (96,97) demonstrated that the cranium is subdivided into a number of semi-independent modules that co-vary with one another. Hence, this study aimed to represent these modules outlined by Smith (97) while also meeting the before-mentioned criterion.

The following working definitions are used to refer to morphology in the respective samples throughout the current investigation: the term robusticity was used to refer to large superstructures such as glabellae, mastoids and wide, flaring zygomatics. This term was, hence, used to explain attributes of size. Subsequent to the mitigation of size, the

characteristic markings and roughenings caused by the large muscles remained. This was referred to as rugosity. These definitions are in-line with those used by Steen (98).

The procedure followed for the digitisation of each curve is detailed below, under the heading of the subset into which they were divided.

3.2.2.1 Zygomatics

Each zygomatic bone comprises two components; an inferior curve and a superior curve. The inferior curve was digitised first and in three parts: from porion (po) to glenoidale (ge), from glenoidale (ge) to the articular eminence (ae) and finally from the articular eminence (ae) to zygomaxillare (zm) (curve number 4 in Figure 3.1). The superior curve comprised two parts: the first from a point on the supramastoid eminence directly above glenoidale, named *superior glenoidale* (sge), to superior zygotemporale (sz), and the second from superior zygotemporale (sz) to frontomalare temporale (fmt) (number 5 in Figure 3.1). The landmark superior glenoidale (sge) had to be created as a starting point for the superior zygomatic curve because the supramastoid tubercle (ss) could not be used as a landmark as it was often bisected during removal of the calotte during dissection.

3.2.2.2 Orbits

The orbits were digitised as three separate sub-curves: a superior curve from frontozygomatic orbitale (fo) to dacryon (d), an inferomedial curve from dacryon (d) to zygomaxillare orbitale (zmo) and an inferolateral curve from zygomaxillare orbitale (zmo) to frontozygomatic orbitale (fo) (curve number 6 in Figure 3.1). Care was taken not to let the stylus dip into the superior orbital notch that was often present on the superior curve. This would have led to distortions in the shape of the curve and subsequent errors in the placement of semilandmarks (72). The inferolateral curve was easily digitised, although it should be noted that at the junction of the zygomatic and maxillary bones (zmo) the suture often presented as a raised area along the curve. Care needed to be taken to ensure smooth tracing by always resting the elbow on the work surface and moving cautiously along this section. Finally, the inferomedial curve data were captured and proved to be the most difficult to trace of all the bony curvatures under investigation. A

defined ridge between dacryon and lachrymal orbitale was often lacking, similar to what was described by Williams (99). This occurred more frequently in females than males. The difficulties in tracing this region were further complicated by damage to the lachrymal bone. These obstacles were overcome by drawing an imaginary line between dacryon and lachrymal orbitale if the ridge was absent or damaged and then tracing the curve with the elbow resting on the work surface for maximum stability.

3.2.2.3 Nasal aperture

The nasal aperture was comprised of a total of six sub-curves with three on each side. These included a superior curve from rhinion (r) to alare (al), a middle curve from alare (al) to nariale (na), and an inferior curve from nariale (na) to the inferior nasal spine (ins) (curve number 7 in Figure 3.1). Although the process of digitisation was not difficult, minor chipping to various parts of the aperture was frequently observed, especially at rhinion and the inferior nasal spine. Damaged areas were “smoothed over” with the stylus where possible by following the original anatomical curvatures. In situations where the damage was too extensive the specimen was excluded.

3.2.2.4 Maxilla

The maxilla was digitised as two individual curves along the maxillary alveolar ridge and the palate. Palate data were captured first and divided into two sub-curves on either side of the maxilla from the posterior aspect of the greater palatine foramen (pf) to the most anterior point on the posterior aspect of the incisors (aic) (curve number 2 in Figure 3.1). The curves were traced as close to the lingual aspect of the dentoalveolar margin as possible. Extreme alveolar resorption often caused the incisive foramen to become the most anterior point of the maxilla, affecting both the maxillary alveolar ridge and the inner palate tracings. The size of the incisive foramen also increased in these cases. Small bony spines, often encountered on the palate, were avoided where possible to minimise distortion.

The maxillary alveolar ridge comprised of two sub-curves running from ectomolare (ecm) to alveolare (ids) on either side (curve number 3 in Figure 3.1). The ridge was traced as closely as possible to the dentoalveolar junction on the buccal side of the maxilla.

Dental caries that were visible as bony lesions (likely as a result of abscesses) were smoothed over where possible. Once again, resting the elbow on the work surface and supporting the stylus with the non-dominant hand helped prevent unwanted deviations of the stylus tip.

3.2.2.5 Basicranium

Representing the only curves on the basicranium, the foramen magnum was digitised as four individual curves, with two curves on each side traced from basion (b) to the posterior aspect of the occipital condyle (poc) and from the occipital condyle (poc) to opisthion (o). The anterior curves on each side were more challenging to trace in some specimens due to an apparent inward flexure of the bony ridge between poc and b. This was overcome by viewing the specimen from directly above whilst digitising the curves to minimise parallax errors by allowing only the external rim of the foramen magnum to be seen.

3.2.2.6 Dental scoring

After digitisation, anterior, posterior and inferior photographs were taken of each cranium. A record of any anomalies and/or variations present on the crania was made by the author. This was done so that outliers could be investigated photographically and morphological anomalies or variation could be excluded as the cause. Finally, the dental state of each specimen was assessed using binomial scoring of each of the maxillary teeth. A score of absent (0) was given if teeth were lost ante-mortem and blunting of the alveolar crests was apparent or alveolar resorption was marked. A score of present (1) was given if teeth were either physically present or in cases where skulls displayed post-mortem tooth loss evidenced by well-defined alveoli with minimal blunting of alveolar crests. The data were then captured in a *MS Excel* spreadsheet.

3.2.3 Data Resampling and Reworking

As semilandmarks were taken at a fixed distance from one another and not at bony landmarks, the number of points on each curve varied depending on the length of the curve and therefore needed to be standardised. In order to do this, the coordinates recorded for the fixed landmarks initially and those at the beginning and end of each curve

were averaged and the original *MS Excel* spreadsheet of data points was converted to a text file. This was then imported into the freely available morphological analysis program *Morpheus* (<http://www.morphometrics.org/id6.html>). *Morpheus* allows a user defined number of landmarks to be resampled from each curve. This procedure is then automatically repeated across all specimens. The number of points to be resampled was determined by randomly sampling ten specimens and determining the average length of each of the five curves under investigation. Each curve length was then divided by 5mm, 7mm, and 10mm to determine which distance provided the minimum number of points that best defined all the curves. A 7mm interval was selected. The number of semilandmarks which define each curve in the subset is detailed in Table 3.3. This number includes “helper landmarks” that needed to be removed later. Helper landmarks were added to assist in representing the curve form better (100) as semilandmarks do not slide along the curves themselves but along tangent vectors to the curves (101). As a result, more complicated curves have a greater bending energy. More points are needed to minimise this energy or misrepresentation of the curve shape may occur. Helper landmarks assist in reducing distortion by helping to align semilandmarks. Unlike semilandmarks, they do not contribute to the overall Procrustes distance as they are removed prior to any analyses (100).

3.2.4 Statistical Analyses

3.2.4.1 Repeatability

Observer error was assessed by comparing the Procrustes distances between paired specimens of the entire sample with those of repeated measurements retaken from 15 individuals. The effects of allometry on between-specimen variation were accounted for by multiple regressions on the logarithm of centroid size. Failure to account for allometry could obscure the effects of measurement error. Figure 3.2 A and B shows the results of the analyses before and after the effects of allometry were accounted for, respectively.

The difference between partial Procrustes superimposed original and repeated configurations were modelled on the mean shape to further evaluate measurement error. In order to illustrate error at each landmark, a wireframe mesh was produced with 95%

confidence ellipses around landmark scatters (Figure 3.3). Although error is averaged among the landmarks through Procrustes superimposition methods, those with excessive error will generally stand out, given that there are enough well placed repeatable landmarks to anchor the configuration.

3.2.4.2 Preliminary analyses

Preliminary refining of the dataset was required before the main analyses could be run. This included mitigation of asymmetry, removing outliers and sectioning the main dataset into the subsets needed for the subset analyses. These procedures are described in this section.

Klingenberg et al. (102) defined two types of bilateral symmetry. The first, known as matching symmetry, occurs when mirror images of a structure occupy opposite sides of an organism (e.g. the left and right arm). The second, known as object symmetry, occurs when symmetry exists along two sides of a midline of the same structure, as is seen in the human skull. Certain degrees of developmental asymmetry occur naturally in even the most symmetric of objects (102,103). Although the study of asymmetry is the focus of many studies, it was beyond the scope of this investigation and needed to be controlled for. Failure to do so would introduce additional variation to the dataset that would obscure results and lead to spurious conclusions. Asymmetry was removed by finding unilateral landmarks, which lie in the midline of the cranium, and zeroing them. Bilateral landmarks from the left side of the cranium were then reflected onto the right and relabelled (102). Mean configurations of a specimen and its reflection, after Procrustes superimposition, are considered symmetric. By running analyses on the symmetric component of the data, any asymmetry was eliminated together with any variation associated with it. The morphological analysis program *Morphologika* (104) was used for preliminary visualisation of the raw data. This included preliminary partial Procrustes superimpositions (PPS) and principal components analyses (PCA) that were used to analyse the overall distribution of the data and to identify outliers.

After the data were visually assessed in *Morphologika*, data and classifier files were read into the statistical software *R* (version 3.1.3, R Core Team, 2015). Outliers were identified in *Morphologika* as any points far removed from the main cluster in the

scatterplot of principal component one. Renderings of each specimen's landmarks were also assessed to ensure that no errors were made during data collection. Once identified, outliers were removed and PPS was performed on the symmetric component of the remaining data. Semilandmarks, including helper landmarks, were slid using a thin-plate spline deformation (with minimum bending energy) (31) and centroid size was saved. Thereafter, the helper landmarks were removed, resulting in a reduction in the total number of landmarks per specimen from 281 landmarks to 158. Centroid size was also recalculated based on the reduced number of landmarks.

3.2.4.3 Analysis of tooth loss

After preliminary analyses, the following set of statistical procedures was conducted using programmed algorithms and scripts in the statistical program *R* (version 3.1.3, R Core Team, 2015). These procedures were repeated for the skull in its entirety as well as for each of the subsets listed in Table 3.3.

Full Procrustes superimposition permits centroid sizes to vary and allows for the attainment of true minimal distances among specimens. Despite this, partial Procrustes superimposition (PPS) is often the preferred superimposition method as, after tangent space projection, it reflects the true distance between specimens better than full Procrustes superimposition (102). An uncentered correlation coefficient was therefore used to test the difference between the two techniques, and PPS was found to produce less distortion due to projection. Therefore, PPS was used to align landmarks by translation, scaling, and rotation (60,105) and the resulting data were projected orthogonally to the tangent plane. The thin plate spline algorithm outlined in Gunz (106,107) was used to allow semilandmarks to slide with each iteration, rather than minimising Procrustes distance. Helper landmarks were utilised because sliding-semilandmarks are shifted along a tangent to the curve with each iteration during Procrustes superimposition, and not along the curve itself. These helper points were then discarded prior to any statistical analysis (100). Finally, permutation tests were employed to determine whether significant size and age differences exist between the male and female groups.

In this investigation, the analysis of dental loss was categorical and scored as absent (0) or present (1). Although the accepted method for analysing relationships between categorical data is by multiple correspondence analysis (108), the question arose whether an ordination method, such as principal components analysis (PCA) or 2-Block partial least squares (PLS), could also be used to investigate such relationships. Both PCA and multiple correspondence analysis were run on the binary dental data and the results were compared by means of an uncentered correlation coefficient. A correlation of 0.998 was found, suggesting that PLS is an appropriate method for assessing categorical data. PLS was thus employed to assess the effects of dental loss on the morphology of the face and basicranium.

Next, the RV coefficient (109) was used to assess whether a significant amount of covariation exists between the two blocks of data (tooth loss and cranial shape). This coefficient is superficially comparable with Pearson's correlation coefficient in that zero represents no association and one a perfect association (the amount of covariation between X and Y expressed as a fraction of the total variation in blocks X and Y). The significance of the covariation was tested using a permutation test to assess whether the coefficient obtained is significantly greater than that resulting by chance (110). Where significant covariation existed this was explored using PLS. PLS is a relatively new dimension reducing technique that explores *covariation between* a set number of variables or blocks, as opposed to PCA which explores *variation within* a block (60,111). Due to the fact that the dependant variable, in this case dental loss had been specified, PLS is a better technique than PCA for this study (112). Vector diagrams and colour coded polygon figures were used to visualise the effects of dental loss on craniofacial morphology.

3.3 RESULTS

3.3.1 Repeatability

Results of the Procrustes distance analyses on the repeated measurements, Figure 3.2 A, show that they did not fall within the range of the paired comparisons which

indicates that the degree of measurement error is well below the 5% requirement. Figure 3.2 B shows the effect of the mitigation of allometry on the results. A minimal reduction of overall variability is seen, but the degree of measurement error remains unchanged. Hence, measurement error was deemed within acceptable limits. These results are visually depicted in Figure 3.3 in which smaller ellipses are indicative of lower degrees of error as compared with larger ellipses. Furthermore, circular ellipses illustrate less directional error than do the more elliptically shaped ones.

Despite being within the 5% acceptable limit, Figure 3.3 shows that the largest amount of measurement error existed along the orbital margins and the outer aspect of the maxillary alveolar margin. Despite the fact that Procrustes superimposition averages out disparities between landmarks, this method highlights potentially problematic landmarks as there are many well-defined highly repeatable landmarks to “anchor” the configurations.

3.3.2 Global Analyses

A significant covariation was observed between tooth loss and cranial shape ($RV = 0.373$, $p < 0.001$), and a two-block PLS analysis was used to elucidate the association between variables (Figure 3.4).

The first PLS vector accounted for 72.01% of the total covariation seen between dental loss and cranial morphology. Similarly factors two, three and four accounted for 4.66%, 3.59% and 2.76% of the covariation in the sample respectively. In Figure 3.4, all edentulous individuals cluster at the bottom of the graph for factor one, independent of skull shape, whereas the remaining vectors only account for a tiny fraction of the covariation and do not align with the order of tooth loss. The statistical program *R* was used to construct vector diagrams (Figure 3.5 a3, i3 and l3) and polygon representations with a colour spectrum illustrating relative changes of polygon area (Figure 3.5 a-l 1 and 2). The use of both image types facilitates an understanding of the changes taking place in each structure as the vector diagrams show how, and in which direction, each structure is changing. The polygon images also give an indication as to the localised relative shape changes using a colour gradient.

In the polygon representations of morphological change (Figure 3.5 a-l 1 and 2), two images are presented. One represents completely edentulous individuals and the other representing dentate individuals. Polygons that experience insignificant change in an area are green in colour, whereas spectra tending toward red and blue are indicative of increasing and decreasing relative polygon area, respectively. The colour red itself indicates a two-fold increase in area, whilst blue represents a halving in area. It is unsurprising that these images indicate that the greatest change associated with tooth loss is the marked recession of the alveolar bone of the maxilla, which seems somewhat localised in the anterior third of this structure. This severe resorption of bone leads to a marked decrease in facial height and prognathism. There is also a significant decrease in the length of the bony bar that extends from the approximate position of the canine jugum to the infraorbital margin near zygomaxillare orbitale (zmo). This is likely to be a result of the decrease in prognathism due to alveolar resorption. As the resorption of bone is not limited to the labial and buccal surfaces of the maxilla, but also occurs on the lingual surface, there is a noticeable increase in the width of the palate, making it appear more hyperbolic.

In the vector diagrams (Figure 3.5 a3 i3 and l3) the two extreme morphologies represented in the data set are superimposed as reference and target images and vectors/arrows are used to show the magnitude and direction of the change that occurs between them. In this case the red image is the reference image that represents completely edentulous samples, whilst the blue image is the target image representing the dentate samples. These images also show that the greatest variation is present in the maxilla, but the vectors further highlight the fact that a larger degree of resorption occurs in a posteromedial direction around the labial/buccal surface. A relatively smaller degree of resorption occurs in an anterolateral direction about the lingual/palatal surface.

Additionally, it is apparent that there is an inferior and anterior flexion of the basicranium relative to the viscerocranium such that the external occipital protuberance comes to lie more inferiorly following tooth loss. The mastoid processes appear to move both inferiorly and anteriorly. The relative size of the basicranium also appears marginally larger in the edentulous individuals. From the vector diagrams it also become apparent

that the zygomatic bones shift inferiorly and bizygomatic breadth becomes relatively larger with tooth loss. Finally, both the protrusion of the nasal bones and the size of the orbits appear to undergo a relative increase in cases of extensive tooth loss. It should be noted however, that these observations are relative and it is likely that a decrease in the size of the facial skeleton is responsible for these outcomes rather than an absolute increase in the size of the aforementioned structures.

3.3.3 Individual Curve Analyses

When each of the subsets (basicranium, maxillary alveolar ridge, zygomatic arch, nasal aperture and orbital rim) was analysed individually, the alveolus was the only structure significantly affected by tooth loss. This effect proved to be highly significant ($p < 0.001$), as expected. The first vector of the two-block PLS accounts for 82.72% of the covariation between dental loss and maxillary shape, followed by only 5.56%, 2.50% and 2.28% being accounted for by the next three vectors. The dramatic reduction in the thickness of the alveolar bone is striking (Figure 3.6, a and b). The anterior third of the maxilla experiences particularly extreme reduction of bone and it appears as though virtually no bone remains. This severe reduction in bone causes an overall relative widening of the bony palate that results in a more hyperbolic shape. The vector diagram in Figure 3.6 (b) clearly illustrates that the loss of bone associated with edentulism is not limited to the labial/buccal surface, but occurs along the lingual surface as well. The depth of the incisive canal, represented by the triangular eminence of bone that appears to extend below the alveolar margin in Figure 3.6 (a to c), is seen to undergo a relative migration anteriorly and reduce in depth in the images representing the edentulous configuration.

3.4 DISCUSSION

3.4.1 Repeatability

Bookstein (70) describes three types of landmarks based on the quality and quantity of the data they define: Type I, Type II and Type III. Type I landmarks occur at the intersection of tissues (e.g. zygomaxillareorbitale – a landmark located on the rim of

the orbit that is at the intersection of the maxilla and zygomatic bones). Type II are points that represent minima and maxima on structures and which vary, in part, depending on the orientation of the object under investigation (e.g. mastoidale – which is located at the tip of the mastoid process). Type III are geometrically determined landmarks that represent extremes (e.g. alveolone - measured where the midline of the palate is crossed by a straight line connecting the posterior aspects of the alveolar crests). Type III landmarks also include semilandmarks. In Figure 3.2, it the Bookstein Type I landmarks (including basion, opisthion, posterior occipital condyle, nasion, rhinion, frontozygomaticorbitale and zygomaxillareorbitale) that display the lowest level of intra-observer error. On the other hand, Type II landmarks such as mastoidale, nuchal crest and auricular eminence as well as the Type III semilandmarks all display a greater amount of intra-observer error. This is in accordance with the results of Bareito-Andrés and colleagues (113) that found semilandmarks taken on the neurocranium showed the greatest level of measurement error. These are Type III landmarks that the authors described as being “difficult to visualise and localise” (113).

Aside from errors associated with landmark types, there were specific regions that displayed larger amounts of measurement error. These include the superomedial and inferolateral aspects of the orbits as well as both labial and lingual aspects of the maxilla. The former may reflect the difficulty in defining a curve between dacryon and lachrymal orbitale as well as damage to the lacrimal bone. The relatively large degree of observer error recorded for the maxilla may have been as a result of the degree of recession of the alveolar ridges. Finally, a relatively large degree of measurement error is seen at glabella, the mastoids and frontotemporale. This was not unexpected as these are all Type II and Type III landmarks, which by definition, are prone to more error. Errors may be reduced in future studies by first applying dental clay to smooth the irregular surfaces before digitisation and perhaps by positioning skulls in such a way that all surfaces are more easily accessed.

3.4.2 Global Observations

This study investigated the effect of tooth loss on cranial morphology and quantified its effects on the palate and maxillary alveolar ridges. Results show that

edentulous crania have reduced facial height and prognathism, globally, and that only the maxilla is significantly affected when analysed regionally.

The alveolar ridges of the maxilla are so thin, delicate and labile (73) that alveolar resorption following tooth loss is severe. Even a reduction of crown height resulting from tooth wear leads to a decrease in anterior upper facial height (91). Studies conducted on monkeys showed that the highest rate of resorption occurs within the first few months following extraction and that lack of oestrogen may have a significant effect on continued resorption (114). This extreme resorption may be further accelerated by smoking, as demonstrated by Saldanha et al. (115).

Although several studies, most of an orthodontic nature, have assessed the effects of edentulism on the mandible and maxilla, very few have considered its effects on other bony structures of the cranium. In the current investigation, global analyses of the entire face and basicranium revealed that tooth loss has significant effects on the cranium including severe resorption of maxillary alveolar bone with a concomitant decrease in alveolar prognathism. When dentate and edentulous crania were compared, a relative increase in both orbit size and projection of the nasal aperture, a relative increase in the width of the zygomatics together with inferior and anterior flexion of the basicranium relative to the viscerocranium was also seen with tooth loss. When each curve was analysed individually, however, only the maxillary alveolus proved to be significantly affected. This is surprising since the current study hypothesised that tooth loss would affect the zygomatics as the masseter muscle has its origins on the arch. This muscle, together with the medial pterygoid, has been shown to atrophy with tooth loss (83), resulting in reduced bite force in edentulous individuals (84,85). Accordingly, this bone should experience a decrease in mechanical loading and hence a degree of reduction, which was not observed. Richard et al. (116) examined the effects of aging on the craniofacial skeleton, and observed a decrease in the anterior projection of the zygomatics, which may support the idea that this bone experiences some degree of atrophy over time. However, the cortical bone mass of the zygomatics seems rather stable irrespective of tooth loss. This is demonstrated by the fact that severe maxillary alveolar recession can be treated by anchoring fixed dental prostheses by means of four

zygomatic implants (117). The lack of significant changes to the zygomatics and other regions in the current study suggests that many of the differences observed in the preceding analysis may have resulted as an artefact from the Procrustes superimposition likely on account of the Pinocchio Effect. The Pinocchio Effect refers to the even distribution of variation across all landmarks which are superimposed using a generalised least-squares procedure (118,119). This results in an “averaging out” of landmark variation and may lead to erroneous conclusions about measurement error and morphology (118,119). However, the extremely large number of edentulous crania in the current sample and the sample size itself may also have influenced outcomes. Low masticatory strains along structures located furthest from the chewing apparatus, including the frontal bone and periorbital regions, have been demonstrated by a number of authors (85,120,121). This would suggest that mastication has little effect on these regions and would explain why no alteration to their structure was induced by tooth loss. Conversely, differences in cortical bone thicknesses between the skulls of dentate and edentulous individuals have been demonstrated by Dechow and associates (85), with edentulous individuals showing statistically thinner cortical bone even in the frontal and zygomatic bones. This may suggest that despite the lack of gross morphological changes in structures far removed from the masticatory complex, the removal of forces does result in complex histological adaptations.

3.4.3 Individual Curve Observations

Regarding the specific modifications of the alveolus, both the labial/buccal and lingual/palatal surface of alveolar bone were seen to resorb, but bony tissue of the buccal plate appears to resorb to a greater extent. Pietrokofski and Massler (92) analysed the effects of unilateral tooth extraction on the degree of alveolar bone loss and also tested the degree of symmetry in edentulous dental arches. Similar to our results, these authors reported that the labial/buccal surface underwent resorption at a greater rate than the lingual/palatal surface, resulting in a posterior shift of the anterior-most point of the maxillary alveolar ridge with an associated decrease in total palatal arch length. These findings are supported by Tallgren (122). Pietrokofski and Massler (92) commented that the total amount of tissue resorption was significantly greater in the molar region as

compared to the premolar and incisor region. They additionally found that the absolute amount of tissue lost in the molar region exceeded that of the other regions of the palatal arch.

The severe degree of maxillary bone resorption seen in this study results in a dramatic decrease in alveolar prognathism as well as a decrease in upper facial height. Numerous authors have noted a marked shortening of the maxilla in the event of extensive tooth loss (75,79,80,89,123). The degree to which the bone is resorbed varies as partially edentulous individuals experience less bone loss than those that are completely edentulous (78). Additionally, individuals with better fitting dentures experience less resorption (124), while females lose bony tissue faster and to a larger degree than do males (125).

The decreases in facial height and prognathism seen in this sample can be extrapolated to samples of other populations as there is no fundamental reason to assume the biomechanical processes involved in alveolar resorption will be different. The degree of alveolar resorption in response to tooth loss may vary, however, as nutrition, age (126,127), population (128) and SxD (129) affect bone turnover rates. As forensic anthropologists rely on various cranial measurements for the estimation of sex (1,5,20) and ancestry (51,130), a decrease in upper facial height will ultimately affect the accuracy of discriminant functions that make use of these measurements. Prognathism is a characteristic ascribed to black crania (43,47,131), and thus, reduced prognathism due to tooth loss may complicate ancestry estimation. This applies especially when assessments are performed by inexperienced observers.

The marked alveolar resorption of both the labial/buccal and lingual/palatal surface of the maxilla leads to an increase in the hyperbolic form of the palate. This is important as the shape of the palate may be qualitatively assessed in the estimation of ancestry (8,132). Furthermore, in a review of the 17 most commonly used traits to assign sex, palate shape ranked 13th with sexing accuracies of up to 88.8% being reported (36). As male palates are generally deeper and narrower, the increased hyperbolic nature of the palate with tooth loss would alter the appearance of male palates such that they take on a more feminine configuration. Additionally, as palate shape in black individuals is

generally more hyperbolic, the increase hyperbolic nature of the palate of edentulous white individuals may also lead to an incorrect ancestry assessment.

Finally, this study demonstrated that a decrease in maxillary prognathism leads to a reduction in the length of the bony bar between the canine jugum and the intersection of the zygomatic and maxillary bones at the orbital rim. Pessa et al. (133) support this finding as they noted a similar change in individuals between the ages of 53 and 76. They found that the elderly and infants display a similar ratio of maxillary height to orbit height. This ratio was, however, found to be greater in young individuals. The reduced ratio in the elderly was attributed to a downward expansion of the orbital shelf with an associated upward migration of the nasal aperture. Pessa et al. (133) did not specify whether the elderly individuals used in their investigation were edentulous or not, but lack of dentition would also lead to a reduced ratio and would be another point of correspondence between elderly and infant craniofacial skeletal proportions.

3.5 CONCLUSIONS

This analysis not only elucidates the bony changes that result from maxillary tooth loss, it also illustrates the importance of considering the effects of tooth loss during the compilation of a biological profile as various structural changes may result in the misclassification of skeletal remains. As demonstrated here, care should be taken when measuring or assessing factors such as upper facial height, prognathism and palatal shape (hyperbolism) for biological profiles, especially in cases where individuals exhibit severe tooth loss. During the global analyses, tooth loss related changes were demonstrated in the size of the orbits, the degree of projection of the nasal aperture, bizygomatic breadth and the shape and projection of the maxilla. When assessed in isolation, however, only maxillary changes proved significant. Specifically, these changes include severe alveolar bone resorption that resulted in a decrease in both alveolar prognathism and upper facial height. Resorption along both labial/buccal and lingual/palatal surfaces was shown to result in an increased palatal hyperbolism. However, it is possible that the extremely skewed ratio of edentulous to dentate individuals could have influenced results obtained. Alternatively, partial Procrustes

superimposition may have failed to maintain biological relationships between regions and the sliding semilandmarks used to represent curve shape may have been inadequate. Further research using more balanced samples is required to clarify this. Despite this, the current investigation demonstrates the advantage of using GMM techniques to visualise tooth loss related changes to the face and maxilla. It also provides the groundwork for future research aimed at improving current standards and deriving new standards for the assessment of partially or fully edentulous cranial material.

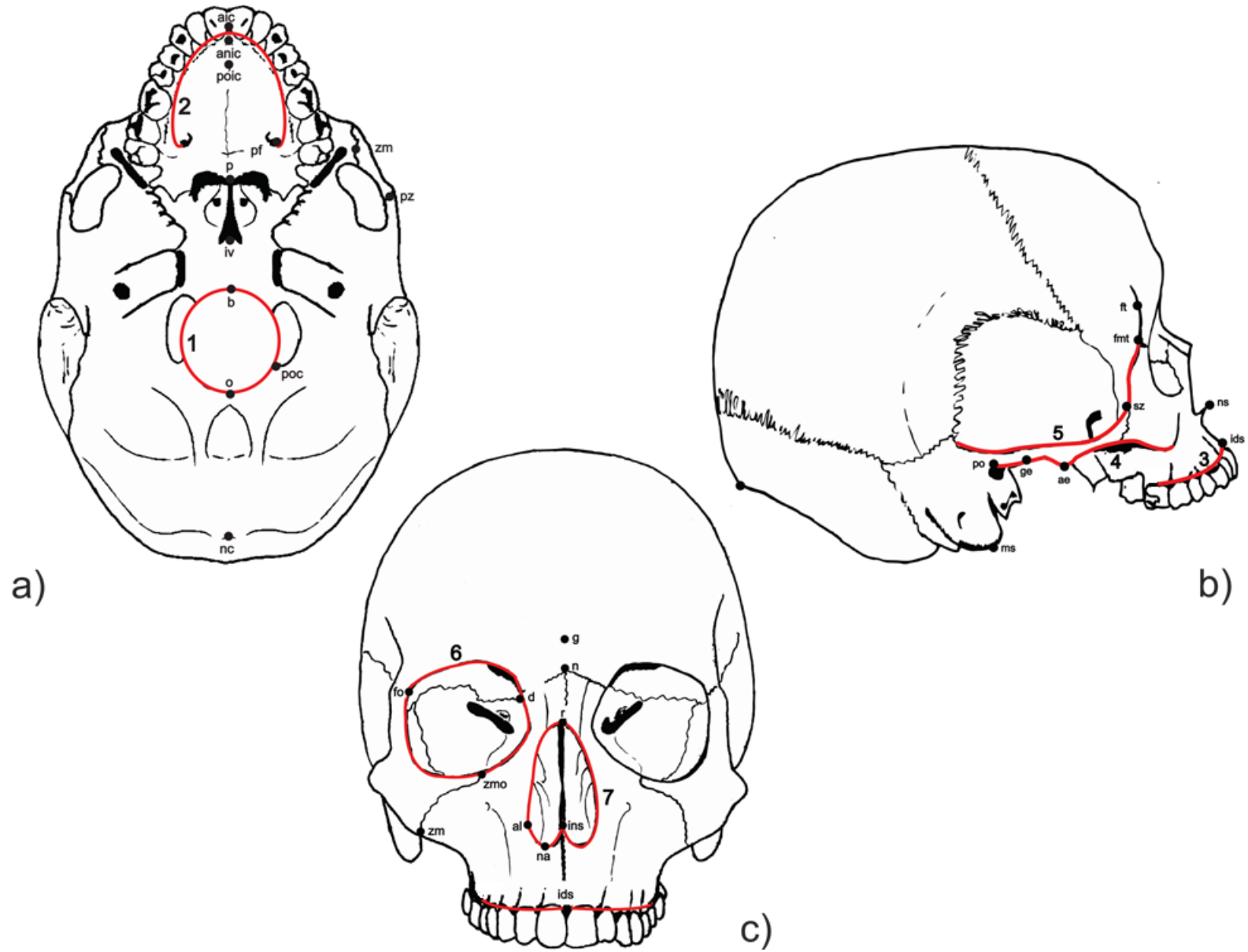


Figure 3.1 Illustration of the landmarks and curves used in this study: a) Inferior view; b) Lateral view; c) Anterior view. Abbreviation and number index correspond to curve numbers in Table 3.2.

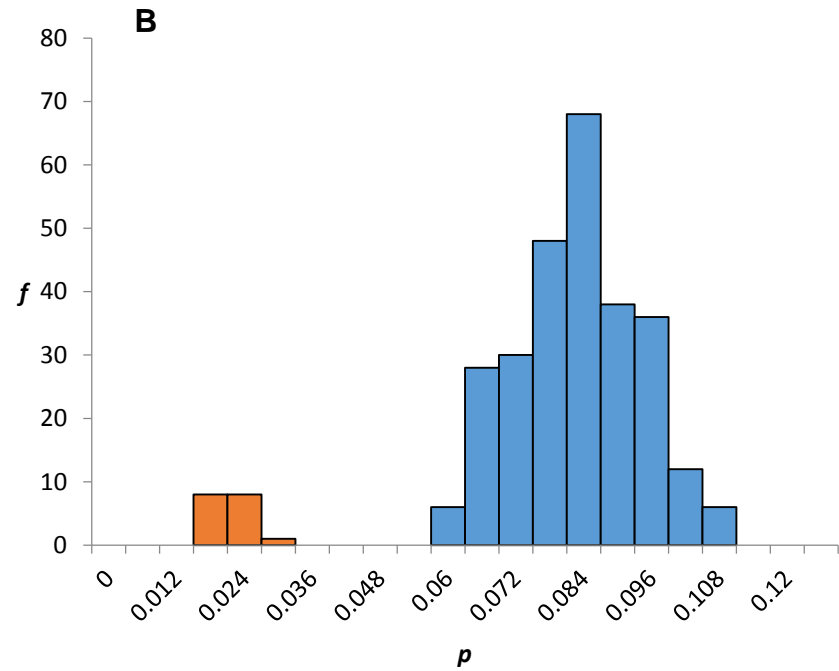
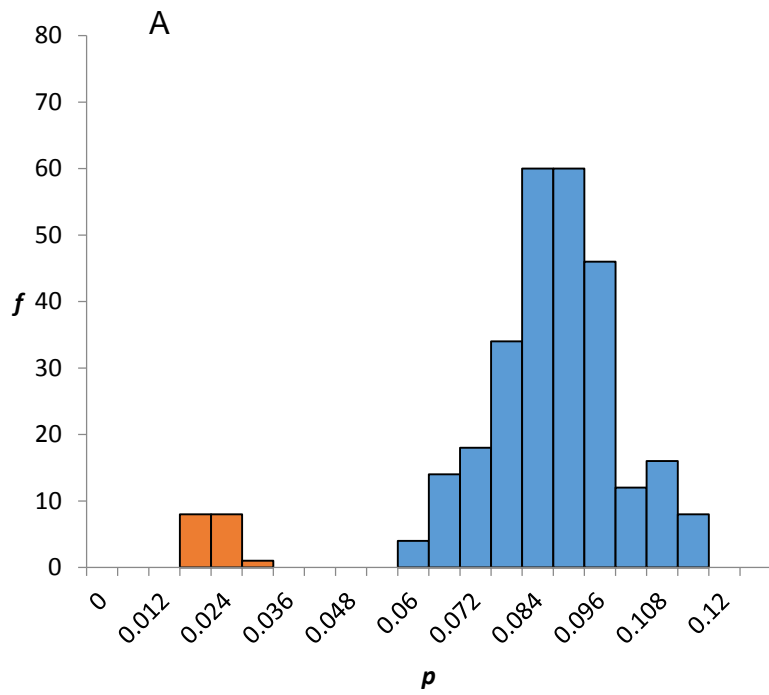


Figure 3.2 Histograms of the results of the tests measuring intra-observer repeatability. A) Frequency of the Procrustes distances between all possible paired observations in the sample (blue) and between the repeated observations (red). B) Relative effect of measurement error after accounting for the influence of allometry in the sample (blue) and between repeated observations (red).

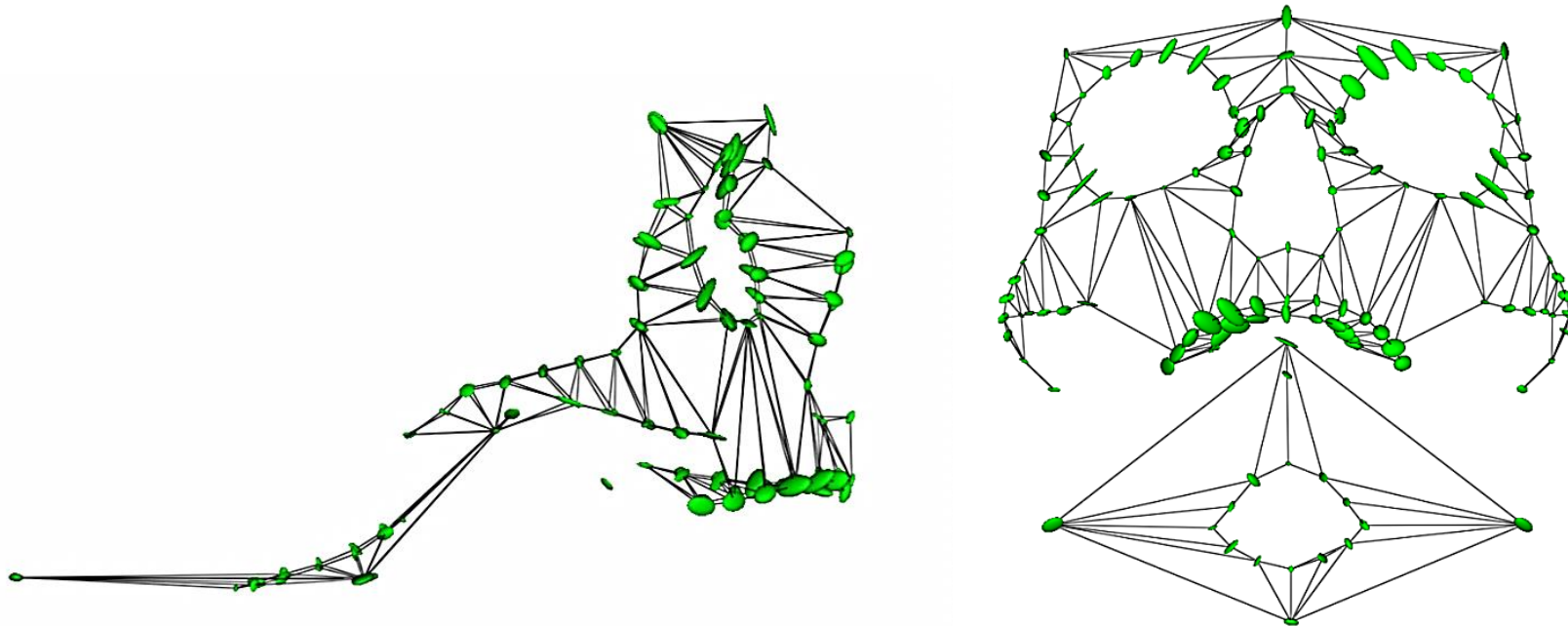


Figure 3.3 Lateral (left) and anterior (right) wireframe illustrations of observer error. Ellipses depict the degree of error produced at each landmark. Larger ellipse = greater amount of measurement error. More elliptically shaped ellipses = higher degree of directional error.

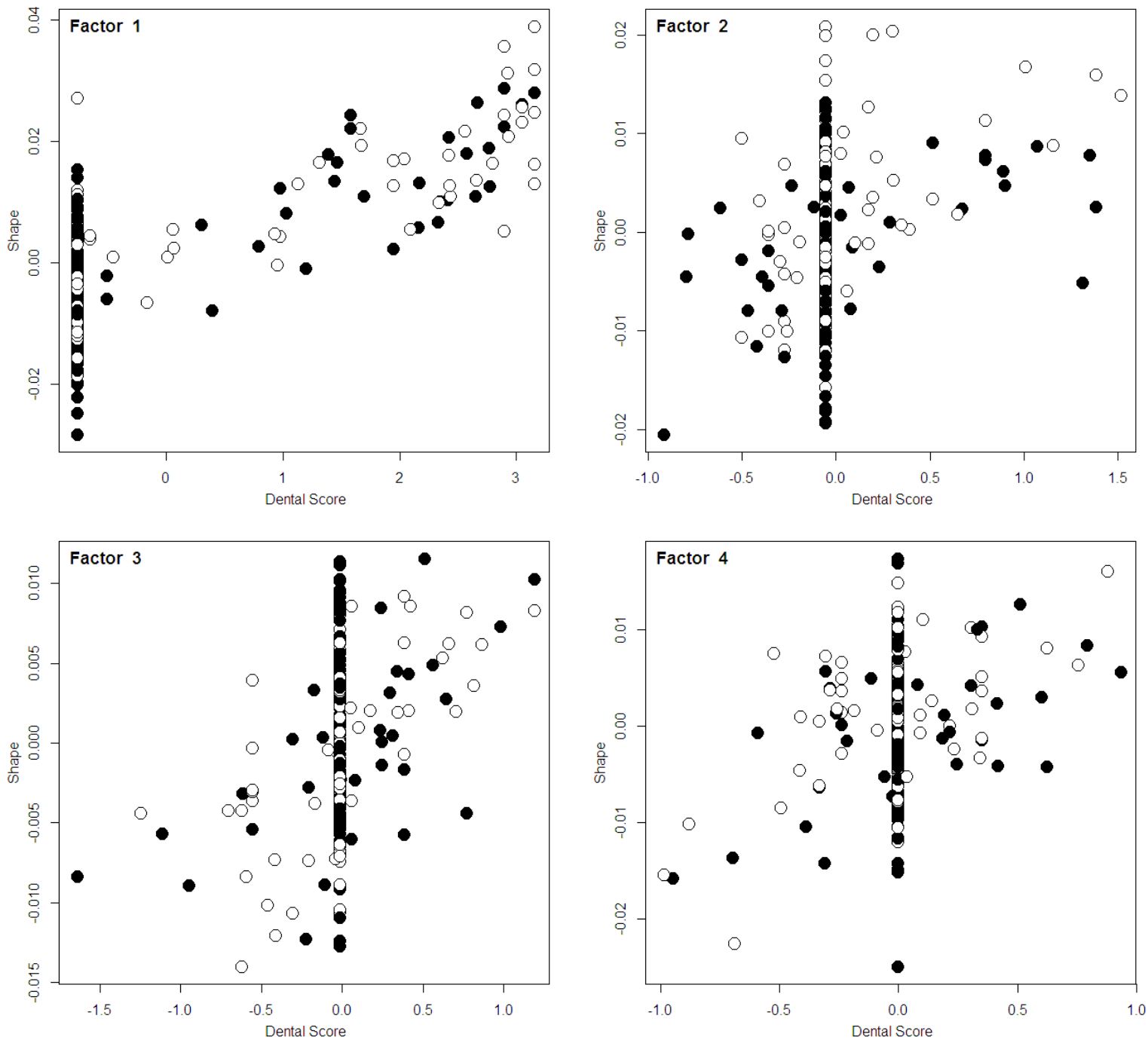


Figure 3.4 Results of the 2-Block partial least squares (PLS) analyses showing the first four vectors. Closed circles indicate female specimens, Open circles represent male specimens. The specimens that are all clustering along a straight line represent those that are completely edentulous.

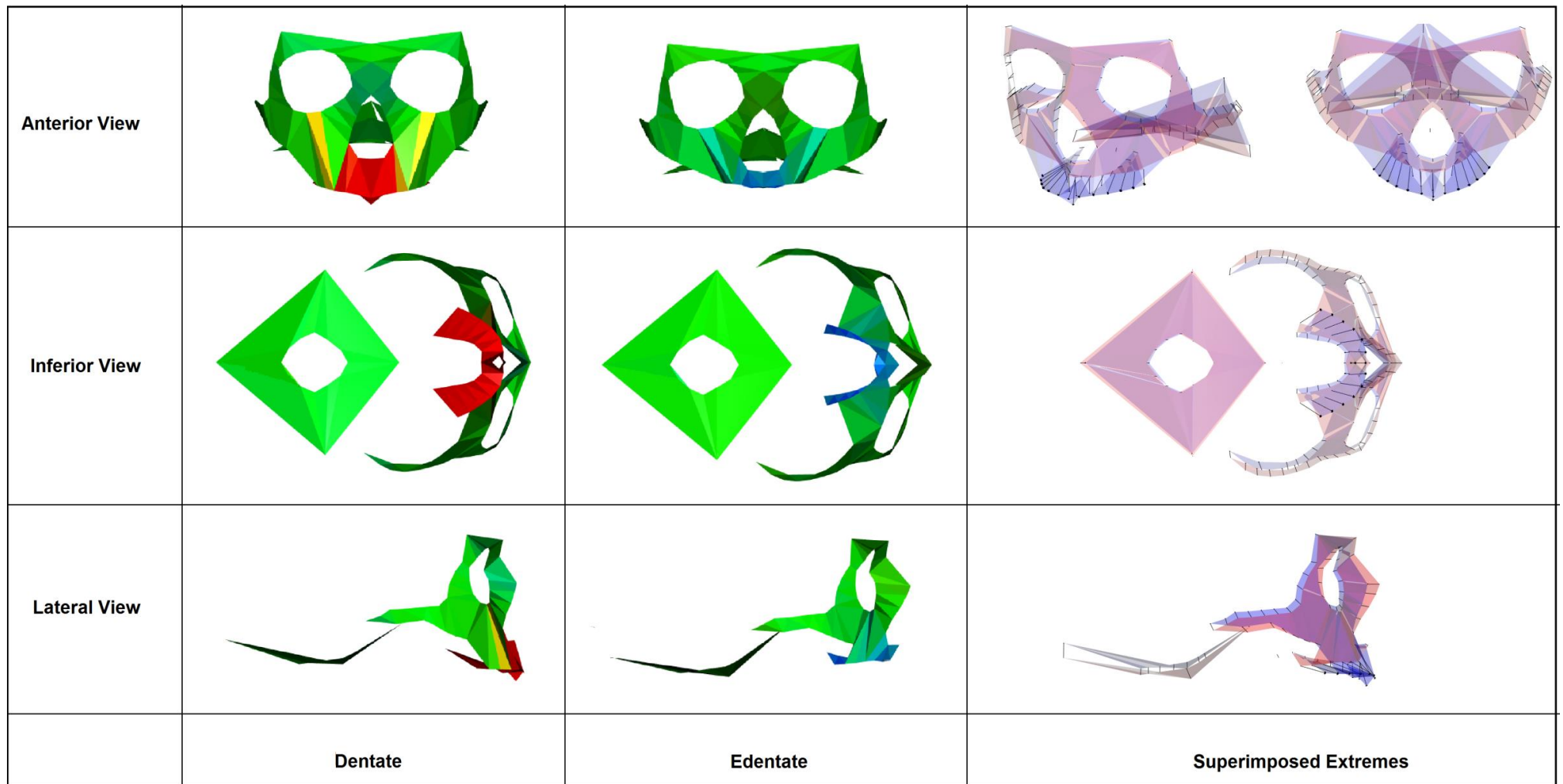


Figure 3.5 Anterior, inferior and lateral side by side representations (left) and vector diagrams (right) illustrating the changes in skull morphology associated with dental loss. Green areas are equivalent; Red indicates a large increase; and Blue shows a large decrease. The gradation of colours between red and blue (from yellow to turquoise) indicate morphologies that lie between the two extremes. In the vector diagrams on the right, arrows indicate the change in a structure of a completely edentulous individual (red), to a completely dentate individual (blue). The size of the arrows in the figure represents the relative magnitude of the structural change.

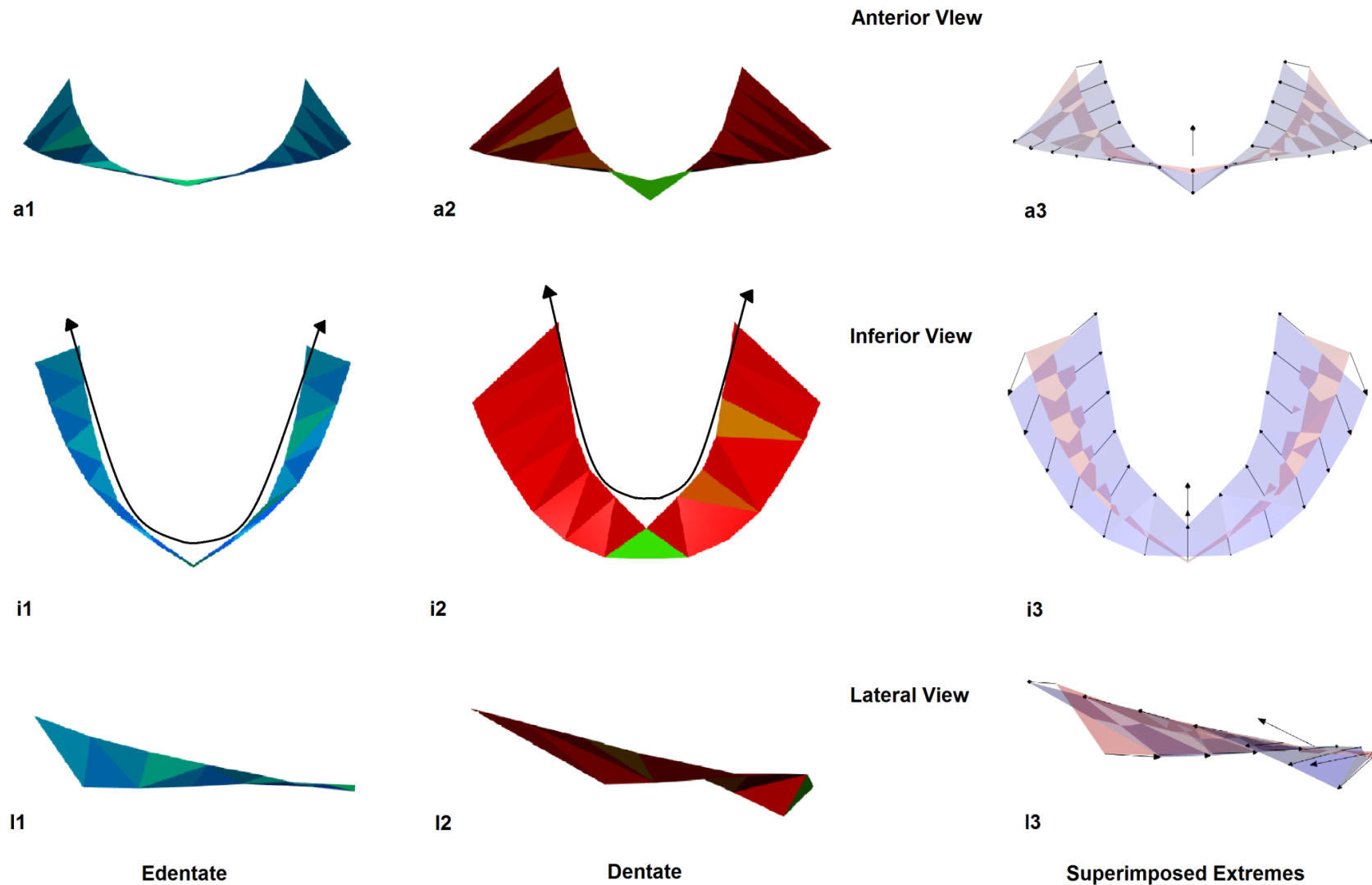


Figure 3.6 Anterior, inferior and lateral coloured representations (left) and vector diagrams (right) of the structural changes in the morphology of the maxilla associated with tooth loss. In the side by side illustrations, green areas are equivalent, red indicates a large increase, and blue shows a large decrease. The gradation of colours between red and blue (from yellow to turquoise) indicate morphologies that lie between the two extremes. In the vector diagrams on the right, arrows indicate the change in a structure from edentulous (red), to dentate, (blue). The size of the arrows in the figure represents the relative amount of structural change.

Table 3.1 Age distribution of sample by decade and dental state, Std. Dev =standard deviation (n= 229).

Age interval	Male		Female	
	Total sample	Edentulous individuals	Total sample	Edentulous individuals
18-29	1	1	2	0
30-39	5	1	1	0
40-49	22	10	8	4
50-59	25	16	21	12
60-69	36	26	45	28
70-79	11	9	13	9
80-89	13	12	16	12
90-95	5	4	5	1
Total	118	79	111	66
Overall age interval (years)	28 – 95	28-95	19 – 95	45-95
Mean age (years)	62	68	66	68
Std. Dev (years)	15	13	14	13

Table 3.2: Landmark number, definitions and abbreviations for all fixed landmarks used in this study

Number	Landmark	Abbreviations	Definition
1	Nuchal crest	nc	The most posteriorly projecting point on the superior nuchal crest of the occiput
2	Opisthion	o	The point on the middle of the posterior curve of foramen magnum
3&5	Posterior occipital condyle	poc	Where the posterior margin of the occipital condyle comes into contact with foramen magnum
4	Basion	ba	The point in the middle of the anterior aspect of foramen magnum
6	Inferior vomer	iv	Point of contact between the sphenoid and vomer bones
7	Palatine	p	Point on the interpalatine suture, laying most posteriorly
8	Posterior incisive canal	poic	Posterior most point on the incisive canal
9	Anterior incisive canal	anic	Anterior most point on the incisive canal
10&11	Palatine foramen	pf	Most anterolateral point on the palatine foramen
12	Intermaxillary	aic	Point between the central incisors posteriorly
13&20	Mastoidale	ms	Point situated on the greatest projection of the mastoid
14&21	Porion	po	Point midway on the superior margin of the external acoustic meatus
15&22	Glenoidale	ge	Point directly above the glenoid fossa on the zygoma
16&23	Articular eminence	ae	The most inferolateral point on the articular eminence
17&24	Posterior zygotemporale	pz	Point at the junction between the zygomatic and temporal bones, inferiorly
18&25	Zygomaxillare	zm	Point at the junction between the zygomatic and maxillary bones, inferiorly

Table 3.2 (continued) Landmark number, definitions and abbreviations for all fixed landmarks used in this study.

Number	Landmark	Abbreviations	Definition
19&26	Superior zygotemporale	sz	Point at the junction between the zygomatic and temporal bones superiorly
27	Glabella	g	The greatest anterior projection midsagittal aspect of the frontal bone at the level of the supraorbital ridges
28	Nasion	n	Point between the internasal suture and nasofrontal suture
29	Rhinion	r	The most inferior point on the internasal suture.
30	Inferior nasal spine	ins	Tip of the nasal spine on the intermaxillary suture
31	Alveolare	ids	Point between the central incisors anteriorly
32&37	Frontomalare temporale	fmt	Point at the junction of the frontal and zygomatic bones posteriorly
33&38	Frontozygomatic orbitale	fo	Point where the frontal and zygomatic bones meet anteriorly on the orbital margin
34&39	Frontotemporale	ft	Points on the frontal bone across which the bone is narrowest
35&40	Dacryon	d	Point where the sutures of the frontal, maxillary and lachrymal bones meet
36&41	Zygomaxillare orbitale	zmo	Point of junction between the zygomatic and maxillary bones on the orbital margin
42&44	Nariale	na	The most inferior extent of the nasal aperture adjacent to the nasal spine
43&45	Alare	al	The widest point on the lateral margin of the nasal aperture

Table 3.3 Subset breakdown and description of curves and semilandmarks. Curve numbers correspond to those in Figure. 3.1.

Subset	Curves	SSL*
Basicranium	1. Foramen magnum	16
Alveolus	2. Inner palate	12
	3. Outer palate	14
Zygoma	4. Inferior zygoma	11
	5. Superior zygoma	11
Orbit Aperture	6. Orbit	18
Nasal Aperture	7. Nasal	16

*Number of sliding semilandmarks

CHAPTER FOUR

Morphological variation in white South African crania: sexual dimorphism and allometry

4.1 INTRODUCTION

The phenotypic expression of sex has been studied in a number of species, from plants to people, and across numerous disciplines. Sexual dimorphism (SxD) in human populations in particular has been investigated for decades by evolutionary biologists, archaeologists and forensic anthropologists alike. Understanding and documenting SxD, its expression and causes, is imperative to understanding contemporary and archaeological human population variation, and when compiling a biological profile in forensic anthropology (6,8).

The estimation of sex is traditionally achieved by either morphological (qualitative) or metric (quantitative) means. Morphological analyses have been employed since the 1700's. These involve the visual assessment or scoring of differences between various bony regions, with a focus on elements of the skull and pelvis (6,18,42). This method is advantageous in that it is simple to use, time efficient, allows the description of characteristics that are not easily measured, and does not require expensive equipment. It is, therefore, often applied in the field as a preliminary assessment. Major drawbacks of morphological analyses are that they are highly subjective and require a skilled, experienced observer to estimate sex accurately and with high precision. Furthermore, these methods are seldom subjected to rigorous statistical testing and often difficult to reproduce due to subjectivity and ill-defined methodology (6,18).

Skeletal measurements from various bones are collected and sex differences related to size are explored. Measurements that are sexually dimorphic are subsequently used to generate discriminant functions for the estimation of sex for unknown skeletal remains (6). When compared to the morphological method, the metric method is less subjective, easier to reproduce if landmarks are well-defined, does not require a highly experienced observer and can be subjected to a battery of multivariate statistical analyses. The accurate collection of measurements is, however, time consuming and requires the use of equipment and software that can be costly. Furthermore, problems arise when there are few anatomical landmarks across the area of interest or remains are damaged or fragmentary (1,5,6,63). Perhaps the most important caveat regarding standard metric methods is that they collapse three-dimensional (3-D) forms into linear, 2-D measurements and therefore do not maintain the geometric integrity of the form being investigated (55,56).

When the sexes are compared, the largest and most obvious difference between them is their size, as is true for most multivariate datasets (29). Size differences between males and females are evident even to the untrained eye. Byers (9) reports that females are generally about 92% the size of their male counterparts. This is a major limiting factor of both the metric and morphological sexing methods as the majority of the differences between the sexes explained by these methods are due to size. Geometric morphometric methods (GMM) are a relatively new suite of techniques for analysing morphological characteristics by metric means. It eliminates some of the problems experienced by traditional techniques in quantifying shape variables (6,55,56). This method is based upon a technique known as generalised Procrustes superimposition (GPA), which is usually applied to 2-D or Cartesian coordinates representing homologous landmarks that can be acquired from photographs using a digitiser or surface scan, or even from CT scans. GPA involves the use of *least squares parameters* to superimpose acquired coordinates onto one another by means of translation, scaling and rotation (56,59). This not only allows morphological traits to be investigated quantitatively whilst maintaining geometric integrity, it also allows the analysis of shape following the mitigation of size.

The efficacy of GMM has been demonstrated by a number of studies (3,59,63–65,69,134). Green and Curnoe (64) used GMM to demonstrate significant differences in the cranial shape of Southeast Asian males and females, even when differences were undetectable using traditional techniques. Similarly, Franklin et al. (2) found differences among the crania of indigenous South African populations that earlier studies found to be homogenous. Finally, Pretorius and colleagues (69) demonstrated shape differences in the orbits of black South Africans that proved to be highly dimorphic despite being undetected using traditional craniometrics.

The effect that size has on shape, or allometry, has been the focus of an increasing number of recent studies, including work in evolutionary biology (25,29,135–137). Understanding allometry is imperative to comprehending the morphological variation associated with SxD as size and shape variation are intimately intertwined. This is especially true when using GMM where size is standardised across all specimens, but the resultant effect of size on shape remains. Rosas and Bastir (30) used GMM to demonstrate the relationship between SxD and allometry on a European sample. After mitigating size and its effects on shape, the authors found that males

have larger nasopharyngeal spaces, piriform apertures and pharynxes as well as more pronounced muscles markings. Females have increased prognathism of both the maxilla and mandible. They postulate that the larger upper respiratory structures in males may facilitate increased oxygen intake in order to affect greater metabolic demands. They also warn that allometry may complicate the estimation of SxD (30). Gonzalez and colleagues (138) used GMM to analyse allometry in the face, vault and basicranium of 283 adults and subadults of various populations from South America. They demonstrated that while allometry significantly affects the face and vault, its effects on the basicranium were insignificant. They also found that an increase in size leads to an increase in the height of the face together with an increased length of the vault for both evolutionary and ontogenetic allometry. They concluded that the pattern of morphological shape change associated with size is the same regardless of whether the change in size is brought about by ontogenetic changes within populations or by mean size changes between populations (138). Most recently, Mitteroecker and associates (137) analysed the relationship between masculinity and SxD by photographing Viennese females and males and having female participants rate the male photographs on a scale from most feminine to most masculine. They also implemented 2-D GMM to analyse SxD based on landmarks and semilandmarks on each of the photographs. Both the allometric and non-allometric components of SxD were analysed. Faces rated as more masculine were characterised by wider dimensions and noses, a greater interorbital distance, thinner lips, and a broader lower jaw. Males had thicker eyebrows that were positioned more inferiorly, thinner lips, smaller eyes and more massive and squared lower jaws when compared to female configurations. The allometric component was very similar to the user rating of masculinity, demonstrating that an increase in the size and angular nature of the lower jaw and a thinning of the lips is associated with increased size. The non-allometric component, on the other hand, corresponded to the SxD analysis demonstrating that masculinity and SxD do not always approximate one another to the degree many researchers presume they do (137).

Building on these previous studies, aims of the current investigation were to identify sexually dimorphic regions within the crania of white South Africans using GMM, both globally and in each of the subsets outlined in Chapter 3. Next, both the

allometric (CA) and non-allometric (NASXD) components of SxD were analysed individually to elucidate the role of each of these factors in the morphological variation of white South African crania. This too was conducted both globally and on each of the cranial subsets.

4.2 MATERIALS AND METHODS

4.2.1 Materials

The crania of 227 specimens were selected from the Raymond A. Dart Collection of Human Skeletons (Dart Collection), by filtering out white individuals, aged 18 to 95 from the Collection's catalogue. The sample consisted of 114 white males and white 113 females (Table 4.1). Most of the white remains in the dataset are from donated individuals who are mainly of Dutch, German, French, British, and Portuguese descent (13,67). Refer to section 3.2.1 for a more detailed description of the history of white South Africans.

The ages of the sampled individuals ranged between 19 and 95 years (mean = 64 ± 14 years) to ensure that the crania had an adult configuration and also to include a broad spectrum of adult cranial morphologies. All individuals were born in the 20th century (1923 to 1995) to represent the contemporary population and avoid a secular trend. Regardless, a secular trend is generally associated with size and this factor is addressed directly in the current study. Crania displaying varying dental states (Table 3.1), including completely edentulous specimens, were included due to the relative paucity of dentate white crania within the collection and because the effect of edentulism could be readily mitigated (refer to Chapter 3.2.4 for a detailed description). Crania exhibiting any other damage, pathology, or missing landmarks were excluded as normal variation was the focus of this investigation and because GMM analyses require a fixed number of landmarks to be digitised across all specimens. The neurocranium was excluded from this investigation as the skull vault had been removed from most of the specimens during the process of laboratory dissections. Rearticulation may have introduced unwanted error.

4.2.2 Data Collection Procedure

Each cranium was secured in a fixed, inverted anterior facing, position to ensure that all landmarks and curves could be digitised without reorienting the cranium. Fixed landmarks on each cranium were digitised using a Microscribe® 3-DX digitiser with a cited accuracy of 0.25mm (Immersion Corp). Following this, curve data were captured by tracing the surface of each curve as a continuous stream of points, known as semilandmarks, registered at 0.5mm intervals between the fixed landmarks. Table 3.2 provides a definition of the landmarks that are illustrated along with the curves captured in Figure 3.1. Landmarks involving the neurocranium were omitted as the skull vault is conventionally removed during dissection and subsequent rearticulation would introduce unwanted error.

4.2.3 Data Resampling and Reworking

The number of points on each curve needed to be standardised as semilandmarks were taken at a fixed distance from one another and not at bony landmarks. The data were imported into the morphological analysis program *Morpheus* (<http://www.morphometrics.org>) and points were resampled such that an equal number of semilandmarks represent homologous curves among the specimens. The number of points for each curve was chosen so that an average spacing of approximately 7mm lay between adjacent semilandmarks (determined from 10 randomly selected crania). This ensured that the inherently “deficient” semilandmarks could be treated as homologous anatomical landmarks (72). See Section 3.2.3 for more details.

4.2.4 Statistical Analyses

4.2.4.1 Preliminary analyses

Before the global analyses could commence, preliminary analyses were run to eliminate unwanted variables such as the effect of tooth loss, clean the data of outliers and prepare subset data. As the study of asymmetry was beyond the scope of this investigation, the symmetric component of the data was obtained using the statistical program *MorphoJ* version 2.0. (www.flywings.org.uk) (139). Outliers were identified in *MorphoJ* as any points that did not cluster with the main dataset in a scatterplot of the first principal component. Regional subsets were extracted and are listed in Table 3.3. Subsets consist of curves defined by semilandmarks located between two fixed

landmarks. The start and end points of each curve, together with the number of semilandmarks employed to define the curve, are also given in Table 3.3.

As specimens with varying dental states were included in this analysis, the effects of tooth loss on cranial morphology needed to be mitigated before SxD could be assessed. To do this, a PLS analysis was run to determine the effects of tooth loss on cranial form and Burnaby's (140) method was then used to mitigate the effect. Burnaby's method mitigates the effect of tooth loss by projecting data points onto a subspace that is perpendicular to the vector of tooth loss (28,140). Next a Pearson's product-moment correlation test was run to determine whether an association existed between tooth loss and size. Residuals from a linear regression were used to account for the effect of tooth loss on centroid size measures.

To test whether the effects of sex on cranial form were greater than those produced by chance, a permutation test was run to randomise sex assignment and mean Procrustes distance between the groups was analysed. The effects of age were investigated by running a permutation test to randomise age and testing whether the sum of the form linear regression residuals is significantly smaller than that obtained by chance. If significant, the effects of age were mitigated using Burnaby's method (140). Finally, the subsets detailed in Table 3.3 were extracted. The statistical analyses detailed below were run on the global data as well as each of these subsets to examine the effects of overall sexual dimorphism (SxD), common allometry (CA) and non-allometric sexual dimorphism (NASXD) on cranial form.

4.2.4.2 Analysis of overall sexual dimorphism

Following the mitigation of the effects of tooth loss and age on cranial form, data representing each of the five subsets (Table 3.3) were extracted from the main dataset and saved as individual text files. The subset data were superimposed using PPS and orthogonally projected to the tangent plane. Principal components analysis (PCAs) were then run as a dimension reducing technique, and to determine where the greatest variance within the sample lay. To calculate the number of principal components (PCs) that best describe variation without over-fitting, a logistic regression analysis was run using the generalised linear model function in *R* (R Core Team, 2015). Results were plotted and visually assessed to determine where accuracies

plateau (Figure 4.4). The chosen number of PCs were used in further logistic regression analyses that elucidated the contribution of each PC.

Finally, vector diagrams, wireframes and surface scan deformation images were created to illustrate the results of the logistic regressions. Vector diagrams draw a vector of the relative magnitude and direction of variation of a landmark from the reference (e.g. female) to the target form (e.g. male) allowing for the interpretation of the variation at each landmark. Wireframes were created using the *rgl* package (<https://r-forge.r-project.org/projects/rgl/>) in *R*. These represent a superimposition of the mean configuration of the two groups under investigation (e.g. average male configuration superimposed onto the average female configuration). Wireframe images are more intuitive and represent overall variation in shape better than the vector diagrams, but determining the extent of the variation they depict is more difficult. Vector diagram and wireframe images were also used to visualise variation in each of the subsets.

Surface scan deformations were only created for visualisation of the global results (these illustrations make use of the *rgl* package as well as customised algorithms in *R* to display differences between a mean shape and its extreme). Images were created by selecting a cranium that was determined to lie close to the mean configuration between males and females and taking a scan of it. The position of the fixed landmarks used in this investigation were located on the scan and all the data points that make up the current dataset were projected onto the scan. The difference between the mean and the extreme shape of the dichotomous variable under investigation was mathematically determined (i.e. the mean male and female shapes were determined as well as the extreme male and female configurations). Using the mean shapes as a reference, the original scan was warped to display the change in shape from the mean to the extreme (target) and the changes in surface areas were coloured in spectra of light to dark blue when the area in question diminished in size, and in spectra of light to dark red when the area in question enlarged. White areas represent areas of the cranium where no landmarks were placed or very little change was observed.

4.2.4.3 Analysis of allometry

Allometry (CA) was calculated as the common (shared) allometry, derived from mean centred data, where the average of both the males and females were subtracted from their respective configurations and subjected to linear regression. Prior to visualising the effects of CA, its significance was tested following the same procedure as for age. If the effects of allometry were found to be significant ($p < 0.05$), the effects on cranial form were plotted using vector diagrams and surface scan deformations.

4.2.4.4 Analysis of non-allometric sexual dimorphism

Finally, any remaining size effect associated with CA was removed by using Burnaby's method (140). The significance of the remaining non-allometric (size independent) SxD was tested using a permutation test (10,000 iterations) to randomise sex and the sum of the form linear regression residuals were measured to determine whether they were significantly smaller than that obtained by chance. If significant, PCA was run as a data reduction tool to allow for discrimination using a handful of PCs. The results of the discriminant analyses were plotted to determine the number of PCs that best describe the differences without over-fitting. This number of PCs was used in a logistic regression to illustrate the effect of NASXD on cranial form. As was done to illustrate SxD and CA, the effects of NASXD were plotted using vector diagrams and surface scan deformations.

4.3 RESULTS

4.3.1 Preliminary Analyses

The symmetric component of the data was extracted and the effects of tooth loss were abated. Permutation tests were run to determine whether the effects associated with tooth loss were significantly associated with cranial size. The association was found to be significant ($p = 0.0278$) and, therefore, the effects were corrected by regressing residuals on the mean. Although not quite significant ($p = 0.0770$), the possible effect of age on cranial form was mitigated using Burnaby's method. Sex proved to be highly significant ($p < 0.0001$).

4.3.2 Global Analyses

4.3.2.1 Overall sexual dimorphism

Following the preliminary analyses, data were subjected to PCA to reduce dimensionality and produce PCs that were used as dependent variables in the subsequent logistic regressions. Figure 4.1 shows the results of the PCA. From the figure, it is clear that PC1 accounted for 15% of the variance in the sample, whilst PC2, PC3, PC4 each contributed 12%, 8% and 6% of the variance, respectively. The PC score of PC1 was plotted against PC2 (Figure 4.1 A), PC2 was plotted against PC3 (Figure 4.1 B) and PC3 against PC4 (Figure 4.1 C). In all three plots, the scatter of the points appears random with no clear pattern or separation of the sexes. Finally, the histogram shows the relative contribution of each PC to overall variation (Figure 4.1D).

Logistic regression was used to model the PCs and to determine the optimal number needed to discriminate sex with maximum accuracy but without overfitting the data. Figure 4.2 shows a plot of the relative contribution of the PCs to the cumulative accuracy of sex discrimination. The figure demonstrates how accuracy increases up to the 25th PC after which there is sudden drop between the 26th and 28th PCs before the accuracy levels off. This indicates that 25 PCs are the optimal number to use to describe SxD within the dataset without overfitting it. Using 25 PCs results in a sex discrimination accuracy of 90.55%.

In terms of the global differences between males and females (Figure 4.3), it is clear that the male configuration has a relatively greater rugosity than that of the female. The projection of the nose and inferior nasal spine, the zygomatics and lateral extent of frontotemporale display the greatest deviations in rugosity between the sexes, with the male nose and nasal spine projecting more anteriorly than the female's and assuming a relatively broader configuration. Male zygomatics also appear to have greater lateral projection relative to the more gracile, less projecting female zygomatics. The anterior maxilla in males is also relatively larger than in females and also displays a greater anterior projection, although to a lesser extent than observed in the overall nasal and zygomatic shapes. The inferolateral projection of the mastoids and posterior projection of the external occipital protuberance in males are both more pronounced than those of females, but markedly less than what is seen in the nose and zygomatics (as indicated by the comparatively pale shade of red in Figure 4.3).

Female orbits, however, appear to be relatively larger than that of males due to a more medial positioning of dacryon (d), a more inferior positioning of zygomaxillare orbitale (zmo), and a more lateral positioning of frontomalare orbitale (fo). This is

indicated by the deep red colour over these landmarks and, to a smaller degree, the corresponding orbital margins. The posterior aspects of the female alveolar margins and palate are also relatively larger than those of males, although not to degree seen in the orbits. The pale red colour of the margins of the foramen magnum and mandibular fossae indicate that the foramen and the area associated with the landmark glenoidale (ge) are relatively larger in females than in males. This is due to the overall smaller size of the female viscerocranium. It is imperative to reiterate, however, that no landmarks were placed along the calotte, the squama of the temporal bones, regions of the basicranium other than the foramen magnum and glenoidale, or anywhere on the frontal bones barring glabella and frontotemporale. For this reason, no inferences can be drawn about these regions, despite how they may appear in Figure 4.3.

4.3.2.2 Common allometry

The common allometric component was calculated using least squares regression on mean-centred data, where the male and female means were subtracted from the respective data, and the grand mean added. The significance of the influence of size on shape was found to be significant ($p < 0.0001$). PCA and logistic regression analyses were run on this dataset to determine the effects of allometry on cranial form. Figure 4.4 shows the allometric differences in morphology between small and large individuals. Nasal projection and the size of the maxilla appear relatively bigger in larger individuals and the glabellar region and zygomatics appear relatively larger in smaller individuals. Although differences exist between large and small zygomatics, the magnitude of the differences (as indicated by the saturation of the colour) is greatly reduced when compared to the difference between males and females (Figure 4.3). Projection of the nasal bones also appears greater in larger individuals and the saturation of the colour in Figure 4.3 shows that nasal projection has a large allometric component. On the contrary, projection of the inferior nasal spine and the lateral projection of the nasal aperture appear mostly unshaded and, hence, largely unaffected by allometry. The projection of glabella, the mastoid processes and the external occipital protuberance, however, appear to have a large allometric component as indicated by the deeper saturation of colour over these regions. From Figure 4.4, it is apparent that smaller individuals have relatively larger mastoid processes and a more projecting external occipital protuberance. A larger degree of glabellar projection

was also demonstrated in smaller individuals when compared with their larger counterparts. The posterior third of the palate in smaller individuals also appears relatively bigger than that in larger individuals while the opposite is true about the anterior palatal portions. Lastly, the orbits of smaller individuals seem relatively bigger than those of larger individuals. This is indicated by the red shading along the curves of the orbit in the renderings of smaller individuals (Figure 4.4).

4.3.2.3 Non-allometric sexual dimorphism

Before further analyses were run, the effects of common allometry were mitigated and size was adjusted accordingly. The remaining size-independent shape differences between the sexes proved significant ($p = 0.0381$). Further logistic regressions were run (accuracy of discrimination: 85%) so that the effects of the remaining NASXD could be visualised. The resulting effects seen during this analysis were very similar to those seen during the analysis of SxD before CA was accounted for. In order to visualise the similarities, Figures 4.5 and 4.6 show a comparison between the results of the analyses of SxD and NASXD for each sex. The figures represent morphological variations between the mean shape to the extreme male and extreme female shape, as predicted by the logistic regression on PCs. Although their effects are very similar, there is a much greater saturation of colour in the images of NASXD, illustrating that the relative differences between the sexes have been amplified. This is apparent in the zygomatic process of the maxilla and the periorbital regions (females in Figure 4.5, males in Figure 4.6). To the contrary, saturation of colour on the nasal bones and around the nasal aperture decreased, relative to what was seen for SxD. This illustrates that the differences in nasal aperture projection between the sexes is largely on account of allometry. As the effect of size was mitigated when producing these images, the saturation indicating nasal differences is also diminished.

4.3.3 Subset Analyses

After analysing the cranium in global analyses, the data were divided into five subsets because all areas under investigation in this study demonstrated significant sex and size-related differences. Moreover, use of subsets allows for nuanced differences to be more easily perceptible as their influences are not over-shadowed by more obvious global differences.

4.3.3.1 Basicranium - Sexual dimorphism

Prior to visualisation, permutation tests were run to test whether SxD influences basicranial shape. The results were significant ($p= 0.0160$). Logistic regression was then run on the optimal number of PCs to elucidate the sex differences in the basicranium and a classification accuracy of 75.77% was achieved. To demonstrate these differences, vector diagrams and wireframe images were created using the results of the logistic regression (Figure 4.7). From the anterior view vector diagrams and wireframe images, it is most apparent that the mastoid process (ms) in males projects more laterally and inferiorly than in females. When viewed laterally, it is apparent that the nuchal crest (nc) in females lies superior to that of males while the relative position of the inferior vomer (iv) in females lies inferior to that of males. This positioning of the female basicranium is once again apparent in the superior view, that also demonstrates how the female foramen magnum is relatively larger. This difference is not due to the difference in position of the structures in question as both the anterior and posterior margins of the foramen magnum are greater in length in females than males.

4.3.3.2 Basicranium - Common allometry

A significant association ($p < 0.0001$) between mean-adjusted basicranial shape and size exists. In order to better visualise the more subtle difference brought about by CA, a twofold magnification was applied to all images generated. In both the superior and lateral views (Figure 4.7), it is apparent that smaller individuals have more inferiorly and laterally positioned mastoids, together with a more anteroinferiorly positioned nuchal crest, contrasting with the results of the SxD analyses. The relatively greater lateral projection of small mastoids (purple) is also seen when viewed from above. Despite the foramen magnum of the larger basicranial specimens appearing bigger posteriorly, they are actually similar in size. This apparent difference stems from the fact that the posterior aspect of the basicranium in larger individuals is relatively more anteriorly flexed about the foramen magnum, causing the nuchal crest and posterior aspect of foramen magnum to lie superior to that of smaller individuals. Hence, CA does not significantly affect the relative size of the foramen magnum but rather the flexure of the basicranium relative to the viscerocranium.

After the effect of size (CA) was accounted for, no further NASXD effect

remained ($p = 0.9986$) and, hence, no further analyses were run on this subset.

4.3.3.3 Maxilla - Sexual dimorphism

Permutation tests were run for the maxillary subset and the association between maxillary shape and sex was deemed significant ($p < 0.0001$). Subsequent logistic regression analyses discriminated between male and female maxillae with 81.94% accuracy. These results were used to visualise the effects of SxD on maxillary morphology. From a superior view (Figure 4.8), it is clear that the palatine foramen (pf) in females lies posterior relative to males and, despite the fact that the labial/buccal curves (from ids to ecm on either side) of male and female maxillae are equivalent, the shape and depth of the palate (aic to pf on either side) varies between the sexes. The male palate (blue) is narrower anteriorly and is also deeper, especially the anterior two-thirds. The incisive foramen (poic to anic) in males also lies more anteriorly. Finally, the anterior view of the maxillae further clarifies that the relative position of the female maxilla is superior to that of the male, except where male palate depth dips below that of the female.

4.3.3.4 Maxilla - Common allometry

After the effects of SxD were mitigated and a permutation test proved that CA is present and that there is an association between size and shape ($p < 0.0001$), vector diagrams and wireframe images were produced with a twofold magnification. This aided in the visualisation of the shape differences associated with CA.

The superior view in Figure 4.8 shows that the palatine foramina (pf) on the posteroinferior surface of the palate of smaller individuals lies posterior to that of larger individuals. The incisive foramen (poic to anic) of smaller individuals also lies more superior. These results directly contrast with what was observed for these foramina during the analysis of SxD. It is also evident that the alveolar process of the maxilla of smaller individuals is relatively thinner throughout its length in a mediolateral direction, especially anteriorly. This was not seen when SxD was investigated. When viewed from a lateral perspective (Figure 4.8), it becomes apparent that the disparate palate depth previously noted between males and females has been mitigated. It is also evident that the relative position of the maxilla in small individuals lies in the same horizontal plane as large individuals in the CA images, again opposing what was seen

during the investigation of SxD. The anterior view reinforces the result that palate depth and the relative position of the maxillae are equivalent independent of size and hence, not influenced by allometry. After CA was accounted for, no NASXD remained ($p = 0.9927$) and, therefore, no further analyses were conducted on the maxillae.

4.3.3.5 Zygomatics - Sexual dimorphism

As with the previous analyses, permutation test results indicated that a significant portion of the differences between male and female zygomatic bones can be attributed to SxD ($p < 0.001$). Subsequent logistic regression analyses indicate that sex can be discriminated with an accuracy of 77.53%. From the images generated (Figure 4.9), the anterior view suggests that while both frontomolare temporale (fmt) and zygomaxillare (zm) are more laterally positioned in females, the body of the male zygomatic bone projects more laterally. This is further reinforced by the lateral view from which it is apparent that the male zygomatic arch is superoinferiorly wider throughout its length. It also becomes apparent that the portion of the arch represented by the articular eminence (ae) in females is more laterally projecting. The fact that the arch extends further posteriorly in females can also be seen, as indicated by the more posterior placement of porion (po) in females. In the superior view images, the more lateral projection of the anterior portion (fmt and zm) of the female zygomatic is clearly demonstrated together with the extensive lateral flaring of the male zygomatic body.

4.3.3.6 Zygomatics - Common allometry

As permutation tests were significant ($p < 0.0001$), vector diagrams and wireframe images were investigated for morphological variation associated with CA (Figure 4.9). The results depicted in the images produced for CA correspond to those that were produced during the investigation of SxD. The results show that the zygomatics of smaller individuals are relatively bigger than that of larger individuals. This is evident from a lateral view (magnification = 4). Larger zygomatics are also seen to project more laterally. The middle third of the zygomatic arch, however, displays a greater lateral projection when smaller, but not over the region represented by the articular eminence (ae). It is evident, however, that the degree of lateral projection of the curve is much reduced when compared to that seen in the analysis of SxD. Finally, the slight posterior positioning of porion (po) seen in female zygomatic bones in the

analyses of SxD is no longer apparent as porion appears to assume a similar position, irrespective of size.

4.3.3.7 Zygomatics - Non-allometric sexual dimorphism

After the effects of CA were accounted for using Burnaby's method (140), the data were subjected to a permutation test to determine whether any association remained between morphology and NASXD. The results were significant ($p = 0.0020$) and so further PCA and logistic regression analyses were run so that images could be produced to assess the association between zygomatic morphology and NASXD. The logistic regression analyses have a sex discrimination accuracy of 76.65%. Similar to the results obtained in the global analyses, eliminating the effects of allometry on morphology enhanced the related differences between the sexes. In Figure 4.10, SxD and NASXD are shown side by side to highlight how the morphological differences seen previously in Figure 4.9 have been magnified by eliminating the effects of CA.

4.3.3.8 Orbits - Sexual dimorphism

The association between orbit morphology and SxD was determined to be significant ($p < 0.0001$) and wireframe images were used to assess the differences detected. Figure 4.1 has orientation markers added to aid in understanding the rotation of the orbit in each of the views. Additionally, the landmark lachrymal orbitale (lo) has been added to the images to aid in descriptions, even though it was not a landmark captured during digitising.

From these images of SxD, it appears as though some of the more obvious size differences between male and female orbits, seen during the global analyses (Figure 4.3), have been lost or obscured. In some areas such as the superomedial and inferolateral walls, the female orbit does still appear to be relatively larger but the inferomedial wall of the male orbit seems both larger and more prominent. In the male orbit, frontomolare orbitale (fo) (the most lateral point) and dacryon (d) both lie posteriorly relative to females. The most medial point, lachrymal orbitale (lo), lays both more posteriorly and more laterally in males, contributing to the more flexed appearance of the male orbit about the horizontal axis at the level of lachrymal orbitale (lo).

4.3.3.9 Orbits - Allometry

As the association between size and orbit morphology were proven to be significant ($p < 0.0001$), wireframes were again used to explore the variation (Figure 4.11). The anterior view of the allometry images shows that as centroid size increases there appears to be a decrease in the size and degree of projection of the superolateral and inferomedial orbital margin, together with a concomitant increase in the size of the superomedial margin. The degree of flexion between the extremes appears less marked, although frontomale orbitale (fo) does move anteriorly with increased CA. After the effects of size on shape were eliminated, permutation test revealed that no variation associated with NASXD remained ($p = 0.4144$).

4.3.3.10 Nasal aperture - Sexual dimorphism

The effect of sex on nasal aperture shape was shown to be significant ($p < 0.0001$). Subsequent logistic regression analysis shows that discrimination accuracy between male and female nasal apertures is 67.40%. This was used to visualise the effects of SxD on nasal morphology.

In the anterior view images representing SxD (Figure 4.12), the female nasal aperture is seen as being relatively wider than that of males, while the male nose protrudes more. The male nasion (n) also lies superior to that of the female. In a superior view, the protrusion of the male inferior nasal spine (ins) is seen to be greater, while in the lateral view it becomes clear that the spine is also directed more inferiorly in males. Alare (al) in males also lies medial relative to females in this view, reinforcing that the male aperture is relatively narrower. In both inferior and lateral views, alare (al) in males also lies posterior to females. This orientation of alare (al) seems to contribute to the mediolaterally narrow nasal aperture in males, which may in turn contribute to their increased nasal protrusion. As a whole, the female nasal aperture appears to be somewhat less prominent as well as shorter and wider.

4.3.3.11 Nasal aperture - Allometry

Once the influence of allometry was determined, it is apparent that size and SxD have similar effects on nasal aperture shape. The images of allometric effect (Figure 4.12) show that as the aperture gets larger there is a relative decrease in its width, accompanied by an anteroinferior movement of the nasal spine and superoanterior movement of nasion (n). This is very similar to what was seen in the images of SxD. The relative protrusion of the inferior nasal spine (ins), however, is

seen to be more marked in smaller individuals, which contradicts what was found in the analysis of SxD. When CA was accounted for and permutation tests run, the association with NASXD was found to be non-significant ($p = 0.4097$) and, hence, no further analyses were run on the nasal aperture.

4.4 DISCUSSION

Despite the availability of large South African skeletal collections, there is a paucity of research pertaining to white cranial morphology and morphometry. This is because of the high incidence of edentulism in this population that renders large proportions of the collections unusable. In the previous chapter of this thesis (Chapter 3) we delved into the effects of edentulism on cranial morphology and mitigated these effects through GMM. In the current chapter, we took advantage of the large number of white South African crania accessible following the mitigation of tooth loss, and aimed to expand upon the current knowledge of the cranial morphology of white South African males and females. Furthermore, this chapter detailed the aspects of cranial SxD that are a result of the influence of size (allometric) and those that are size-independent (non-allometric). Finally, we elucidated the complex synergistic and antagonistic relationship between SxD and allometry.

4.4.1 General Findings

This study demonstrated significant SxD in crania on a global scale, and in each of the subsets analysed regionally. The nasal bones, inferior nasal spine and zygomatics displayed the greatest amount of SxD. Significant CA effects were also found both globally and regionally. Once the effect of size was removed, however, NASXD differences were only significant in the zygomatics.

Sex differences in human populations have been assessed since pre-Darwinian times. Most scientists regard SxD to be the result of sexual selection. Larger males are more likely to be successful in combat with other males and, hence, stand a better chance of acquiring a mate (33,141). A less accepted hypothesis is propagated by Shine (33), who postulated that SxD may also be due to ecological causes. This hypothesis is often dismissed as inapplicable to humans due to a lack of supporting evidence and because of the difficulties scientists face in testing the theory. However it is a common occurrence in bird species (33). Numerous studies have investigated

the possible causes of robusticity, especially in the cranium, and describe three main reasons for this phenomenon: 1) Genetic drift 2) Climate 3) Functional model: relating to the differential use of masticatory complexes (22,142).

The mechanisms that bring about SxD and its evolution in a range of species, have also been extensively studied (141,143–145). Sexual selection, genetics, nutritional status and environmental factors have all been shown to affect the degree of human as well as nonhuman SxD (38,145–147). Badyaev (141) states that despite high levels of genetic correlation between the sexes, SxD exists in a multitude of species including human and nonhuman primates. He demonstrated how differences in growth rates and duration between the sexes are some of the general causes of SxD. Differential timing, duration and concentration of growth hormone result in variations in the sensitivity of tissues to the hormone and thus a differential growth response. Badyaev (141) also asserts that males and females respond differently to environmental changes with males being more sensitive. This would then explain why a decrease in male robusticity, and hence SxD, is seen in situations of increased nutritional stress (38,141). Holden and Mace (148) showed that the preferential treatment of children of one gender in various human cultures effects SxD as the gender that contributes more to subsistence is generally better nourished. The same authors found a significant correlation between a gender-based division of labour and SxD. Bulygina and colleagues (149) proposed four factors that influence SxD in the cranium in particular, namely the 1) initial differences that manifest *in utero*; 2) differences in the size-shape relationship; 3) fact that males experience a particular type of heterochrony, known as hypermorphosis, later in development; and 4) differences between male and female growth trajectories at puberty.

Sexual dimorphism (SxD) proved to be a significant factor in each of the analyses of this study, including both the global analyses that encompassed the viscerocranium and basicranium, and each of the subset analyses. This is a foreseeable result as SxD has long been demonstrated between human males and females. Ursi et al. (150) reported that the faces of children as young as three correlate with their adult configuration, whilst true SxD starts to manifest by the age of 14 years. Previous studies demonstrated SxD in each of the structures investigated in this study including the nasal aperture (3,63,151), the zygomatics (3,151), the palate (63,152) and the

orbits (62,63,69). These differences are demonstrated to be significant even in populations which are known to have low levels of SxD.

As size was accounted for during Procrustes superimposition, the question arose whether the scaling effect (allometry) that remained after size removal has an impact on the shape of facial structures. A significant allometric affect was demonstrated, not only in the global analyses, but also to various extents in each of the subsets. Cock (153) defined three levels of allometry: 1) Ontogenetic allometry; 2) Evolutionary allometry ; and 3) Static allometry. Ontogenetic allometry aims to quantify the relationship between size and form during development and, hence, includes samples of different ages (153). Such studies aim to establish the growth stage (age) at which divergent form patterns appear. Ontogenetic allometry studies are often run concomitantly with evolutionary allometry investigations that assess allometric differences between related taxa (28,153). Static allometry determines the relationship between size and shape of individuals in the same age group, usually adults, but can be applied across different species (153). It is often analysed in studies that use GMM analyses, such as the current study, which mitigate size to determine the residual effects it has on shape (30,137,151,154). Static allometric scaling of the human skull has been demonstrated in various European populations including the Czech Republicans (151), Austrians (25), and Portuguese (30). Kimmerle et al. (154), however, found no allometric affects in an American sample (both black and white individuals), contradicting the result of this study as well as the aforementioned investigations. These results will be elaborated upon in the subsequent section.

4.4.2 Detailed Observations

4.4.2.1 Sexual dimorphism

The global analyses reveal a significant degree of SxD in white South Africans, particularly in the markedly greater rugosity of male crania. The deep red colour of the nasal bones, inferior nasal spine, and the zygomatics in the male renderings illustrate that these areas vary most in their expression of robusticity between the sexes. The less saturated red colouration of the basicranium, including the mastoids and external occipital protuberance, suggest that whilst these areas are more rugose in males, it is to a lesser extent than what is seen in the piriform aperture and zygomatics. Females appear to have larger orbits, particularly in the regions of the fixed landmarks, as well

as more rugose posterior maxillae. These results are in line with traditional descriptions of characteristic male and female attributes, including larger, more robust/rugose male skulls with more prominent muscle markings, inferiorly projecting mastoid processes and square orbits (8,42). Once size was accounted for, however, the global analyses of this investigation allude to a number of other traits not seen in older analyses of SxD, including the relatively larger posterior maxilla in females and the fact that differences in the orbits appear to be concentrated at the fixed landmarks.

Some smaller differences between the basicrania of the sexes manifested when this structure was analysed apart from the facial structures. These differences include a relatively larger, elliptical, centrally-placed foramen magnum in females as compared to a smaller, circular, more anteriorly-placed foramen in males. While investigations of structural variations in the basicranium are abundant in evolutionary biology (155), maxillofacial surgery (156), orthodontics (157) and even otorhinolaryngology (158), the vast majority of those that pertain to forensic anthropology centre around the foramen magnum and occipital condyles (36,159–162). Most of these studies were based on simple linear measurements of the foramen magnum including maximum length, breadth and perimeter. Regression analyses based on these variables consistently find male measurements to be greater and achieve sexing accuracies of between 66.5% and 88.0%, depending on the origin of the sample (36,159–162). The results of the current investigation are consistent with those findings and suggest that the foreman magnum deserves further investigation in a South African context.

The occiput is a popular region to investigate for the presence of SxD since it obtains an adults morphology at a young age (159,163). Developing from both intramembranous and endochondral ossification, the occipital bone is comprised of four main parts that arise from the fusion of a number of ossification centres *in utero* (132). The squamous and lateral portions (including the condyles) fuse by age four, whilst synostosis of the basilar part occurs by age eight (159,164). The early fusion of bony elements renders the foramen magnum and occipital condyles largely unaffected by secondary sexual changes (160). This structural stability also makes this region a prime area for the investigation of prepubertal SxD, which has been demonstrated in children as young as eight (159). Furthermore, Lestrel and colleagues (163)

demonstrated that basicranial form is not only conserved across 2000 years of human variation, but also between non-human primates, including gorillas and chimpanzees.

In this investigation, the relatively large female foramen magnum is associated with an overall paucity of bony tissue in the female basicranium when compared to the male. Furthermore, the female basicranium in its entirety is tilted anteriorly about the foramen magnum while it is posteriorly tilted in males. The posterior segment of the male basicranium was also found to be longer, while the anterior segment is marginally shorter. This once again demonstrates the applicability of basicranial analyses for sex determination in South Africa, and the need for analysis of the foramen magnum and anterior and posterior occipital length measures. Finally, no difference in flexion of the basicranium relative to the viscerocranium was apparent between the sexes. Notwithstanding, Rosas et al. (165) demonstrated statistically significant differences in this characteristic between African, Asian and European individuals. Evolutionary biologists have long recognised differences between human cranial base flexure and that of lower primates. Thus, the methodology outlined here could be extrapolated in future research pertaining to GMM analyses of the basicranium for the analyses of SxD during evolutionary and developmental ontogeny. Furthermore, this line of research would be of particular importance for black and white South African populations, as it could assist in identifying subadult individuals.

SxD in the maxillary alveolar ridge appears to reflect a superoinferior thickening in females together with variation in palate shape between the sexes. The female palate in this sample was deeper and, in an anterior view, this difference in palatal depth contributed to a relatively more “V”-shaped palate in females as opposed to a more “U”-shape observed in males. Both ectomolare (ecm) and alveolare (ids) lie more superiorly in the female specimens in this study.

A number of studies that investigate palate shape focus on its use for population discrimination (8,166). The vast majority that did investigate sex differences considered only absolute form and not shape differences independent of size (8,40,41,152,167). While there is a general consensus that palate form in white individuals is parabolic/elliptical and small as compared to the hyperbolic/“U”-shape and larger palate of black individuals (3,168,169), there is less consensus regarding palate shape between the sexes. Although all scholars agree that absolute linear

measurements of male palates are always larger, there are differing results from studies employing univariate statistics and those employing multivariate statistics (41,63,167,168). When linear measurements and univariate statistical analyses were used, male palates were described as having wider, “U”-shapes and female’s as having narrower, shorter parabolic shapes (3,41,152). Bigoni et al. (63), on the other hand, used GMM techniques, much like the current investigation, and found male palates to be relatively narrower and deeper than female’s. The current investigation found that the female palate is narrow anteriorly relative to males and, in contrast to Bigoni et al. (63), the palate of females was deeper. Possible reasons for these disparate results, aside from those mentioned above, include different measuring techniques and geographically distinct samples. Differences between the present results and those of Bigoni et al. (63) could also be due to the edentulous component and temporal difference. Finally, clarification of the relative position of the incisive foramen, palatine foramina and ectomolare provided in this study has not been attempted before.

The female zygomatic bones proved to be more gracile on the whole, with marginally more anterior projection seen along the orbital rim and frontal process. The opposite is true for the males in this sample with greater overall rugosity as well as anterior projection of the majority of the bone. The relative difference in the projection of the zygomatic bones could perhaps be attributed to the greater flexion between the body of the zygomatic bone and the zygomatic arch in males, resulting in a slightly decreased angle as compared to females and a slight increase in the projection of the bone. All these differences are, however, very small and a four-fold magnification was applied in order to effectively visualise them (Figure 4.9). Notwithstanding, the results are significant and represent true morphological shape differences, free from the effect of absolute size. Additionally, the rugosity and lateral extension of the zygomatic bones in males are confirmed by traditional morphometric studies (1,2,20), as these characteristics would result in greater bizygomatic breadth. The results are also in line with morphological descriptions of the zygomatic bone including: robust, high, and rough in males versus gracile, low and smooth in females (170), extension in males versus lack of extension in females (40), and rugged and laterally arched in males versus smooth and compressed in females (41). The current investigation demonstrates the power of GMM to quantitatively describe structures that were

previously difficult to measure and relied heavily on morphological descriptions for sex discrimination.

In traditional qualitative analyses, the orbits are described as round, larger and higher in females and square/TV-like, smaller and lower in males (40,41,170). The global analyses of this investigation failed to demonstrate these characteristics. This is likely because these characteristics are a product of absolute size, which was mitigated in this investigation. The landmarks frontomale orbitale (fo) and lachrymal orbitale (lo) in the male orbit lie posterior to those of the female orbit in the lateral view, resulting in a more flexed appearance of the male orbit. When analysed in isolation, the size differences between male and female orbits became considerably reduced. This could be attributed to the fact that Procrustes superimposition may have dealt with a far greater number of artefacts due to nuisance landmarks, resulting in greater distances needing to be minimised in the global analyses. Despite this, the flexure of the male orbit remained a dominant sex characteristic in the regional analysis of the orbit. Franklin et al.'s (3) illustration of vertical constriction in the glabellar region may account for this difference in orbital flexure. Bigoni et al. (63) demonstrated that male orbits lie somewhat parallel to the frontal plane while females were directed relatively more sagittal, based on the fact that the medial margin in females was shifted more anteriorly and the lateral margin was shifted more posteriorly. We did not find this to be the case in the current sample as both medial and lateral margins of the female orbit lay anterior relative to males. Differences in the geographical origin of the samples used may account for this discrepancy.

This study found the male nasal aperture to be both antero-superiorly longer and narrower compared to females. The male inferior nasal spine also projects further anteriorly, but lies more inferiorly. The glabellar region also projects more anteriorly in males. These outcomes corroborate the morphological descriptions of the male nasal aperture as being high and thin with sharp margins as opposed to a lower, wider nasal aperture with rounder margins in females (40,41). Glabellar robusticity and projection in males have been used as a discriminator of sex in numerous quantitative studies (3,64,170). The present results do, however, contradict metric analyses of nasal aperture measurements, such as those reported for white Americans (171) and white South Africans (1) where the dimensions of males were larger. This is because the

aforementioned studies used absolute measures and the results from the current study are relative and, hence, devoid of size. The GMM analyses of both Bigoni et al. (63) and Franklin et al. (3) give detailed morphological descriptions of differences between the glabellar and nasal regions of the sexes. Aside from the established fact that the male aperture is narrower and taller, Bigoni et al. (63) also describe the nasal base in males as being deeper, and more prominent and interorbital breadth in males as being smaller. In the global results of this study, the male nasal base was also deeper and the nasal bones projected further. However, interorbital breadth between the sexes is comparable. Population specific differences between our sample and that of Bigoni and associates (63) could account for this discrepancy. Furthermore, the current research found no difference in nasal projection, as seen in the curve analyses of the nasal aperture, because only the outline of this structure was analysed with no additional landmarks to act as reference points for projection to be compared. Using transformation grids over smooth-rendered warped means, Franklin et al. (3) demonstrated how sex-linked differences in nasal and glabellar structures are the result of a vertical constriction across the male glabellar region resulting in characteristic male features, including a more sloped forehead and the features previously described. Most recently, McDowell et al. (164,172) used GMM to analyse ancestry differences in South African nasal apertures. They also measured sexual dimorphism using both elliptical Fourier analyses and LDA. Despite high ancestry estimation accuracy, they achieved only 50% sexing accuracy using LDA of elliptical Fourier analyses and 70% using traditional craniometrics. They concluded that the traditional measures achieved better results because SxD in the nasal aperture is on account of size. The current investigation achieved an accuracy of 67% using linear regression, which is similar to McDowell et al's results using traditional measures. This difference may be because the geometry of nasal shape was represented better in the current study, by using sliding-semilandmarks. Additionally linear regression has fewer statistical assumptions (e.g. it doesn't require the sample to be parametric) (173) which may also account for the difference in accuracies between the 3-D methods.

In this analysis, SxD is the dominant factor that drives differences between human skulls. Every structure analysed, both globally and regionally, proved to be significantly affected by SxD. A number of hypotheses about the cause of SxD in the viscerocranium in particular have been put forth. Franklin et al. (3) attribute sex

related differences in the zygomatics and glabellar region to masticatory strain induced by the muscle activity. Although the masseter muscle has been shown to significantly strain the zygomatic bone (174), the effects of masticatory forces on the supraorbital torus and glabella are hotly contested, as relatively low stress and strain effects have been found in the frontal bone (120). Alternatively, Velemínská et al. (151) proposed that prolonged growth of the nasal region of the male face, including the frontal sinus, together with different sizes of certain orbit structures, result in the enlarged glabella. They also assert that this explains the more protrusive nasal bones seen in males. The larger nasal aperture in males has been attributed to the need for increased oxygen intake associated with greater proportions of muscle tissue, and hence, greater metabolic demands in males (30,151). This conjecture is supported by the work of Rosas and Bastir (30) who found larger airway dimensions in males, including an anterior expansion of the nasal aperture and concomitant posterior expansion of the choanae. Furthermore, the nasal bones were shown to increase in angulation relative to glabella and the anterior nasal floor was shown to move inferiorly. Rosas and Bastir (30) contend that this expansion of the male airway is responsible for an upward shift of the nasal and glabellar region, and could perhaps explain the compression of the glabellar region demonstrated by Franklin et al. (3).

4.4.2.2 Allometry

Allometry plays a pivotal role in the elucidation of SxD. This is because allometric effects can modify the expression of SxD either synergistically or antagonistically (30). In other words, the effect of scaling on an object's shape can either accentuate a sexual trait or obscure it. For example, SxD in the nasal aperture produces large apertures in males (30). Conversely, allometry results in smaller apertures. This antagonistic interaction between SxD and size results in male apertures that approximate that of females in size. On the other hand, a synergistic relationship between SxD and allometry is seen in the naso-glabellar region. Allometry causes the glabella region to recede relative to the nasal bones, which SxD causes to lie more superiorly. Together these factors enhance the expression of SxD (30).

Geometric morphometrics (GMM) allows the effect of allometry on SxD to be analysed without the confounding influence of size. The current investigation analysed static allometry through an analysis of size-independent shape differences in adult

white South Africans, and demonstrated significant allometric effects in the global investigation and for each of the subsets. Globally, the rendered images are significantly different from those of SxD and show a clear distinction in the morphology of the upper and lower face with changes in CA. Generally, smaller individuals have larger glabellae, supraorbital regions and nasal bones, while larger individuals have more prominent anterior maxillae. The cranial base of smaller individuals shows more protrusive nuchal crests (nc) and more inferiorly projecting mastoid processes (ms). These differences are discussed in greater detail in the subset discussion below. The vector diagrams used to illustrate differences in each subset allowed for a better understanding of the relative size and direction of the differences between structures. For ease of comparison, the results of SxD and CA were compiled into a single image in Figures 4.5 (females) and 4.6 (males).

In the basicranium, the effect of allometry works antagonistically a that of SxD, particularly in the relative location of foramen magnum, which moves superiorly as structures decrease in size. As size differences in the foramen are no longer apparent when SxD is mitigated, it suggests that SxD was the sole cause of this difference. Smaller individuals also have more inferiorly and laterally positioned mastoids and a more anteroinferiorly positioned nuchal crest. As a result, larger males have relatively less projecting mastoids and superiorly positioned, more projecting nuchal regions, whereas smaller males have more projecting mastoids with a nuchal region that is more inferiorly positioned and less projecting. The opposite is true for females. These results imply that the mastoid processes of relatively large females will approximate those of males, hence confounding sex estimation accuracies of this feature. Furthermore, these SxD and size related differences in basicranial shape explain the underlying morphology associated with population-specific differences. Rosas and Bastir (30) studied the effects of allometry on SxD using a Portuguese sample by applying GMM. To visualise deformations of the skull related to both SxD and allometry, they applied thin plate splines to lateral digitisations from a total of 104 samples. The authors focused on the occipital clivus, represented by the landmarks basion (b) and inferior vomer (iv) in the current investigation. Although they also demonstrated an antagonistic relationship in the basicranium between SxD and CA, and found that the clivus moves inferiorly while the current investigation found it moves superiorly with increasing CA.

When the maxilla was tested for CA, the differences in palate depth seen during the analysis of SxD are no longer apparent. Hence, palate depth can be attributed to SxD only. An antagonistic relationship between SxD and CA once again emerges in the palatal region. The posterior-most aspect of the palate (pf) was seen to extend further backward in smaller individuals when allometry was assessed, but it was more posterior in males in the analysis of SxD. Additionally, the incisive foramen in smaller individuals was also superior to the position in larger individuals. This is demonstrated by the superior position of the foramen in males seen during the analyses of SxD. Overall, smaller individuals have anteroposteriorly longer palates with thin alveolar bone anteriorly as opposed to broader, shorter palates in larger individuals with alveolar bone that is evenly thick throughout its length. Not only was this not seen during the analysis of SxD, but these effects are also independent of both age and dental loss, the effects of which were mitigated in the preliminary analyses. Hence, these palatal features can be entirely attributed to CA. These results are in agreement with Rosas and Bastir (30) who demonstrated positive allometry in the maxilla. Additionally, these authors also demonstrated an increase in maxillary length with size, together with an anterior rotation of the midfacial region, resulting in an increase in prognathism with increased size. Geometric morphometric (GMM) analyses of photographs and surface scans (151,175) showed an increased size of the lower face with an increase in CA, corroborating these findings.

Yet another antagonistic relationship is apparent in the size of the zygomatic bone, which demonstrates an increase in size with a decrease in CA, meaning that smaller individuals will have relatively larger zygomatics. The difference, however, is slight as the images of the effects of CA on zygomatic morphology were magnified four-fold. As larger zygomatics are seen to project more laterally, larger males would have increasingly projecting zygomatics when compared to small females- a clear case of synergism. Lateral projection of the zygomatic is not as pronounced in the renderings of CA as it was when SxD was analysed. This indicates that lateral projection can be largely attributed to SxD. Other differences among zygomatics are very slight, despite being statistically significant.

An antagonistic relationship was also apparent in the orbit. Superior displacement was seen in the superolateral margin of larger individuals, together with

an anteromedial displacement of frontomolare orbitale (fo). Conversely, the superolateral margin lay anteromedial in males and frontomolare orbitale (fo) lay posteriorly. No flexion of the orbit is evident when allometry is analysed and, hence, it can be concluded that orbital flexure is a sexually dimorphic trait. Velemínská et al. (151) also demonstrated an allometric affect pertaining to the orbits, although these authors looked at soft tissue differences and not at bony structures. They found a smaller inter-orbital distance in males as well as more deep-set eyes. These observations were confirmed in the global analyses of CA in the current study. The decrease in glabellar protrusion with an increase in CA, however, is supported by Rosas and Bastir (30) who had similar findings. In the nasal aperture, an increase in size was shown to cause a narrowing and lengthening of the aperture, demonstrating synergism between CA and SxD. In contrast, the relative position of the nasal spine (ins) moved posteriorly and inferiorly in larger individuals, while it moved anteriorly and inferiorly in males. Using 3-D surface models, Velemínská et al. (151) also documented allometric variation in nasal structure that was shown to increase in size and convexity with increased CA. Rosas and Bastir (30), however, demonstrated an antagonistic relationship between SxD and CA as they found the nasal aperture to decrease in size as CA increased, which they attribute to a “counter clock-wise rotation” of the midface associated with relative size increases. Differences in the results of this study when compared to Rosas and Bastir (30) may be attributed to differences in the sample population, the landmarks investigated, the statistical methods employed, the sample size and importantly, the orientation of the dataset, as the aforementioned authors analysed 2-D lateral view digitisations only.

4.4.2.3 Non-allometric sexual dimorphism

Despite an increased saturation of colour in all sexually dimorphic regions of the cranium in the global analysis, only the zygomatic bones demonstrated significant NASXD effects. The resultant effect of NASXD is that SxD in the zygomatics was emphasised. This illustrates that although CA was not completely obscuring the effects of sexually dimorphic traits, it was suppressing them, highlighting the importance of mitigating allometric affects when analysing SxD.

Schaefer et al. (25) demonstrated that in primates displaying a small degree of sexual size dimorphism (such as humans, *Pan troglodytes* and *Pan paniscus*), this

low-level dimorphism is largely due to the non-allometric component. As sexual size dimorphism between larger primates reflects male-male competition, Schaefer et al. (25) propose that the non-allometric component present in smaller primates is associated with male sexual attractiveness. Rosas and Bastir (30) suggest that as much as two-thirds of SxD may be attributable to NASXD in these primates.

4.5 CONCLUSIONS

In conclusion, this study applied GMM to 3-D co-ordinate based data and demonstrated significant SxD, after accounting for size, in the global analyses and in each of the subsets investigated including the basicranium, maxilla, zygomatic bones, orbits and nasal aperture. Similarly, CA was investigated and also found to have a significant effect on the cranium, both during the global and subset analyses. These results highlight the importance of analysing the effects of allometry on the facial skeleton and the importance of isolating allometric effect when analysing SxD. Although some degree of synergism is seen in the relationship between CA and SxD, the majority of the interactions between these two factors is antagonistic. These results demonstrate that caution is warranted in future research on SxD and that more research into allometric effects between human sexes, as well as population groups, is needed.

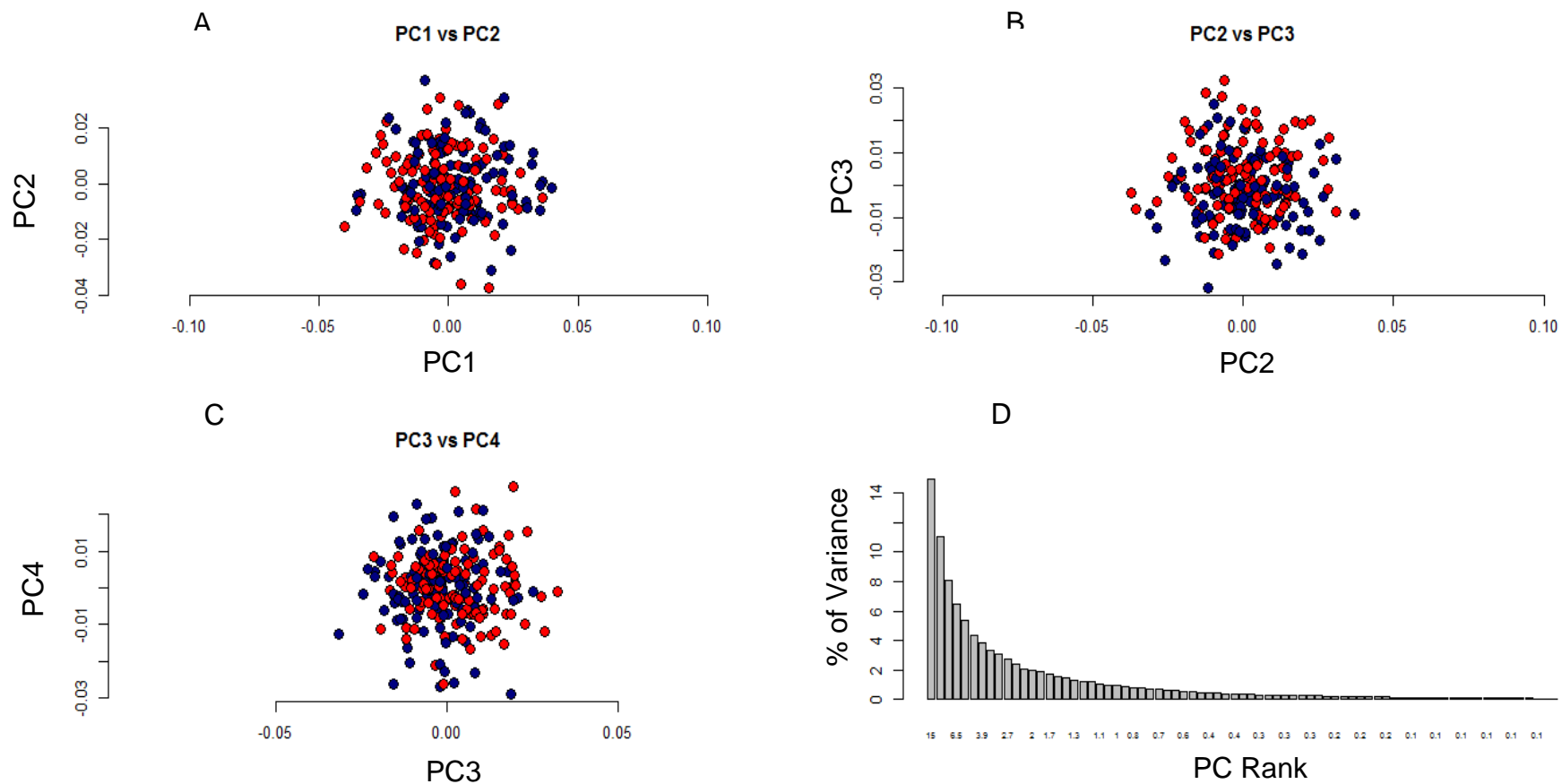


Figure 4.1 Scatter plots of the distribution of male (blue) versus female (red) data points along PC1 vs. PC2 (A), PC2 vs. PC3 (B) and PC3 vs. PC4,(C) as well as a histogram of the percentage of the variance accounted for by each principal component (D).

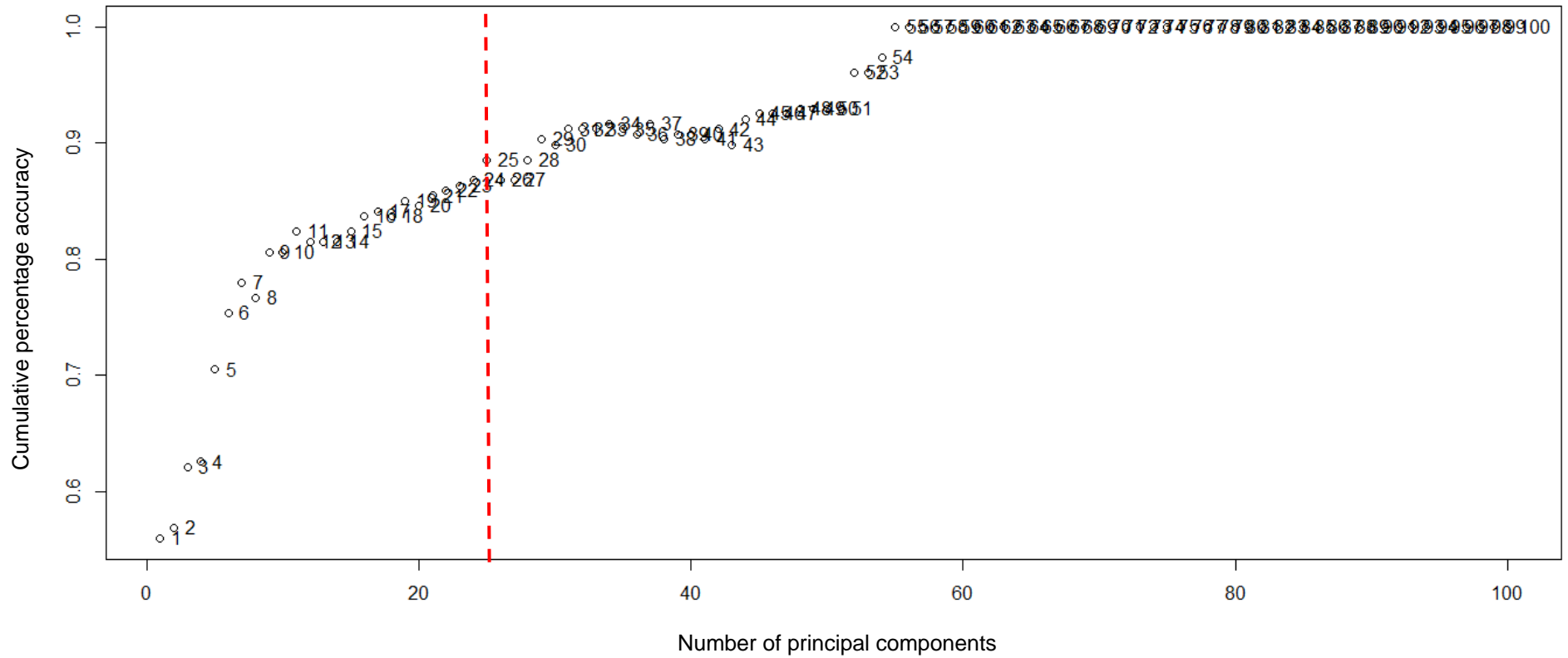
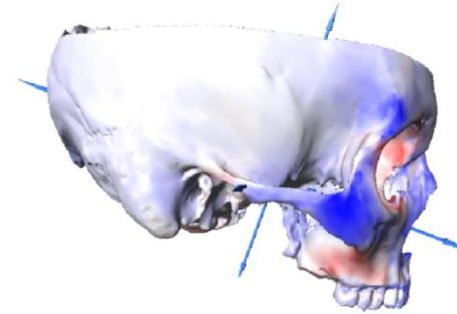
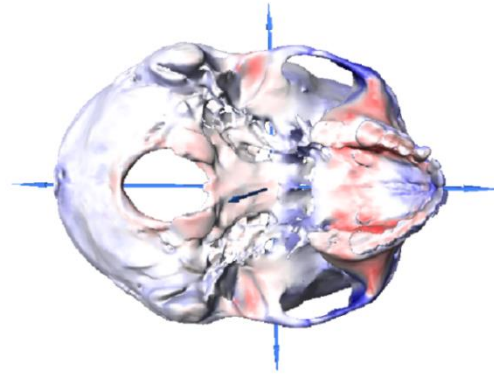
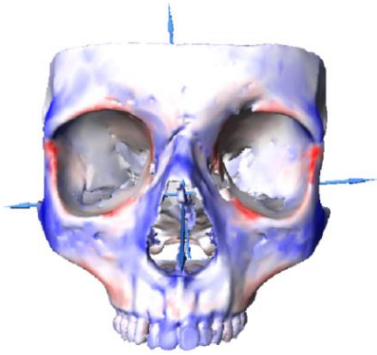


Figure 4.2 Plot of the cumulative contribution of the first 100 principal components for sex discrimination accuracy. The broken line represents the plateau in predictive accuracy at which the number of principal components needed for the regression analysis was chosen.

Female



a)

b)

c)

Male

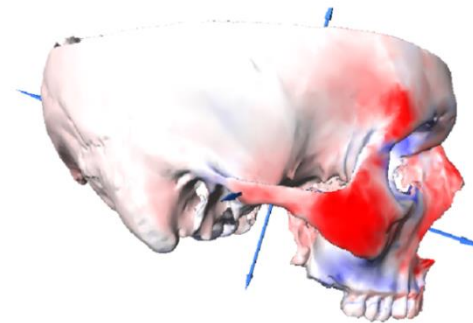
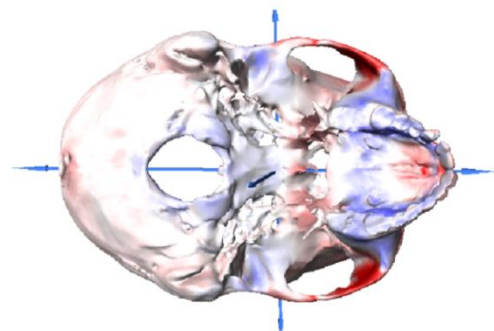
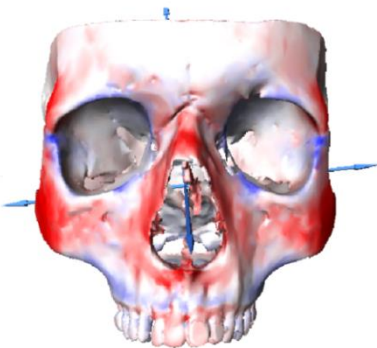
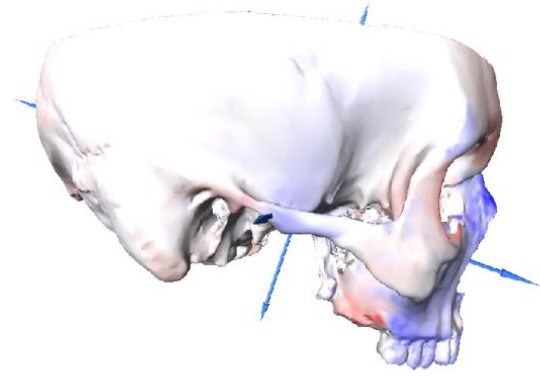
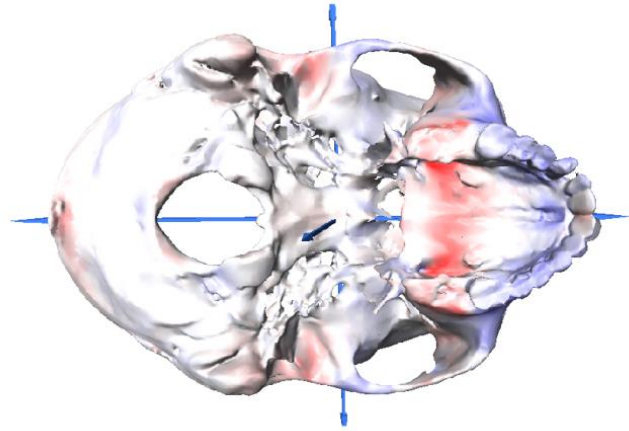
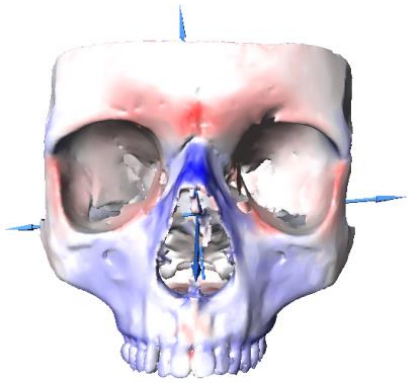


Figure 4.3 Surface scan deformations displaying the relative differences in cranial shape between males and females from anterior (a), inferior (b), and lateral (c) views. In the images, spectra from light blue to dark blue indicate areas that are relatively smaller than areas coloured in spectra of red, from pale to dark red. Note that regions of the neurocranium, and much of the posterior basicranium, were void of landmarks and thus the differences observed here are an artefact of the methods and landmark locations.

Small



Large

a)

b)

c)

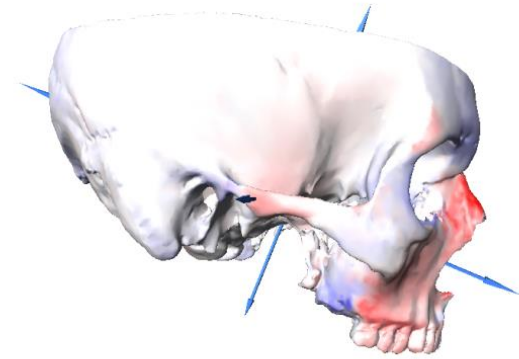
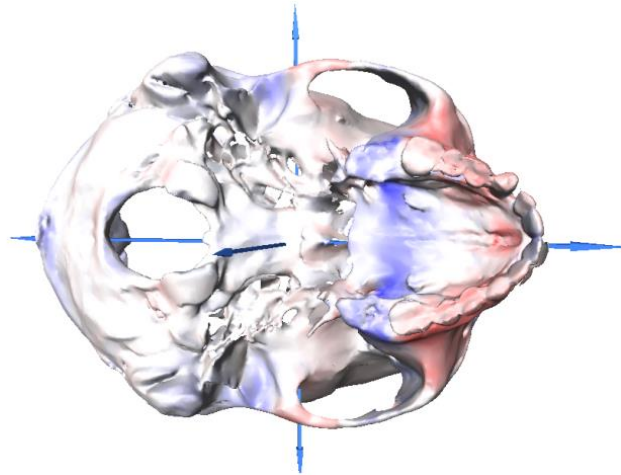
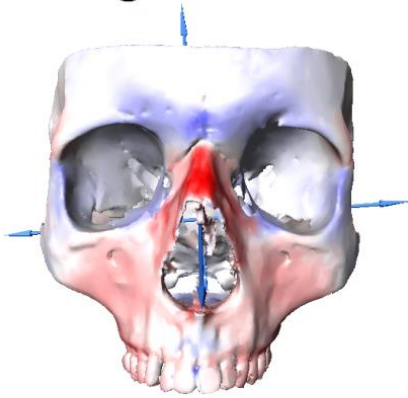
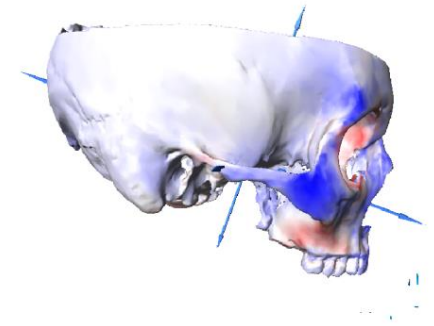
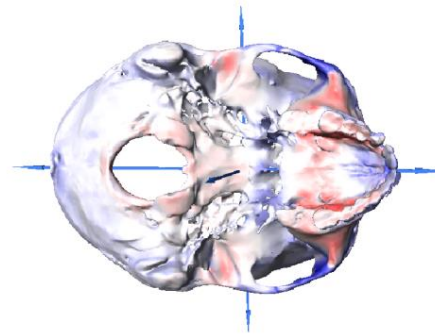
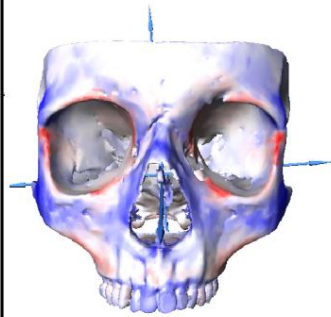


Figure 4.4 Surface scan deformations displaying the relative differences in cranial shape between small and large individuals from anterior (a), inferior (b), and lateral (c) views. In the images, spectra from light blue to dark blue indicate areas that are relatively smaller than areas coloured in spectra of red, from pale to dark red.

Female

Sexual Dimorphism



Non-Allometric Sexual Dimorphism

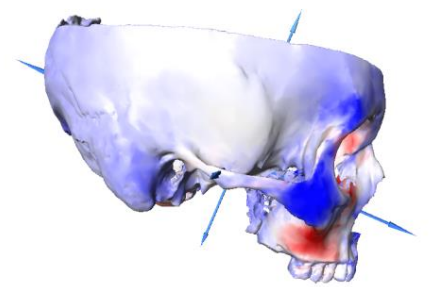
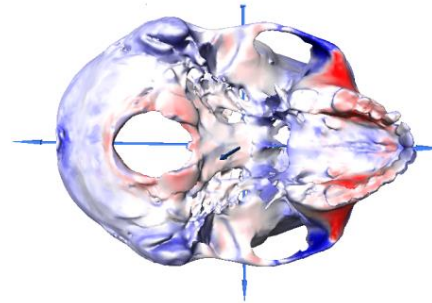
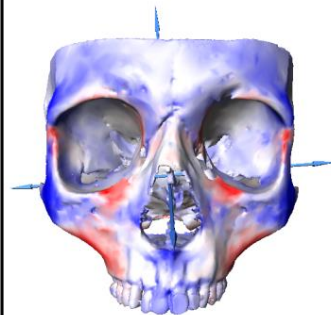
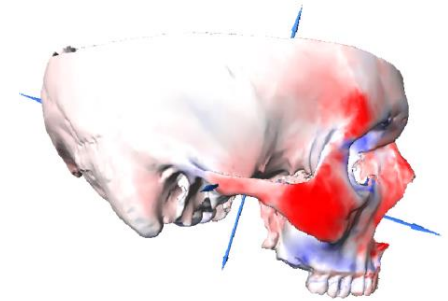
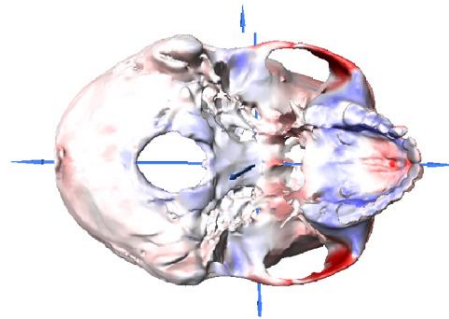
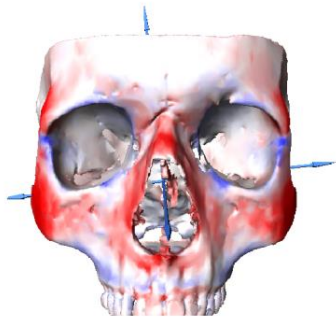


Figure 4.5 Surface scan deformation images of the effects of non-allometric sexual dimorphism on female cranial form shape in anterior (a), inferior (b), and lateral (c) views. Non-allometric sexual dimorphism is also directly compared to sexual dimorphism to demonstrate the similarities and differences between the results. In the images, spectra from light blue to dark blue indicate areas that are relatively smaller than areas coloured in spectra of red, from pale to dark red.

Male

Sexual Dimorphism



**Non-Allometric
Sexual Dimorphism**

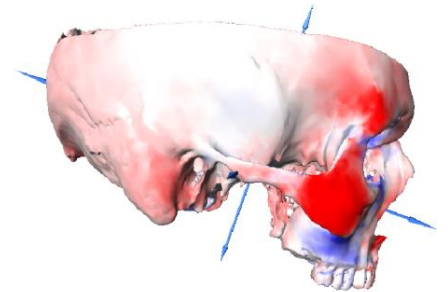
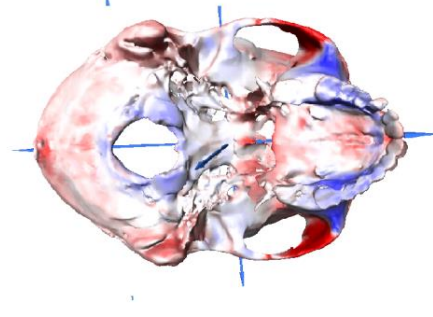
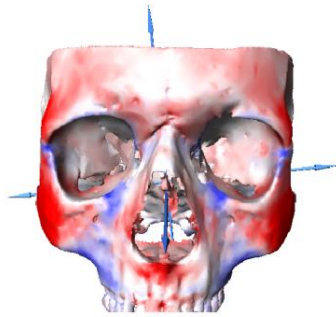


Figure 4.6 Surface scan deformations of the effects of non-allometric sexual dimorphism on male cranial shape in anterior (a), inferior (b), and lateral (c) views. Non-allometric sexual dimorphism is also directly compared to sexual dimorphism to demonstrate the similarities and differences between the results. In the images, spectra from light blue to dark blue indicate areas in which more variation is seen, coloured in spectra of red, from pale to dark red.

Sexual Dimorphism

Common Allometry

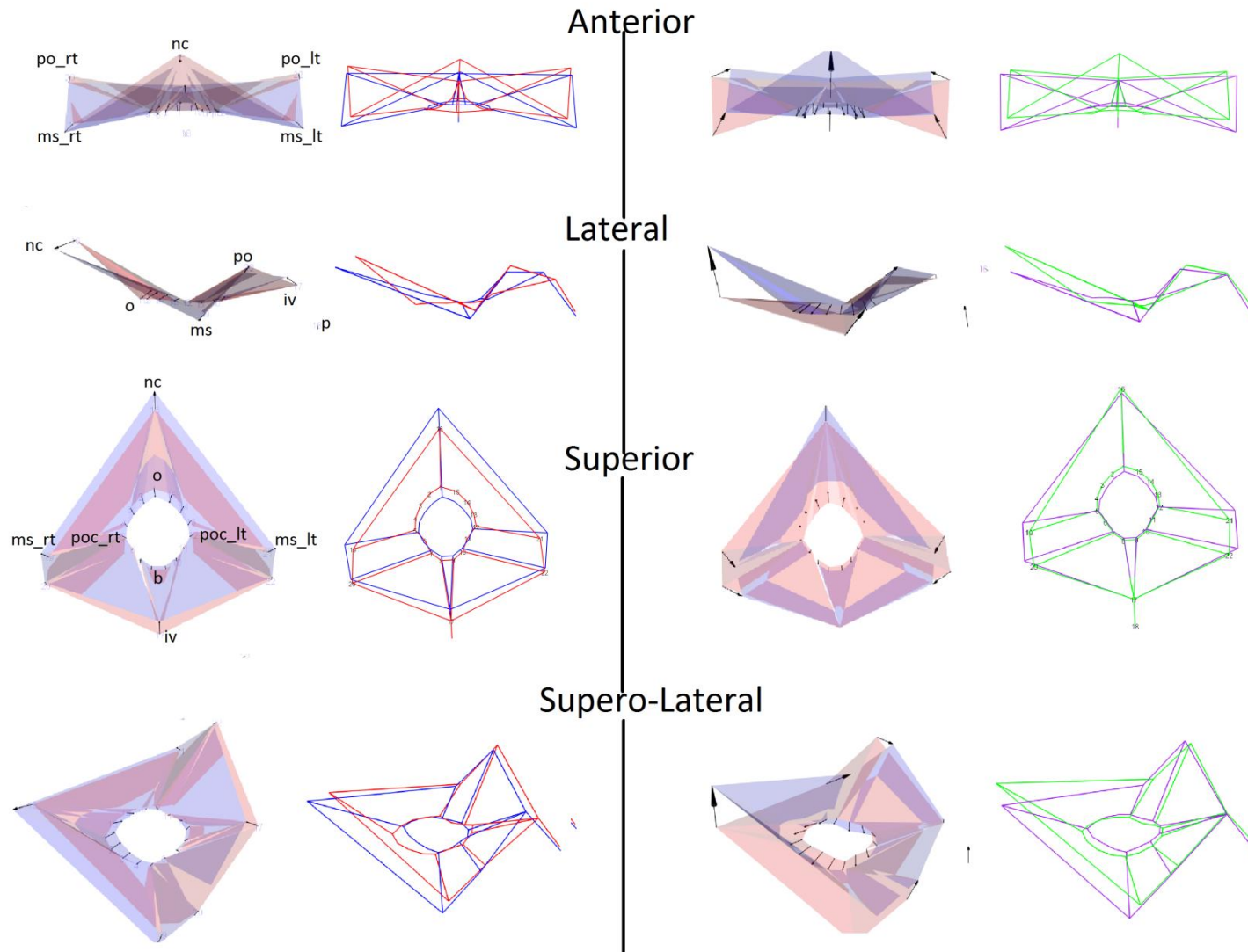


Figure 4.7 Vector diagrams and wireframe images of the differences between male (blue) and female (red) basicrania on the left, and allometric difference between large (green) and small (purple) basicrania on the right. Images displaying variation in common allometry were scaled by a factor of two to aid visualisation.

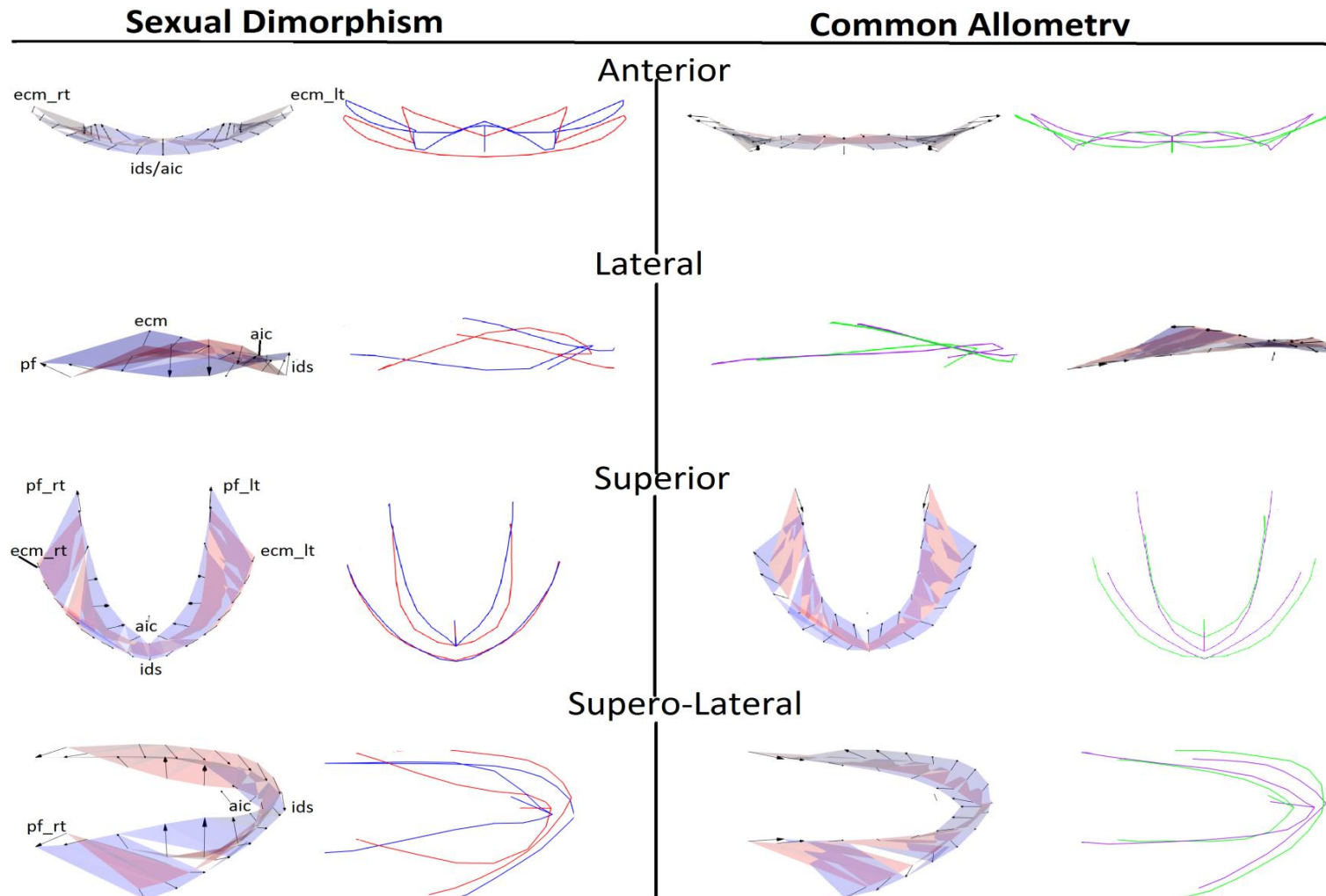


Figure 4.8 Vector diagrams and wireframe images of the differences between male (blue) and female (red) maxillae on the left, and allometric difference between large (green) and small (purple) maxillary dental arcs on the right. Images displaying variation in common allometry were scaled by a factor of two to aid visualisation.

Sexual Dimorphism

Common Allometry

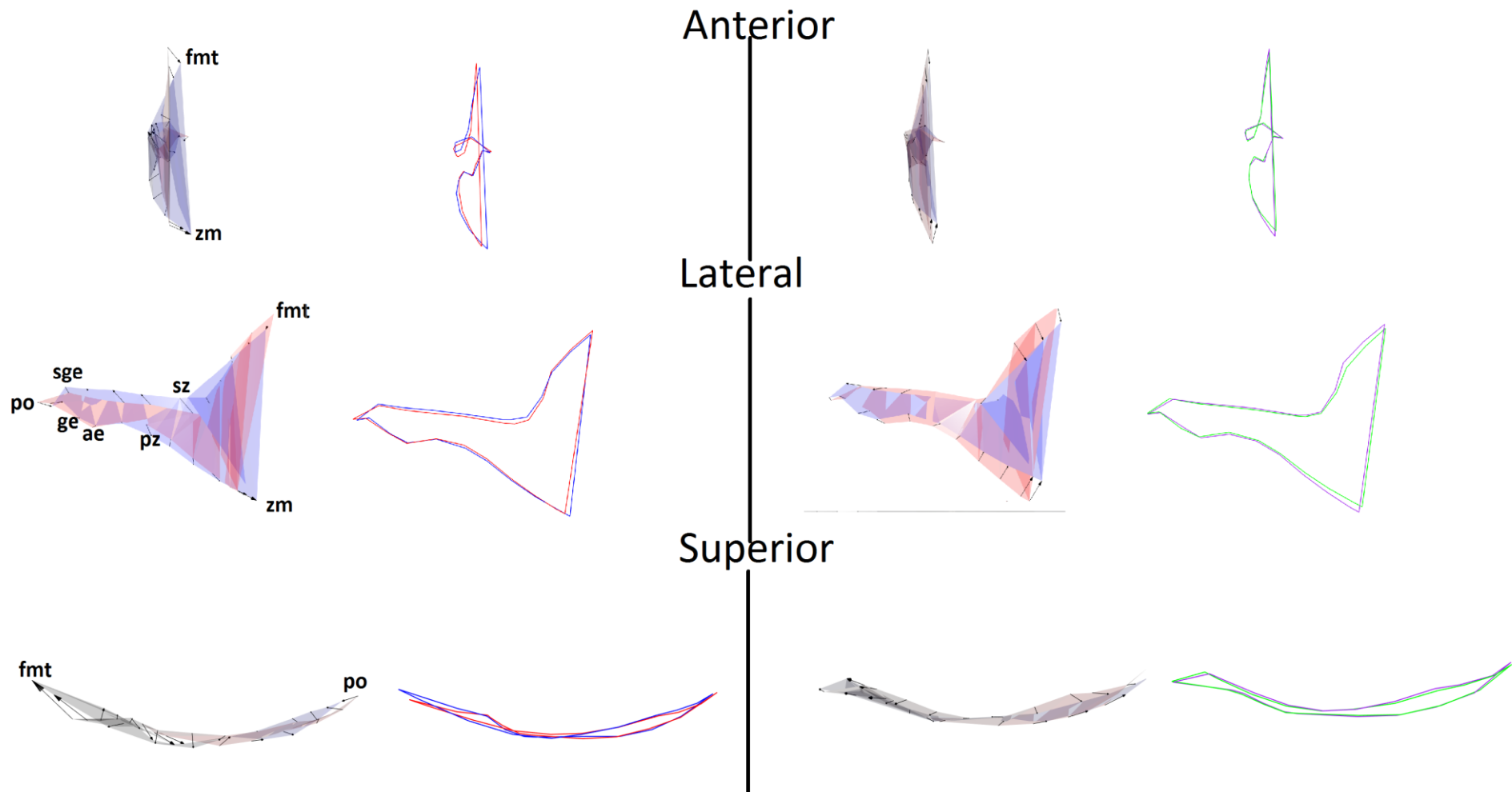


Figure 4.9 Vector diagrams and wireframe images of the differences between male (blue) and female (red) zygomatic bones on the left, and allometric difference between large (green) and small (purple) zygomatic bones on the right. Images displaying variation in common allometry were scaled by a factor of four to aid visualisation.

Sexual Dimorphism

Non-Allometric Sexual Dimorphism

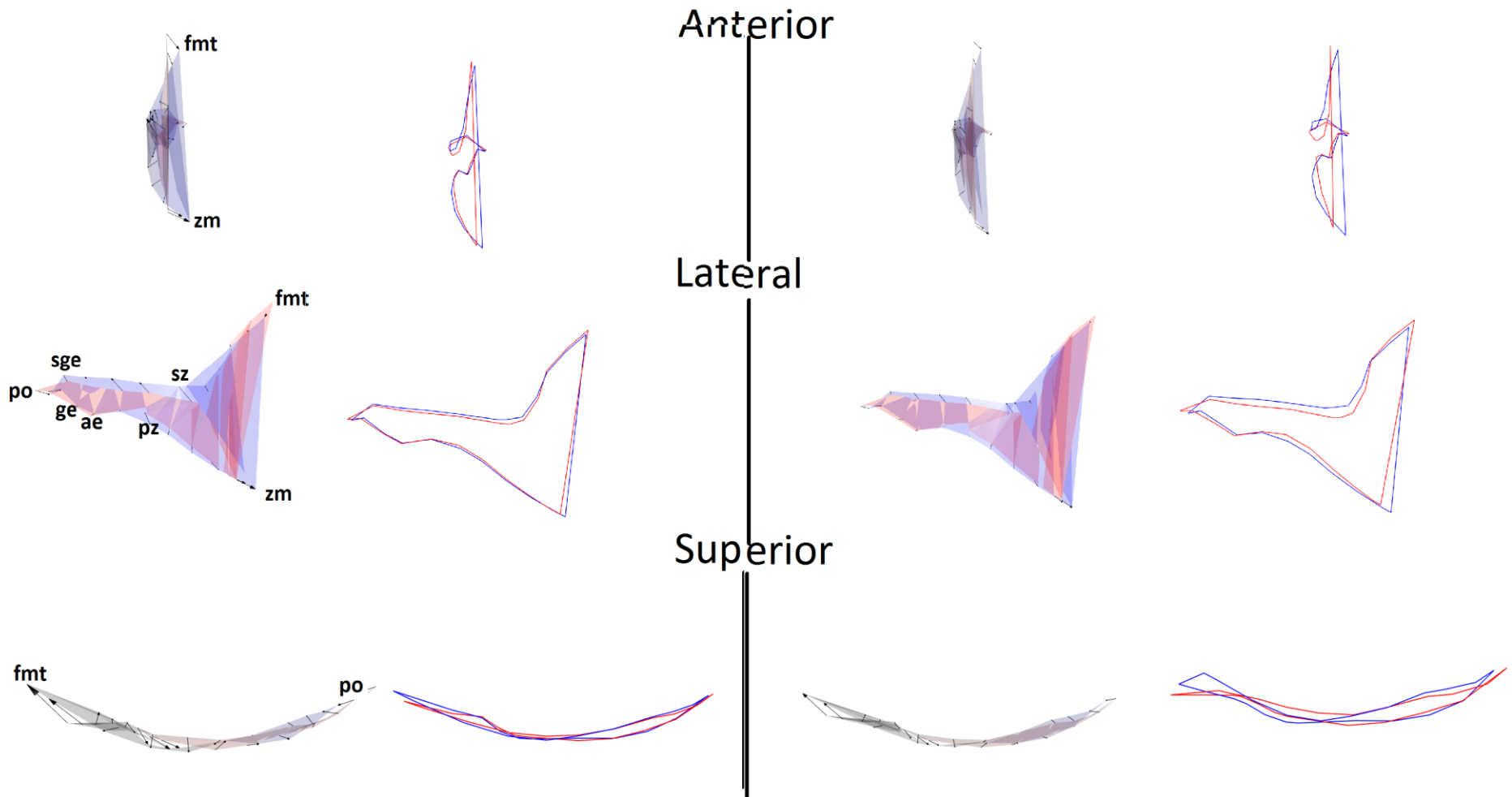


Figure 4.10 Vector diagrams and wireframe images of the differences between male (blue) and female (red) zygomatic bones before removing the effect of size (left), and after removing the effect of size (right). No scaling was necessary.

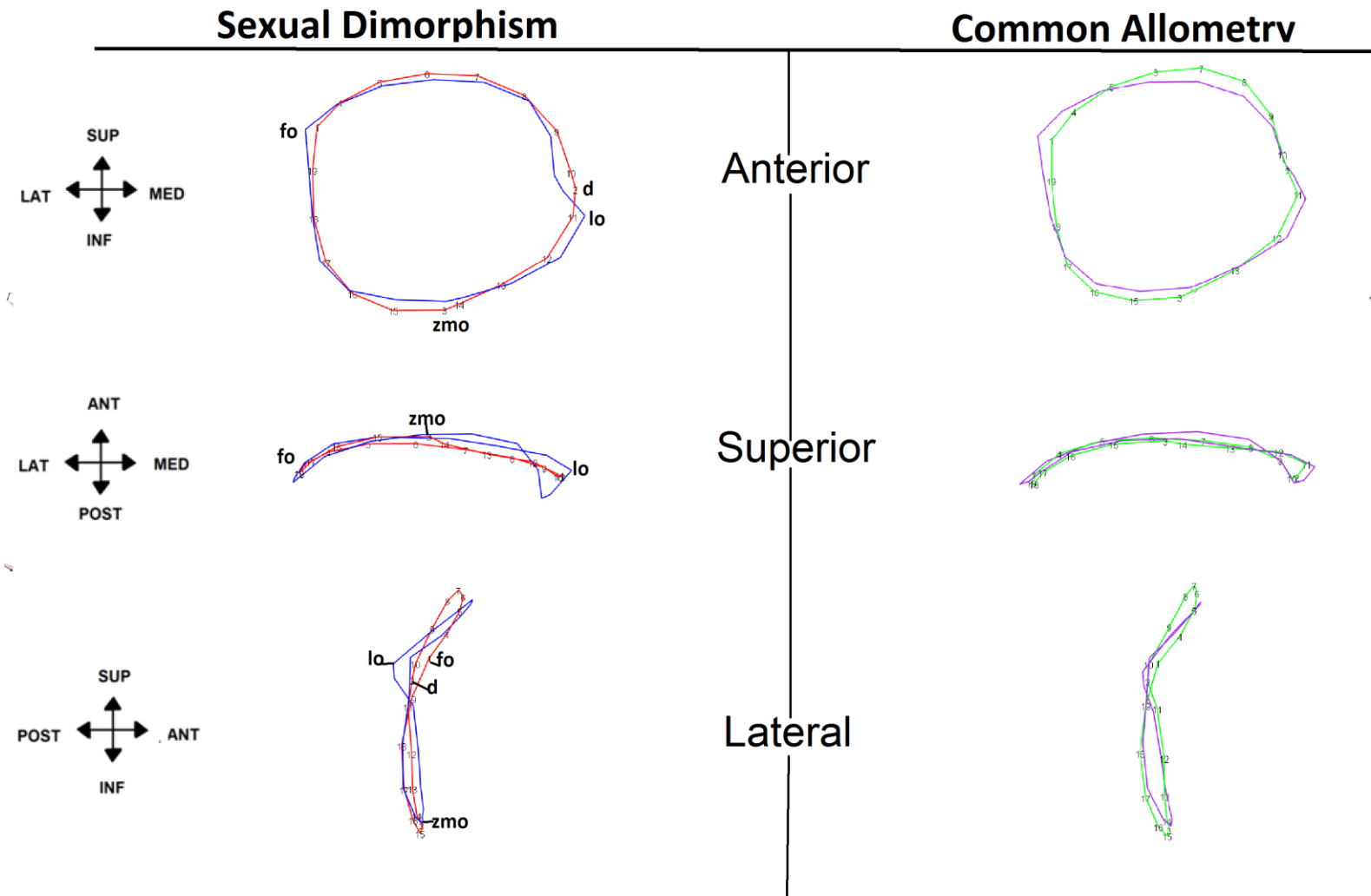


Figure 4.11 Anterior, superior and lateral wireframe images of the morphological changes in the orbits associated with sexual dimorphism (left) and allometry (right). In the images, red indicates female, blue male, while purple indicates small individuals and green large individuals.

Sexual Dimorphism

Common Allometry

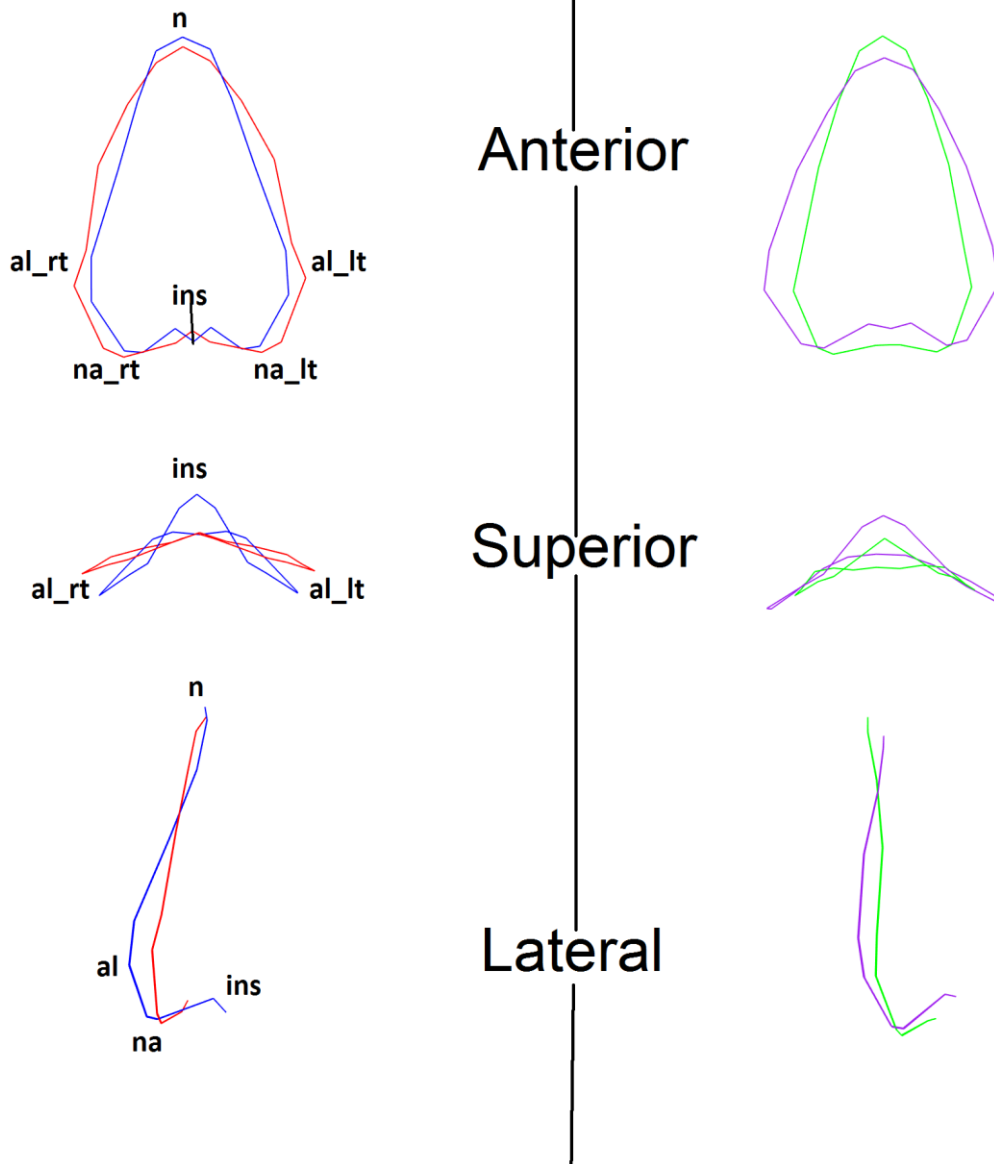


Figure 4.12 Anterior, inferior and lateral wireframe images of the morphological changes in the nasal aperture associated with sexual dimorphism (left) and allometry (right). In the images, red = female, blue = male, purple = small, and green = large.

Table 4.1 Age distribution of sample by decade and dental state. SD= standard deviation (n= 227).

Age interval	Male		Female	
	Total sample	Edentulous individuals	Total sample	Edentulous individuals
18-29	1	1	2	0
30-39	4	1	1	0
40-49	22	11	8	3
50-59	24	16	21	12
60-69	35	22	46	38
70-79	12	10	15	13
80-89	11	10	14	11
90-95	5	4	6	6
Total	114	75	113	86
Overall age interval (years)	28 – 95	28-95	19 – 95	45-95
Mean age (years)	62	64	66	69
SD (years)	14	14	14	14

CHAPTER FIVE

Traditional cranial measurements versus
3-D derived interlandmark distances for
sex estimation in white South Africans

5.1 INTRODUCTION

One of the main tasks facing forensic anthropologists is the accurate estimation of sex, ancestry, age, stature and other individualising factors, when compiling a biological profile for unidentified skeletal remains (9,10). Traditional metric analyses, the often preferred method of data collection, involve measuring distances between a numbers of predefined, biologically homologous landmarks that are representative of the groups of interest. Corresponding measures, known as interlandmark distances (ILDs), are compared using univariate or multivariate statistics. When compared to morphologic analyses, these methods require equipment such as callipers, osteometric boards and mandibulometers, and their measurements are more time consuming to collect and assess, the data are less subjective, easier to reproduce, do not require an experienced observer and can be readily analysed using sophisticated multivariate statistics (6). Most metric studies use linear discriminant analyses (LDA) to derive discriminant functions, which are robust, multivariate means of population and/or sex discrimination. Restrictions of metric methods include that they are applied only to the population from which they were formulated and that the assumptions of the statistical test are met (6,49). These assumptions regarding predictor variables are that 1) they should have a multivariate normal distribution; 2) they should have equal within-group covariance matrices; 3) they should be uncorrelated (i.e. non-multicollinear); and 4) cases should be independent (50,173,176). First described by Fisher (177), LDA is computationally similar to MANOVA and involves deriving a linear discriminant function to predict group membership for a dichotomous variable, using a weighted combination of the most dimorphic predictor variables (6,49). This is achieved by maximising the ratio of between-group to within-group sum of squared distances (49). Due to the practical, real life applicability of discriminant functions and the need for population-specific standards for biological parameters (51,52,178), a plethora of studies are published annually that use traditional metric methods and LDA to define new functions for previously unexplored bony elements and populations (179). Furthermore, many of these publications validate older metric studies, reinforcing the reliability of the traditional forensics. According to the ruling in *Daubert v. Merrell Dow Pharmaceuticals, Inc.* (509 US.579, 1993), validated methods with accuracies greater than 80% and intra-observer error below 10% must be employed for legal purposes (180,181).

The skull is the single most studied bone in the human body. It has been used as a key element in the field of evolutionary biology and its variation is highly correlated with ancestry (8,11). Many scholars have studied the skull by employing a number of different cranial measurements. A range of sexing accuracies were achieved: Black Americans: 82%-86%; White American: 82%-88% (171); Central Europeans: 100% (63); Thai: 74.72%; French: 86% (182); Portuguese: 62.12%-77.86% (71); English: 48.8%-97% (37); West Australians: 79.9%-90% (183); and Indians: 61.3%-88.7% (184).

The earliest study of South African crania to employ discriminant analyses was Rightmire (20). Using 35 cranial variables, he studied different black South African tribes and was able to achieve 100% correct sex estimation in Khoisan individuals and 90.6% in Sotho and Zulu individuals. More recently, İşcan and Steyn (1) conducted similar research on white South Africans using 12 cranial and 5 mandibular measurements and achieved sexing accuracies of between 80% (using only bizygomatic breadth) and 86% (using a combination of cranial measurements). This study was later validated by Robinson and Bidmos (5), not only on a sample derived from Gauteng province, but also on samples from Cape Town and Stellenbosch. The authors found that discriminant functions derived by Steyn and İşcan (1) could be applied to samples from across the country with similar accuracies to those reported in the original study, and hence they suggested that the white population within South Africa is homogenous. Sexual dimorphism (SxD) in the crania of black South Africans has also been investigated by subjecting traditionally obtained, and 3-D derived, ILDs to discriminant analyses. Franklin and colleagues (2) used 3-D derived ILDs to estimate sex in black South Africans. The authors attained maximum sexing accuracies of 80%. In response, Dayal et al. (4) studied the same populations, but by analysing traditional metric ILD and achieved sexing accuracies ranging between 80% and 85%. These results were in line with sexing accuracies of the earlier morphometric study by Franklin and colleagues (2), demonstrating the equivalence of the two studies despite the differences in methodology. Both sets of authors also agreed that there is a need for discriminant functions that can be specifically applied to fragmentary cranial remains, a need which to my knowledge, is yet to be met for South African populations.

The current investigation had two broad aims:

1. To compare the accuracy of the most commonly used traditional cranial measures with all possible ILDs.
2. To derive novel, custom-created discriminant functions for white South African crania using the most accurate ILDs possible, that would be applicable to both intact and fragmentary crania.

In order to achieve these aims the following objectives were outlined:

1. To derive all possible ILDs taken between 45 three-dimensional, fixed landmarks and to determine their sex estimation accuracy using both LR and LDA.
2. To demonstrate the equivalence between ILDs extracted from 3-D data and traditionally measured ILDs by comparing the accuracy of discriminant functions derived in this investigation to those published by Steyn and Işcan (1), which are commonly employed when estimating sex in unidentified white crania in South Africa.
3. To compare the sex estimation accuracy of 17 traditional cranial ILDs commonly assessed in forensic investigations, with that of all possible ILDs derived in this investigation, using both LDA and LR.
4. To derive new discriminant functions from the most accurate 3-D ILDs derived in the current investigation for the basicranium; basicranium and palate combined (termed “basipalate”); and zygomatics; orbits and the combined maxilla and nasal aperture (termed “nasomaxilla”).
5. To use the ILDs determined to be most accurate in each of the above mentioned subsets to derive a novel discriminant function for sexing white crania in their entirety.

5.2 MATERIALS AND METHODS

5.2.1 Materials

Two hundred and twenty seven (227) crania were analysed, including 114 males and 113 females of European descent (white) (Table 4.1). Specimens were selected from the Raymond A. Dart Collection of Human Skeletons (Dart Collection) housed in the School of Anatomical Sciences at the University of the Witwatersrand,

Johannesburg, South Africa. Crania between 19-95 years of age (mean = 64 ± 14 years) were sampled to ensure adult morphologies were represented. Specimens exhibiting varying dental states, including completely edentulous skulls, were included in the study, but samples with any damage, missing landmarks or pathology were excluded. Analyses of the neurocranium were not within the scope of this investigation, as rearticulating the sectioned calotte could introduce unwanted error. For further details on the sample, please refer to Chapter 4.2.1.

5.2.2 Data Collection Procedure

After crania were affixed to the work surface using dental clay, 45 homologous landmarks, common to both traditional and GMM, were collected. The landmarks were digitised using a Microscribe® 3-DX digitiser (Immersion Corp., San Jose, CA) interfaced to a personal computer. Three-dimensional (3-D) Cartesian coordinates of each landmark were recorded in an *MS Excel* spreadsheet in millimetres with up to four decimal places. Curve data were not utilised during this study in order to keep the data as similar to traditional metric data as possible.

5.2.3 Statistical Analyses

5.2.3.1 Preliminary analyses

Raw 3-D data points were read into the statistical program *R* (R Core Team, 2015, version 3.2.2) together with a classifier file containing pertinent information such as specimen number, age, sex and dental state. The statistical program *R* was used to extract only the fixed landmarks in the original data file and to create a new file for the purpose of this investigation. The data were then subjected to generalised Procrustes superimposition using functions from the *Morpho* package (185). Generalised Procrustes superimposition involves the mitigation of size, retained as centroid size for reintroduction later, translation of all configurations about the origin, and finally rotation that aligns corresponding homologous landmarks. The symmetric component of the data was extracted using functions from the *Morpho* package, as evaluation of asymmetry was beyond the scope of this analysis.

The individuals sampled in this investigation possessed a variety of dental states, including complete edentulism. A record of the number of teeth that each specimen possessed was taken using binomial scoring. Zero (0) was scored if teeth

were lost antemortem as evidenced by blunting of the alveolar crests or the presence of marked bone resorption. One (1) was scored if teeth were present or were lost postmortem. The significance of the effect of tooth loss on morphology was therefore tested. Permutation tests revealed a significant covariation between tooth loss and cranial morphology ($RV = 0.06$, $p < 0.001$), and hence, a two-block PLS analysis was run. These results were used to correct for the effects of tooth loss using a modification of Burnaby's (140) method. The residual effects of tooth loss on size were mitigated by regressing size (dependent factor) against the dental scores (independent) and adding any residual variation to the mean size that was not accounted for by the model. The age effect was similarly corrected using Burnaby's method.

Finally, size was reintroduced into the data by multiplying individual sizes by centroid size retained following Procrustes superimposition. This allowed the data to approximate traditional metric data.

5.2.3.2 Sample interlandmark distances

The purpose of this investigation was to determine, mathematically, the ILDs with the most discriminatory power given the set of landmarks collected. As the relative position of all homologous points to each other is retained by the Euclidian coordinates, it is possible to calculate the distance between points using Pythagorean geometry. In this case, the built-in *R* function *dist* was used to calculate ILDs between each of the 45 landmarks, resulting in a total of 990 ILDs. The ability of each ILD to estimate sex was tested using logistic regression (using *R*'s *predict* function from the *stats* package), and linear discriminant analyses (using the *lda* function from the *MASS* package). Finally, the ILDs were ranked in order of greatest predicting power and the top 17 were tabulated (Table 5.2), together with their sexing accuracy achieved using LR and LDA and univariate descriptive statistics.

5.2.3.3 Published interlandmark distances

A total of 17 previously published, commonly used ILDs were chosen to compare to the accuracies of all possible attainable ILDs. These distances were chosen as they are easily attainable from the current set of 3-D landmarks and they are currently measured when constructing biological profiles in South African forensic cases. They have been extensively used by previous authors when creating population-specific discriminant functions and are largely based on traditional ILDs

described by Martin and Saller (186) and Giles and Elliot (171). These ILDs are listed in Table 5.2 together with their sex prediction accuracy, as determined from the current dataset.

5.2.3.4 Validation of 3-D derived interlandmark distances

In order to validate the use of the 3-D derived ILDs and to compare their accuracy with ILDs acquired using the traditional calliper method, 3-D ILDs similar to the those used by Steyn and İşcan (1) were derived. Table 5.1 shows a comparison of the subset used in this study and those from Steyn and İşcan (1), and highlights the measures that varied due to differences in data capture methods. Direct descriptive analyses mimicking those employed by Steyn and İşcan (1) were then conducted and a comparison of the results are shown in Table 5.1. Using a Chi-square test (187), the accuracies achieved by each of the functions derived by Steyn and İşcan (1) were compared to the equivalent function derived in the current investigation to determine whether any differences are statistically significant.

5.2.3.5 Cranial subset landmark selection

The total sample of 990 ILDs were filtered by subsection and ILDs in each region with sex estimation accuracies over 70%, as determined in *R*, were ranked in ascending order. A 70% cut-off was chosen as the inclusion criteria for 3-D derived ILDs to approximate the average sex estimation accuracy achieved using traditional measurements in isolation, despite the law requiring a minimum accuracy of 80% (41). In addition, functions derived from multiple measurements result in higher sex estimation accuracies than when using isolated measurements. Hence, a 70% cut-off takes potential increases in accuracy into account. Cranial data were subdivided into the following subsections: 1) Basicranium only; 2) Basipalate, comprising both basicranium and palate landmarks; 3) Zygoma; 4) Orbits; and 5) Nasomaxilla, comprising both nasal and maxillary landmarks. A breakdown of the specific ILDs used in each of these subsections, their sex estimation accuracy and other univariate descriptors can be found in Table 5.3: basicranium; Table 5.7: basipalate; Table 5.11: zygomatics; Table 5.15: orbit; Table 5.19: nasomaxilla; and Table 5.23: total cranium.

5.2.3.6 Discriminant analyses and discriminant functions

Traditional and 3-D derived cranial ILDs and each of the five subsets of 3-D ILDs (basicranium, basipalate, zygoma, orbit and nasomaxilla) were exported to create six individual spreadsheets of raw data. Each of these spreadsheets was then imported into *SPSS* (version 22). Descriptive statistics including the mean and standard deviation of each ILD were determined and an analysis of variance (ANOVA) was used to test whether the male and female means for each of these measurements differed significantly from one another. These results can be found in Table 5.3: basicranium; Table 5.7: basipalate; Table 5.11: zygomatics; Table 5.15: orbit; Table 5.19: nasomaxilla; and Table 5.20: total cranium. As equal variance and covariance matrices are an assumption of a discriminant analysis, a Box's M test was used to test the null hypothesis of equal population covariance matrices. In order to prove equal covariances, the p-value should exceed 0.001, thus failing to reject the null hypothesis. Following this, both direct and stepwise discriminant analyses were conducted using the *SPSS* system default that minimises Wilk's Lambda. During a direct discriminant analysis, all the chosen independent variables are entered into the function, each variable is assigned an unstandardised coefficient (i.e. weight), and a constant is derived such that the discriminant function is a straight line function, similar to simple linear regression. Raw measurements are multiplied by their respective assigned coefficients and the values are summed, together with the constant, resulting in a discriminant score. This score is then compared to a sectioning point calculated as the average of the means of the dependant variables, in this case the average of the male and female mean. If the discriminant score falls below the sectioning point the unknown individual is assigned as female and, if it lies above the sectioning point, it is assigned as male. The program also calculates standardised coefficients that indicate which independent variable contributes most to the final discriminant equation, and a structure matrix, which denotes the correlation of each independent variable with the final discriminant function. When analysing the data, consistency between structure matrix and standardised coefficient values should be assessed. These coefficients, together with the unstandardised coefficients for the direct discriminant analyses, can be found in Table 5.4: basicranium; Table 5.8: basipalate; Table 5.12: zygomatics; Table 5.16: orbit; Table 5.20: nasomaxilla; Table 5.24: total cranium.

Following the direct discriminant analyses, the data were also subjected to stepwise discriminant analyses in which variables were entered into the function one

at a time in successive steps. In each step, the current variable is compared to variables that came before and only the one that has the most significant effect on the final discriminant function is retained. In this investigation, the system default of minimising Wilk's Lambda and calculating F-ratios was used, with entry being set at $F = 3.84$ and removal at $F = 2.71$. These entry and removal values are *SPSS* pre-set values. Although few investigators specify the entry and removal values used in their respective studies, these were the values used when they did specify (188,189). Unstandardised and standardised coefficients, together with structure matrices, were also calculated during these analyses for each of the variables deemed most significant (Table 5.5: basicranium; Table 5.9: basipalate; Table 5.13: zygomatics; Table 5.17: orbit; Table 5.21: nasomaxilla; and Table 5.25: total cranium). Finally, a Chi-squared test was used to compare the sexing accuracies achieved by the "Cranium" function derived by Steyn and İşcan (1) to the accuracy of the "Total cranium" function derived in the current investigation.

5.2.3.7 Top cranial interlandmark distances and cranial discriminant functions

ILDs determined to have the greatest discriminatory power by stepwise discriminant analyses in each of the five cranial subsets were compiled to represent the top ILDs for the entire cranium. This method of choosing ILDs was used to overcome issues of multicollinearity between the top 20 ILDs. The subset of cranial ILDs was subjected to direct and stepwise discriminant analyses in order to create new discriminant functions and determine whether greater sexing accuracies are possible using these previously unexplored measures of the skull.

5.2.3.8 Validation of discriminant functions

All discriminant functions derived in this study were validated in a bi-step process similar to that used by Ogawa et al. (190): 1) Raw measures from each of the 227 specimens were substituted into the derived discriminant functions and the resulting discriminant score was used to estimate the individual's sex and compare it to the recorded sex, termed "Original" in the tables of discriminant accuracy. The discriminant accuracy is the percentage of the total sample correctly assigned. 2) Each of these results was cross-validated using the leave-one-out or "jack-knife" cross-validation procedure, in which the discriminant function is once again derived, but without including the specimen being assessed. This equation is then used to estimate

the sex of the specimen that was “left out” and the procedure is repeated for each of the 227 specimens. The resulting accuracy, termed “Cross-validated” in the accuracy tables, is the percentage of the sample for which sex was correctly assigned by the new function.

5.3 RESULTS

5.3.1 Three-dimensional Interlandmark Distance Validation

The aim of this section was to demonstrate the applicability of 3-D derived ILDs in forensic anthropology and to demonstrate their equivalence to those collected using callipers. Specific ILDs derived from 3-D Cartesian coordinates were used to create discriminant functions for the entire cranium, vault and face following procedures outlined by Steyn and İşcan (1). Landmarks were taken to approximate those in Steyn and İşcan as closely as possible but, as no mandibular landmarks were collected, no discriminant functions were created for this region. Specific differences in landmark placement are also highlighted in Table 5.1 and detailed below it. Table 5.1 also shows a direct comparison of the results achieved by Steyn and İşcan (1) using ILDs collected using callipers, and that of this investigation, which used 3-D derived ILDs.

From Table 5.1, it is apparent that the average sexing accuracy achieved by the current investigation was, on average, only 3.3% lower than that demonstrated by Steyn and İşcan (1). This demonstrates a high concordance between discriminant functions derived from ILDs mathematically obtained using 3-D landmark data and those that are traditionally measured, despite slight variations in landmark positioning and even omission of certain ILDs. The 3-D derived “Cranium” discriminant function fared worst on average at 80.2%, which is 5.5% lower than the traditional function. Using this function, males were misclassified more frequently than females, 78.9% versus 81.4% respectively. This misclassification rate also exceeds that of traditional ILDs (approximately 21.1% misclassifications, whereas the original function misclassified fewer at 13.6%). Females, on the other hand, were correctly assigned in 81.4% of cases using the 3-D derived function versus 85.1% using the original function. While the 3-D derived “vault” discriminant functions achieved 6.6% lower sex estimation in males, it achieved a marginally better accuracy in females at 81.1% versus 80.9%. On average Steyn and İşcan’s (1) original “Vault” function outperformed

the current method by 3.0%. When “face” discriminant functions were compared, both sexes were more accurately classified using the traditional discriminant functions, although the difference in the average accuracy was only 1.8%. Finally, “bizygomatic” breadth alone assigned on average 6.8% fewer individuals to the correct sex using the newly derived discriminant functions, despite males having a 1.3% greater classification accuracy. The discrepancy in the accuracy of this function between the sexes was much less pronounced using the new function though, with only a 2.0% difference in correctly assigned individuals as opposed to 10.1% noted previously. Despite the differences in accuracy between the functions derived in the two studies, a Chi-square test (187) revealed that none of these differences are statistically significant, reinforcing the equivalence of traditional and 3-D derived ILDs.

5.3.2 Traditional Interlandmark Distances and most accurate 3-D Derived Interlandmark Distances

Seventeen of the most commonly measured ILDs for sex estimation in South Africans were directly compared to a subset of the top 17 derived ILDs from the original sample of 990. This was done to determine the accuracy of traditional ILDs and was achieved using LR. The results are highlighted in Table 5.2. While the range of accuracies for the traditional ILDs ranges were from 52.9% to 79.3%, those of the 3-D derived ILDs ranged from 73.6% to 82.4%. Only 8 of the 17 traditional ILDs achieved above 70.0% sex estimating accuracy compared to 582, or 58.8%, of the total 3-D derived ILDs, using LR. Additionally, only four of the traditional ILDs, including maximum cranial length, bizygomatic breadth, cranial base length and maximum cranial length, feature in the top 17. The most accurate of the 3-D ILDs, a measure from glabella to porion, was 3% more accurate at sex estimation when analysed in isolation compared to maximum cranial length, the most accurate traditional measure. Additionally, 126 of the 3-D derived ILDs scored 77.0% or above, the accuracy of the second leading traditional ILD.

It is important to recognise that 3-D derived ILDs are not an exact replica of traditional ILDs measured using callipers, as they are exclusively taken between homologous landmarks. This is illustrated by the fact that bizygomatic breadth provided the greatest discrimination between the sexes in Steyn and İşcan (1) (80.0% average), but maximum cranial length fared best using 3-D derived ILDs (78.0%).

Regarding the different accuracies provided by LR relative to LDA, the two techniques appear highly correlated with minimal difference in their sex estimation ability when using isolated measures. The difference in accuracy between LR and LDA ranged between 0.0% and 1.8% for the traditional ILDs (mean 0.2%) as well as for 3-D derived ILDs (mean 0.2%). In total, 70.6% of the 17 traditional ILDs displayed no difference in sex estimation ability between LR and LDA, while this was true for 40.1% of 3-D derived ILDs.

5.3.3 Individual Subset Discriminant Analyses

The results reported in the following five subsections (5.3.3.1 to 5.3.3.5) were obtained by filtering the entire body of 990 ILDs by the landmarks that comprise the subset in question and then selecting only measures with sexing accuracies of over 70.0%. Duplicate ILDs, which appear between identical landmarks on opposite sides of the face, were then removed using filtering. Finally, the data were subjected to univariate and multivariate statistical analyses, the results of which are detailed below in three parts for each of the subsets. The first section details both univariate statistics and direct discriminant analyses including the mean, standard deviation, Wilks' Lambda and F-ratio for each of the most accurate ILDs. Sex estimation accuracies, as determined using both LR and LDA, are also included. The second section outlines the stepwise discriminant analysis outcomes including coefficients, centroids and sectioning points for discriminant functions using only the most accurate ILDs as determined by stepwise discriminant analyses. Finally, discriminant accuracies are addressed by directly comparing the accuracies of the discriminant functions derived by both direct and stepwise methods.

5.3.3.1 Basicranium

Univariate Statistics and Direct Discriminant Analyses

Univariate statistics and direct discriminant results are detailed in Table 5.3. A total of five ILDs in the basicranial region provided sex discrimination accuracies above 70.0%. All of these measures span between the mastoid process and other basicranial landmarks such as basion (ba), the posterior occipital condyles (poc) and the inferior vomer (iv). A range of 70.0% to 73.6% (mean = 71.6%) accuracy was achieved for isolated ILDs in the basicranial region, with mastoid to basion (ms-ba) proving most accurate. Two of the five measures are contralateral (on opposite sides of the

cranium), while the other three are ipsilateral (on the same side of the cranium). All group means were significantly different ($p < 0.001$) and Box's M test indicated that population covariance matrices are equal ($p < 0.341$). When LR and LDA are compared the average difference in accuracy between the methods is 0.0%.

Unstandardised and standardised canonical coefficients, as well as structure matrices, are presented in Table 5.4. From the standardised coefficients, it is evident that the ILD from mastoid to inferior vomer (ms-iv) was the greatest contributor, despite not being the most accurate. The structure matrix value, however, demonstrates that ms-ba has the highest correlation with SxD (0.977). In LDA, the unstandardised coefficients are superficially comparable to beta-weights used in linear regression as they represent the fraction of the raw value measured for each of the respective ILDs, which are summed to calculate the discriminant score using the following equation:

$$DS = \beta_0 + \beta_1X_1 + \beta_2X_2 + \beta_3X_3 \dots + \beta_nX_n$$

where DS is the discriminant score, β_0 is the constant, β_1 to β_n are unstandardised coefficients, and X_1 to X_n represent the raw ILD measure. The calculated discriminant score is then compared to the sectioning point, also quoted in Table 5.4, and the specimen is designated female if the score lies below the sectioning point and male if it lies above.

Stepwise Discriminant Analyses

The five ILDs used in the direct discriminant analysis was then subjected to stepwise discriminant analyses the results of which, including the unstandardised coefficient, constant, group centroid and sectioning point, are summarised in Table 5.5. This analysis involved a single step as only the ILD ms-ba was retained for the calculation of the discriminant score. Covariance between the male and female ms-ba measure was equal ($p < 0.341$), according to Box's test.

Discriminant Function Accuracies

Table 5.6 summarises the accuracies of both the direct and stepwise methods. Regarding the average accuracies, it is evident that despite both direct and stepwise *original* accuracies being 74.0%, the direct accuracy suffers a 1.3% decline once cross-validated. Hence, using only a single ILD and the stepwise method, in the case of the basicranium, provided more accurate sex assignment than using all of five the

original ILDs. In all analyses, females classified with greater accuracy than males. Cross-validation of direct discriminant results in females caused a greater decline in accuracy than in males, however, this was not the case when applied to stepwise analysis, as it had no effect on the function's discriminatory power in either group.

5.3.3.2 Basipalate

Univariate Statistics and Direct Discriminant Analyses

In the case of the basipalate, a total of 23 ILDs were capable of discriminating sex with an accuracy of at least 70.0%, despite the addition of only five additional landmarks to the basicranium subset. Univariate statistics, as well as a comparison of the sex estimation accuracy of LR and LDA, can be found in Table 5.7. Of the 23 ILDs originally selected, only 19 were entered into the direct discriminant analysis, the remainder were highly correlated (multicollinear). The lower limit of the range of sex estimation accuracies in this subset was 70.0%, as in the basicranium, however, the upper limit was 3.5% greater at 77.0%. The distance between the palatine foramen and mastoid process on contralateral sides of the cranium (pf_rt-ms_lt) was the most dimorphic measurement. Nearly half of the ILDs in this subset (48.0%) were measured from the mastoid process. The ANOVA was significant for every ILD ($p < 0.001$) and a Box's M test showed that the samples possessed equal covariance matrices ($p = 0.582$). Finally, a comparison of the results produced by LR versus LDA proved LR to be less than 0.1% more accurate when applied to isolated ILDs. Standardised, unstandardised, and structure matrix coefficients, as well as other variables required to construct a discriminant function from the direct discriminant analyses, are presented in Table 5.8. While the anterior palate to nuchal crest measurement (aic-nc) contributed the most to the function, as indicated by its standardised coefficient, the structure matrix showed that pf_rt-ms_lt is most strongly correlated with SxD (0.721). This result is in line with the fact that pf_rt-ms_lt was also the single most accurate ILD in the basipalate subset.

Stepwise Discriminant Analyses

All ILDs that were retained in the direct discriminant analysis were then entered into a stepwise discriminant analysis. Only four of the original 18 ILDs were used in the stepwise discriminant function. Variables pertaining to this discriminant function are outlined in Table 5.9 and include: a diagonal measure from the posterior palate to

the mastoid process (pf_rt-ms_lt), posterior palate to pmuchal crest (pf-nc), mastoid process to anterior palate ipsilaterally (ms-anic) and across the length of palate (poic-iv). No significant difference was present between the covariance matrices of these ILDs as demonstrated using Box's M test ($p = 0.493$).

Discriminant Accuracies

Table 5.10 details the accuracies of the different discriminant methods. Similar to the results seen using basicranial landmarks only, the more parsimonious stepwise discriminant analyses proved more accurate with an average of 80.2% of individuals being correctly classified, as opposed to 78.0% using the direct method. Cross-validation caused a drop in accuracy across the board, although the effect was more pronounced when using direct discriminant analyses. Females were once again discriminated with greater accuracy than males, on average (83.0% vs 78.0% respectively).

5.3.3.3 Zygomatics

Univariate Statistics and Direct Discriminant Analyses

The zygomatics represent the largest subset of ILDs analysed in this investigation, with 29 ILDs having sex prediction accuracies over 70.0%. Only 13 of these were analysed in the direct discriminant analysis. The rest were omitted due to multicollinearity. Direct discriminant analysis results, together with other univariate data, are presented in Table 5.11. All male variables proved significantly larger than those of females ($p < 0.001$), whilst all covariance matrices proved comparable by Box's M test ($p = 0.385$). Individual ILD accuracies (analysed using LR) ranged between 70.1% and 79.3%, with three transverse measures spanning the opposite zygomatics (pz_rt to po_lt, sz-rt to po_lt and sz_rt to ge_lt) proving most dimorphic. Results derived using LR and LDA show high levels of concordance with the average difference in accuracy between the techniques in this subset measuring only 0.4%, in favour of LR.

The direct discriminant constant, coefficients, sectioning point and group centroids for the 13 ILDs that were entered into the analysis are presented in Table 5.12. Standardised coefficients show that sz_rt-pz_lt contributes the most to the equation, whilst sz_rt-po_lt was the most highly correlated with sex.

Stepwise Discriminant Analyses

Following the stepwise discriminant analysis, only two of the 13 ILDs were retained for the resulting discriminant function. Their covariance matrices were comparable ($p= 0.894$). These include sz_rt-po_lt, a measure traversing both zygomatics and the most accurate sex discriminator as determined by LR, and sz-zm measured across a single zygoma and the least accurate measure entered into the direct analysis. Details regarding the discriminant function, including the constant, coefficients, sectioning point, and group centroids are displayed in Table 5.13.

Discriminant Accuracies

Table 5.14 shows a comparison of the accuracies of the discriminant functions detailed above, both original and cross-validated. The average cross-validated, stepwise discriminant accuracy once again proved most accurate with 82.4% of individuals correctly assigned. Interestingly, males classified more accurately than females when subjected to direct discriminant analysis, whilst females were more accurately assigned using stepwise procedures. Cross-validation of the results caused a drop in discriminant accuracies when applied to functions derived using the direct method, but those derived using stepwise methods remained unaffected.

5.3.3.4 Orbit

Univariate Statistics and Direct Discriminant Analyses

Only two ILDs in the orbit subset were deemed accurate enough to be subjected to discriminant analyses: interorbital breadth (d-d) and dacryon to frontomolare temporale (d-fmt) on the contralateral side. Both had accuracies in the low 70's (71.8% and 70.0% respectively). These and other univariate results are presented in Table 5.15. The ANOVA tests showed that male mean values were statistically larger in both cases ($p < 0,001$) and Box's M test showed that they had equal covariance matrices ($p= 0.195$).

Results of the direct discriminant analysis of these ILDs are given in Table 5.16. The table shows that all d-d coefficients are larger than those for d_rt-fmt_lt and contains variables required for the construction of a pertinent discriminant function.

Stepwise Discriminant Analyses

Stepwise analysis of the variables produced a function with only a single ILD, d-d. This, together with other stepwise discriminant function data for the orbits, are presented in Table 5.17.

Discriminant Accuracies

The accuracy of both direct and stepwise analysis of ILDs measured between orbital landmarks are in Table 5.18. The function produced using stepwise discriminant analysis was able to assign 69.3% of males correctly versus 67.5% using direct methods. Although female orbits were more precisely assigned, the method used to derive the function made no difference. Additionally, cross-validation did not affect the accuracy of either function independent of the sex it was applied to.

5.3.3.5 Nasomaxilla

Univariate Statistics and Direct Discriminant Analyses

Nasomaxillary ILDs are representative of the landmarks of both the nasal aperture (nariale (na), alare (al), and rhinion(r) and surrounding maxillary structures that are adjacent to the zygomatics (zygomaxillare (zm) and zygomaxillare orbitale (zmo) and orbits (dacryon (d). Thirteen ILDs with sex discrimination accuracies of over 70.0%, including the traditional measure interorbital breadth, were subjected to univariate and direct discriminant analyses. These results are provided in Table 5.19. Almost half (45.0%) of these measurements included midline landmarks. All measurements of male crania were statistically larger ($p < 0.001$) and LR estimated sex with accuracies between 70.5% and 78.9% from these isolated measures. Covariance matrices were again determined to be equal using Box's M tests ($p = 0.058$). Finally, the ability of LR and LDA to assign sex were assessed and only a minimal difference of 0.2% accuracy in favour of LDA was found.

All 13 ILDs were included in the direct discriminant function. The constant, coefficients, group means and sectioning point are highlighted in Table 5.20. Standardised coefficients indicate that a measure from the inner orbit to nasal spine (d-ins) was the most highly weighted in the function, whilst structure matrices suggested that both na_rt-d_lt and al_rt-d_lt were most highly correlated with sex. Despite this, na_rt-d_lt proved 3.5% more accurate than al_rt-d_lt, despite the apparent similarity between the two measurements.

Stepwise Discriminant Analyses

The ILDs were subjected to stepwise discriminant analyses to refine the function by removing redundant, collinear measures. Five dimensions that possessed equal covariance matrices ($p = 0.156$) were retained for the stepwise function, including the traditional interorbital breadth measure (d-d). In this function, standardised and structure matrix coefficients indicate that d-ins is most highly correlated with sex and also contributes most to the function derived. These results, as well as other parameters of the stepwise function, are found in Table 5.21.

Discriminant Accuracies

Table 5.22 shows a comparison of the accuracies of the direct and stepwise discriminant functions as they were derived originally, and following cross-validation. In this subset, males classified with greater accuracy when the stepwise discriminant method was employed, whilst females classified with greater accuracy using direct discriminant analysis. This finding was unique to the nasomaxillary subset. However, following cross-validation, the stepwise function proved the most accurate on average, surpassing the direct function by nearly 4.0% despite utilising eight fewer ILDs.

5.3.4 Cranial Interlandmark Distances and Discriminant Functions

5.3.4.1 Direct discriminant analyses

As stepwise discriminant analysis was determined not only to be the most parsimonious means of ILD selection, but also the most accurate, all ILDs retained during the stepwise analyses of the subsets were compiled to represent the entire cranium. This subset of 12 ILDs, together with the top two ILDs gleaned from the LR (Table 5.2) but not included in the subset data, were subjected to univariate analyses and then entered into direct discriminant analysis. The means of all male and female ILDs were found to be significantly different using an ANOVA ($p < 0.001$), whilst Box's M tests showed that their covariance matrices were comparable ($p = 0.452$) (Table 5.23). Individual accuracies for the ILDs chosen to represent the cranium as a whole ranged between 70.0% and 82.4%. The measure between porion and glabella (po-g) was the most accurate followed by the traditional measure of maximum cranial length taken between opisthocranium (represented by nc in the current investigation) and glabella (g).

Table 5.24 provides the constant, coefficients, group centroids and sectioning point for the function. Based on the standardised coefficient values, d-ins contributes the most to the function, whilst nc-g was most correlated with sex.

5.3.4.2 Stepwise discriminant analyses

The 14 selected cranial ILDs were entered into a stepwise discriminant analysis that refined the measures to a total of seven all-encompassing cranial ILDs. These are presented in Table 5.25 together with coefficients and other parameters required to construct the discriminant function. A Box's M test revealed that the covariance matrices of these measures were equal ($p= 0.609$). Interestingly, three of these measures (including maximum cranial length (nc-g), interorbital breadth (d-d), and nasal height (n-ins) are traditional ILDs that have been used for decades (171). Additionally, the standardised coefficients reveal that nc-g correlates most strongly with sex, whereas the novel measurement between dacryon and the inferior nasal spine (d-ins) was most highly weighted in this function.

5.3.4.3 Discriminant accuracies

Original and cross-validated accuracies of both the direct and stepwise discriminant functions are presented in Table 5.26. They reveal that stepwise analyses outperform direct analyses, at least with regards to sex estimation from cranial landmarks. On average, 88.2% of individuals were assigned to the correct sex using only seven ILDs and the discriminant function below:

$$DS = -25.24 + 0.085X_1 + 0.119X_2 + 0.145X_3 + 0.358X_4 + 0.128X_5 \\ + (-0.214)X_6 + (-0.158)X_7$$

Where **DS** is the discriminant score that indicates female if smaller than the sectioning point and male if greater (Table 5.25), X_{1-7} measured variables are defined in Table 5.25.

Following the pattern seen in most of the subsets, females were classified with greater accuracy than males, independent of the discriminant method used. Cross-validation led to a slight decrease in accuracy, however, the stepwise method still outperformed the direct method in terms of accuracy in all cases.

5.4 DISCUSSION

The current chapter of this thesis assessed the efficacy of all possible cranial ILDs, derived from digitiser-acquired coordinate data for estimating sex in a white South African population. It also attempted to validate the use of 3-D derived ILDs using previously published discriminant functions and finally, to derive new discriminant functions using the most accurate, custom ILDs for both intact and fragmentary crania. Results indicate that the novel 3-D derived ILDs outperform some commonly used measures. Additionally, 3-D derived discriminant functions compared well with traditional cranial measures as this study achieved comparable sexing accuracies using 3-D derived discriminant functions. All differences between the sexing accuracies achieved in the current investigation and those derived previously (1) were proven to be insignificant. Newly created cranial discriminant functions achieved high sexing accuracies and offer five new functions that are applicable to fragmentary remains.

In recent years, the number of studies that derive morphometric data from digital datasets has steadily increased, with numerous investigators obtaining ILD data from CT scans (183,191,192) and digitiser-acquired Cartesian coordinate data (2,37,51,52,63,71,172,193). The current investigation derived all possible ILDs, a total of 990, from 45 3-D data points and assessed each individual measure's ability to assign sex using both LDA and LR. The accuracy of the top 17 ILDs ranged from 73.6% to 82.4% (mean = 77.3%), in contrast with the 17 common traditional ILDs assessed that had accuracies ranging between 52.9% and 79.3% (mean = 66.9%). Three of the most commonly measured cranial ILDs (foramen length and breadth and maxillo-alveolar length) performed only slightly better than chance (56%-59.5%), while less than half of the subset predicted sex with accuracies greater than 70%. In comparison, not only were all the top 17 ILDs able to predict sex with over 70% accuracy, but a total of 580 (58.8%) measures derived in this study could do so. Four of the top ILDs correspond to commonly-measured traditional ILDs. These include maximal cranial length, bizygomatic breadth, cranial base height and opisthion to glabella. The single most accurate measure in the current study was taken from glabella-porion (82.4%) and closely approximates the novel measure glabella-zygion (87.5%-88.0%) found to be the most accurate in Franklin et al.'s (194) investigation of Western Australians (194). These results suggest that the most accurate measures in

the current research should be used to supplement traditional cranial measures, rather than replace them, at least when applied to white South Africans.

The methods employed in this investigation modelled that of Franklin and colleagues' (2) investigation on SxD in South African black individuals, chronicling the morphology of this population using GMM (2). In their work, the authors used Pythagorean geometry to derive ILDs that approximate traditional cranial measures. Our investigation shares an additional similarity with Franklin and colleagues' (194) study of the crania of Western Australians that also used 3-D derived ILDs, in that it also determined novel measures with high sex allocation accuracies (194). Since then, a number of other investigators have used similar methods of practically employing GMM through derived ILDs, including McDowell and associate's (164) investigation of nasal size and shape in black and white South Africans (164); L'Abbé and associates' (52) test of the precision of the forensic anthropology statistical package FORDISC 3 when applied to black and white South African cranial measurements in the context of sex and ancestry estimation (52); Franklin and colleagues' (183) assessment of SxD in Western Australians; and McDowell and colleagues' (172) study that elucidated mid-facial differences between South African populations.

5.4.1 Three-dimensional interlandmark distance validation

This study derived discriminant functions from the 3-D ILDs and compared them with the Steyn and İşcan (1) analysis of white South Africans. The purpose of this was twofold; 1) to validate the use of 3-D derived ILDs for sex estimation in white South Africans; and 2) determine whether adapting traditional cranial discriminant functions for 3-D ILDs would negatively impact sex estimation accuracies. An average decline in accuracy of only 3.4% using was achieved using the functions derived in this investigation, compared to Steyn and İşcan's (1). The accuracy of the "Cranium" function derived from 3-D data had the highest drop in accuracy. A decline of 7.5% was noted in males, and 5.5% (to 80.2%) on average. This was expected as the measure from basion to bregma was omitted in the current investigation due to the exclusion of the cranial vault. The "Face" function was most similar between the two investigations, with only a 1.8% drop in accuracy in the 3-D derived function. This was somewhat surprising as two of the three ILDs used to create the current function had to be modified slightly to suit the 3-D landmarks available. These modifications were

necessary to approximate the landmarks used in traditional cranial measurements. These results demonstrate that the landmarks used in this study to approximate those in Steyn and İşcan's study are a good match. The "Vault" function had a decline in sexing accuracy of 3%, however, despite the fact that the 3-D ILDs were identical between two studies. The ability of the "Vault" function to assign sex in females was nearly identical, however (0.2% increase in accuracy). This suggests that the female sample in the two studies was more similar than the male sample. These difference proved insignificant when tested using a Chi-square test.

Finally, the sex bias between the studies (defined as the male percent accuracy minus the female percent accuracy for any given function) was compared. The average bias in the current study was 2%, compared with 5% in Steyn and İşcan's analysis (1). The most notable bias was observed in Steyn and İşcan's (1) "Bizygomatic" function, in which females classified with 10% greater accuracy than males (85.1% versus 75%). The same function produced a much lower bias of 2% (in favour of females) in the current study. Once again, the differences proved not to be statistically significantly different. Possible reasons for the differences include a larger sample size in the current study (227 individuals versus 91 individuals), variations in the age of the specimens between the samples (♂ 63 years, ♀ 65 years in the current investigation versus ♂ 65 years, ♀ 67 years in Steyn and İşcan (1), and the asymmetry tooth loss corrections in the current study. Any of the aforementioned reasons, but especially the asymmetry and tooth loss corrections, could have resulted in a larger average bizygomatic breadth measure in females, and hence fewer correct classifications. Despite being counterintuitive, this represents a positive outcome of tooth loss correction. This is because the correction may have mitigated the effect of bone resorption, which may have been the cause of the smaller measures in females. Furthermore, a low sex bias is favourable, especially in bioarcheology as pointed out by Walker (42), as it limits erroneous conclusions about the distribution of the sexes in burial or disaster sites.

5.4.2 Traditional Interlandmark Distances and most accurate 3-D Derived Interlandmark Distances

A measure of the distance between each of the 45 homologous fixed landmarks produced a total of 990 unique, non-repetitive ILDs. Both LDA and LR were then

applied to each of these measures to determine the difference in sex estimation accuracy between them. LDA is the most commonly used statistical method by which anthropologists assess population and sex differences (6). Assumptions of the technique include, amongst others, that all variables be normally distributed, have equal covariance matrices, be uncorrelated with one another, and that there be less predictor variables than the sample size (71). When large subsets of variables are assessed, such as in the current investigation, testing for normality of each of these variables becomes impractical and therefore it becomes important to consider alternative means of assessing independent variables. LR offers an ideal alternative as it is less constrained by assumptions and can be applied to nonparametric data, whereas, in instances of non-normality, LDA negatively impacts the fit of the model and its prediction capabilities, even in large samples (195). When using LDA, violation of the assumption of normality can attribute false significance to variables that are then erroneously included in discriminant functions, even with infinitely large samples. LDA is not appropriate when the independent variables are binary, such as in qualitative data (195).

In this investigation, each individual ILDs sex assignment potential was assessed independently and in the context of cranial subsets. A very high correlation between the methods was found in all cases with a maximum difference of 1.76% seen for isolated measures. Concordance between the methods was highest in the basicranium with no difference on average between the methods. For the basipalate, the result was less than 0.1%, for the global cranial measures, 0.16%, and for nasomaxilla, a 0.2% difference on average. A maximum average difference between LDA and LR was demonstrated in the zygomatics and orbits, both at 0.4%.

LR was more accurate for all subsections except the nasomaxilla, suggesting that at least some of the variables in the current investigation may have a nonparametric distribution. These differences cannot be attributed to unequal covariance matrices because Box's M test demonstrated that all covariances were homogenous during the discriminant analyses. The use of LR in deriving skeletal standards is becoming increasingly commonplace due to its robustness, a lack of underlying assumptions and the ease with which it can be applied to dichotomous variables (167,196–199). Lei and Koehly (48) did a comprehensive analysis of the difference in classification accuracy between LDA and LR with regards to a number of data parameters including 1) the degree of group separation, 2) covariance equality;

3) sample size and 4) cut score. They found that there is a complicated interplay between the above-mentioned factors and prediction accuracy, and concluded that the research question being addressed may be more important than the data distribution when deciding between LDA and LR (48). Pohar and colleagues (173) demonstrated that LDA performs better when the data are normally distributed, but that the predictive power of the methods become more similar as sample size increases to over 50 specimens due to the fact that the data approach normality. LDA also performed better on greater than three categorised variables, whereas LR had a greater predicative power in cases of less than three variables. Both the population group and sex to which the method is applied may also affect its accuracy, as demonstrated by Shah et al. (200). They found that LR displayed greater predictive accuracies in males, whereas LDA fared better in their female counterparts, although the accuracy of LR was found to be greater overall. Additionally, Dong et al. (62) found that while LDA had a greater predictive accuracy, LR has a lower sex bias when applied to Chinese mandibles. Overall, these studies suggest that LDA performs better when the dataset is normally distributed and includes a relatively low number of samples, whereas LR is more robust due it is not subject to as many assumptions. These findings are corroborated by our results. Even so, they offer only a cursory look at these multivariate statistical techniques. Despite this, our results suggest that, in the current investigation, the difference between them is sufficiently small to warrant the use of LDA for the derivation of discriminant functions. The large sample size used in the current investigation likely resulted in the equivalence between LR and LDA demonstrated.

5.4.3 Global Cranial and Individual Subset Discriminant Analyses

The final aim of this investigation was to derive discriminant functions for both fragmentary remains and the cranium as a whole. The cranium was divided into five regions (basicranium, basipalate, zygoma, nasomaxilla and orbits) and both direct and stepwise analyses were conducted on all regional ILDs that provided sexing accuracies greater than 70%. Due to the incidence of corpse maiming, scavenger activity, fires and explosions, the need for anthropological standards that can be applied to fragmentary remains is of paramount importance (2,4,161). This is particularly true of crania in South African as they are the most frequently recovered

skeletal element (164). While numerous publications can be applied to sex estimation of fragmentary remains, none have derived functions specifically for this purpose (5,201–203). The current study also used the most statistically accurate ILDs for each region. This approach enhances the applicability of the functions not only due to their accuracy, but also because they are tailor-made for each region, thus, increases the number of cases in which they may be applicable. In the current study, stepwise discriminant analyses proved more accurate and more parsimonious than direct discriminant analyses. Leave-one-out-cross-validation was used to validate sexing accuracies, and hence reduce bias, as the case being classified is left out when the function is derived. The effect of cross-validation on the derived accuracies was, however, very slight with only the nasomaxillary and overall cranial function showing any decline (0.9% and 0.8% respectively), pointing to the efficacy of the functions.

Across the five regions, the discriminatory ability of the functions ranged from 71.8% for the orbits to 83.7% for the nasomaxilla. A combination of the most accurate ILDs from each region provided 88.2% sexing accuracy for the cranium as a whole, which is well above the 80% level dictated by the Daubert criterion.

5.4.3.1 Basicranium and basipalate

The functions for the basicranium and basipalate were derived to create an equation for situations where damage to basicranial or palatal landmarks could prohibit the application of available standards. A function for the palate alone was not provided, however, as none of the ILDs from this region made the cut-off of 70.0%. Interestingly, a large difference in accuracy was found between the equations, with the basicranium function sexing 74.0% of the sample correctly, as opposed to 80.2% using the basipalate function. These results demonstrate the advantage of assessing individual regions in isolation. Our results compare well with that of Suazo et al. (152) who assessed Brazilian skull bases and attained sexing accuracies of 75.5% from palatal measurements. Our results did however provide better results than those of Lima et al.'s (167) investigation of Brazilian skull base and palate measurements (63.0% to 65.0%). These studies illustrate the discriminatory power of palatal measures as opposed to basicranial measures when estimating sex.

5.4.3.2 Orbit

Despite the orbit having the lowest discriminant accuracy of the five regions investigated (71.8%), the single measure used to derive the orbit function (interorbital breadth) still provided a superior classification accuracy to two-thirds of commonly used traditional measures. This result is similar to that of Bigoni et al.'s (63) analysis of Central Europeans in which 74% of individuals were correctly assigned based on orbit structure, and it falls on the lower end of the range (73.3%-80.0%) attained by Pretorius et al. (69) in their investigation of black South Africans.

5.4.3.3 Zygomatics and nasomaxilla

The functions attained for the zygomatic and nasomaxillary regions provided high sexing accuracies of 82.4% and 83.7%, respectively. Despite the subsets sharing some common landmarks, the discriminant functions have no ILDs in common. Previous studies attained accuracies ranging between 78.0% and 90.0% using bizygomatic breadth. It was found to be the most sexually dimorphic measurement in each of the following populations: white (1,5) and black South Africans (2,4), Cretans (188), Australians (183), Japanese (190), and Gujarati Indians (184). For this reason, high discriminatory accuracies were expected when assessing this region. The favourable results obtained from the nasomaxillary functions (83.7%) were, however, surprising. McDowell and associates (164,172) studied the region in great detail in three South African populations using ILDs derived from 3-D data. They found that while size differences exist in this region between the populations, shape dimorphism was relatively low, citing accuracies of 65.9% for males and 71.4% for females (164,172). In their analysis of Central Europeans using GMM, Bigoni et al. (63) achieved significantly better sexing accuracies in this region of 76.8% in females and 77.4% in males. Bastir et al. (27) described dimorphism in the midfacial region and postulated that these differences may be as a result of larger airways in males as a response to greater energy requirements. The current investigation's accuracies of 84.2% in males and 83.7% in females outweighs the results obtained from the same population in McDowell's (164,172) investigation. This is a testament to the benefits of the novel ILDs derived in this investigation, as well as the benefits of a larger sample size, and finally, mitigation of the effects of tooth loss inevitably present in the aforementioned studies.

5.4.3.4 Total cranial function

The benefits of deriving novel 3-D ILDs are also exemplified by the high classification accuracies attained by the total cranial formula in this study ($\text{♀} = 90.3\%$, $\text{♂} = 86.0\%$, cross validated). The 88.2% aggregate accuracy is slightly higher than that of Steyn and İşcan's (1) cranial function (86.0%) as well as that of Robinson and Bidmos' (5) validation of the aforementioned function (87.8%), although not significantly so. Our results fall well within the accuracies seen in South Indians: 85.7% (204); Gujarati Indians: 88.7% (184); Western Australians: 90.0% (183); Cretans: 88.2% (188); black South Africans: 77.0%-85.0% (4,51); and Americans: 86.6% (205).

5.5 CONCLUSIONS

The need for population-specific standards for the estimation of sex is well established. Anthropologists are constantly developing new standards for various skeletal elements and validating established ones, however, there remains a paucity of research exploring variation in white South Africans. This investigation helps to fill the void by using white South African cranial data in which the effect of tooth loss was controlled for. This vastly increased the number of specimens available for study from this underrepresented population group. A sample of 227 specimens was used to develop a new, more accurate set of discriminant functions for estimating sex from white South African crania, ultimately demonstrating 88.2% average accuracy. In addition, functions were specifically formulated for fragmentary remains with accuracies ranging from 74.0% to 83.2%. This research did not, however, rely on traditionally defined interlandmark distances, but instead used GMM to derive new measures of superior accuracy. Finally, this study emphasises the successful approach where the critical evaluation of accepted methodology is expanded through the application of new techniques of data capturing and analysis.

Table 5.1 Comparison of the sex estimation accuracy of the discriminant functions derived by Steyn and İşcan (S&I. 1998) (1) and the functions derived by the current investigation (Current) using 3-D derived interlandmark distances.

Discriminant functions	(S&I. 1998)	Current	(S&I. 1998)	Current	(S&I. 1998)	Current	(S&I. 1998)	Current
	ILD ^a	Abbreviation	Males		Female		Average	
Cranium	Bizygomatic ^b	sz_rt - sz_lt						
	Basion-nasion	ba - na						
	Nasal height	ins - na	86.4	78.9	85.1	81.4	85.7	80.2
	Cranial length	nc - g						
	Nasal breadth	na_rt - na_lt						
	Basion-bregma ^c	Not measured						
Vault	Cranial length	nc - g						
	Basion-nasion	ba - na	86.4	79.8	80.9	81.1	83.5	80.5
	Max. frontal br.	fmt_rt - fmt_lt						
Face	Bizygomatic ^b	sz_rt - sz_lt						
	Nasal height	ins - na	79.5	78.1	82.6	80.5	81.1	79.3
	Basion to prosthion ^d	ba - ins						
Bizygomatic	Bizygomatic ^b	sz_rt - sz_lt	75.0	76.3	85.1	78.3	80.2	77.3

^b sz_rt-sz_lt was used to approximate bizygomatic breadth as it was found to be the most accurate measure to traverse the zygoma.

^c As the callote was not measured in this investigation, this measurement was not included when the discriminant function for the cranium was assessed.

^d Prosthion (defined as the most anterior projection of the maxilla) is not a fixed landmark and was therefore not included in this investigation. Rather, Alveolare (ids) was included as an approximation of this measurement.

Table 5.2 Comparison of the accuracy of traditional cranial interlandmark distances with the most accurate interlandmark distances derived in the current investigation. Both logistic regression (LR) and direct discriminant function accuracies (LDA) are listed. Isp = ipsilateral; Cntr = contralateral.

Traditional interlandmark distances			Top 3-D derived interlandmark distances		
ILD	LR	LDA	ILD	LR	LDA
Max cranial length	79.30	77.53	Porion to glabella	82.38	82.38
Bizygomatic breadth ^b	77.97	77.53	Mastoid to superior zygotemporale (Cntr.)	81.50	81.06
Cranial base length	74.45	75.33	Glabella to mastoid	81.06	80.62
Opisthion to glabella	74.01	73.13	Max cranial length	79.30	77.53
Biauricular breadth	73.13	73.13	Nariale to dacryon (Cntr.)	78.85	79.30
Interorbital breadth	71.81	71.81	Alare to auricular eminence (Cntr.)	78.41	78.41
Nasal height	71.37	71.37	Rhinion to glenoidale	77.97	77.97
Basion to prosthion ^c	70.04	70.04	Dacryon to posterior zygotemporale (Cntr.)	77.53	77.09
Upper face breadth	68.72	68.72	Inferior vomer to rhinion	77.09	77.09
Biorbital breadth ^d	66.52	66.52	Palatine to mastoid	76.65	76.65

Table 5.2 (continued) Comparison of the accuracy of traditional cranial interlandmark distances with the most accurate interlandmark distances derived in the current investigation. Both logistic regression (LR) and direct discriminant function accuracies (LDA) are listed. Ips = ipsilateral; Cntr = contralateral.

Traditional interlandmark distances			Top 3-D derived interlandmark distances		
ILD	LR	LDA	ILD	LR	LDA
Upper facial height ^e	63.00	63.44	Pos. occipital condyle to zygomaxillare orbitale (Ips.)	76.21	76.21
Min frontal breadth	61.67	61.67	Frontozygomatic orbitale to mastoid (Ips.)	75.77	75.33
Nasal width	60.35	60.35	Inf. vomer to inf. nasal spine	75.33	75.33
Maxillo-alveolar length ^f	59.47	59.47	Bizygomatic breadth ^b	77.97	77.53
Foramen- Max breadth	58.15	58.15	Cranial base length	74.45	75.33
Foramen- Max length	55.95	55.95	Opisthion to glabella	74.01	73.13
Orbital breadth ^g	52.86	52.86	Basion to mastoid	73.57	74.01

^b sz_rt-sz_lt was used to approximate bizygomatic breadth, as it was found to be the most accurate measure across the zygoma.

^c Alveolare (ids) was included in this ILD to approximate prosthion, and defined as the most anterior projection of the maxilla. Prosthion is not a fixed landmark and was therefore not included in this investigation.

^d Biorbital breadth is traditionally measured from the point ectoconchion, which is refined as the intersection of the most anterior surface of the lateral border of the orbit and a line bisecting the orbit along its long axis, on either orbit. Frontozygomatic orbitale (fo) was used to approximate ectoconchion in this analysis.

^e Upper facial height was originally defined as a measure from nasion (n) to prosthion. Prosthion, which was defined as the most anterior projection of the maxilla, is not a fixed landmark and was therefore not included in this investigation. Alveolare (ids) was included in this ILD to approximate prosthion.

^f Maxillo-alveolar length was originally measured from prosthion to alveolon. In this study, palatine (p) was used to approximate alveolon and ids to approximate prosthion.

^g Orbital breadth was measured from dacryon to ectoconchion. Frontozygomatic orbitale (fo) was used to approximate ectoconchion in this analysis.

Table 5.3 Individual ILD sex estimation accuracies achieved by logistic regression (LR) and linear discriminant analyses (LDA), as well as univariate statistics including means, standard deviations (SD), Wilks' lambda and F-ratios for basicranial landmarks.

ILD	LR	LDA	Male		Female		Wilks' Lambda	F*
			Mean	SD	Mean	SD		
ms-ba	73.57	74.01	54.72	2.59	51.81	2.38	0.74	77.42
ms-ms	72.69	72.25	105.28	5.39	99.75	4.58	0.76	69.31
ms_rt-poc-lt	71.81	71.81	69.97	3.35	66.72	2.81	0.78	62.64
ms-poc	70.04	70.04	37.87	2.66	35.44	2.29	0.81	54.21
ms-iv	70.04	70.04	68.65	3.10	65.28	3.20	0.78	64.91

* Significant at $p < 0.001$

Table 5.4 Direct discriminant analysis function coefficients, group centroids and sectioning points for all basicranial interlandmark distances that achieved discrimination accuracies of 70.0% or above.

ILD	Standardised Coefficients	Structure Matrix	Unstandardised Coefficients	Group Centroids
ms-ba	0.366	0.977	0.147	M= 0.595
ms-ms	-0.215	0.924	-0.043	F= -0.601
ms_rt-poc-lt	0.324	0.879	0.105	
ms-poc	0.272	0.817	0.110	
ms-iv	0.374	0.894	0.119	
Constant			-22.55	
Sectioning Point			-0.003	

Table 5.5 Stepwise discriminant analysis results for the best basicranial interlandmark distances including coefficients, centroids and sectioning points.

ILD	Standardised Coefficients	Structure Matrix	Unstandardised Coefficients	Group Centroids
ms-ba	1.0	1.0	0.401	M= 0.581 F= -0.587
Constant			-21.390	
Sectioning point			-0.003	

Table 5.6 Comparison of sex estimation accuracies achieved using original and cross-validated basicranial discriminant functions (derived by both direct and stepwise procedures).

	Total N	Males		Females		Average %
		%	N	%	N	
<u>Direct</u>						
Original	227	71.9	82/114	76.1	86/113	74.0
Cross-validated	227	71.1	81/114	74.3	84/113	72.7
<u>Stepwise</u>						
Original	227	71.1	81/114	77.0	87/113	74.0
Cross-validated	227	71.1	81/114	77.0	87/113	74.0

Table 5.7 Individual ILD sex estimation accuracies achieved by logistic regression (LR) and linear discriminant analyses (LDA), as well as univariate statistics including means, standard deviations (SD), Wilks' lambda and F-ratios for basipalate landmarks.

ILD	LR	LDA	Male		Female		Wilks' Lambda	F ^β
			Mean	SD	Mean	SD		
pf_rt-ms_lt	77.09	77.09	91.75	3.70	86.94	3.69	0.70	96.17
ms-p	76.65	76.65	74.05	3.15	70.29	3.62	0.76	69.93
ms-pf	74.89	74.89	70.73	3.56	66.90	3.62	0.78	64.45
ms-b	73.57	74.01	54.72	2.59	51.81	2.38	0.74	77.42
pf-nc	72.69	73.13	131.95	5.54	125.17	5.93	0.74	79.20
poic-nc	72.69	72.69	162.19	6.53	154.73	6.81	0.76	70.93
ms-ms	72.69	72.25	105.28	5.39	99.75	4.58	0.76	69.31
pf-b	72.25	72.25	52.52	2.68	49.72	2.62	0.78	63.64
ms-poic	72.25	72.25	104.74	3.95	100.08	4.31	0.76	72.00
ms-anic	72.25	71.81	110.34	4.30	105.68	4.95	0.80	57.65
anic-nc*	71.81	71.81	168.88	6.71	161.47	7.21	0.78	64.40
aic-b	71.81	71.81	89.97	3.43	86.39	3.71	0.80	57.22
ms_rt-poc_lt	71.81	71.81	69.97	3.35	66.72	2.81	0.78	62.64
anic-iv	71.81	70.48	67.74	3.43	64.25	3.77	0.81	53.29
aic-iv	71.81	71.81	70.12	3.53	66.45	3.80	0.80	56.80
aic-nc	71.37	71.37	170.88	6.56	163.30	7.13	0.76	69.64
ms-aic*	71.37	70.93	111.99	4.30	107.17	4.90	0.78	62.03
aic-poc_rt	70.93	70.93	109.10	4.14	104.87	4.27	0.80	57.21
p-nc	70.04	69.60	122.62	5.46	116.60	6.08	0.79	61.53
ms-poc	70.04	70.04	37.87	2.66	35.44	2.29	0.81	54.21
poic-b*	70.04	70.04	81.15	3.36	77.72	3.27	0.79	60.98
poic-iv	70.04	70.04	60.57	3.49	56.85	3.60	0.78	62.49
ms-iv*	70.04	70.04	68.65	3.10	65.28	3.20	0.78	64.91

^β Significant at $p < 0.001$; *ILD's not entered into the direct discriminant function due to multicollinearity

Table 5.8 Direct discriminant analysis function coefficients, group centroids and sectioning points for all basipalate interlandmark distances that achieved discrimination accuracies of 70.0% or above.

ILD	Standardised Coefficients	Structure Matrix	Unstandardised Coefficients	Group Centroids
pf_rt-ms_lt	2.985	0.721	0.807	M= 0.898
ms-p	-0.149	0.615	-0.044	F= -0.906
ms-pf	1.039	0.591	0.290	
b-b	-1.916	0.647	-0.769	
pf-nc	2.836	0.655	0.494	
poic-nc	2.563	0.620	0.384	
ms-ms	-0.160	0.612	-0.032	
pf-b	-2.770	0.587	-1.046	
ms-poic	-3.417	0.624	-0.827	
ms-anic	1.383	0.559	0.299	
aic-b	2.954	0.556	0.827	
ms_rt-poc_lt	0.851	0.582	0.275	
anic-iv	-1.320	0.537	-0.366	
aic-iv	0.492	0.554	0.134	
aic-nc	-5.843	0.614	-0.853	
aic-poc_rt	-0.522	0.556	-0.124	
p-nc	0.406	0.577	0.070	
ms-poc	0.677	0.542	0.273	
poic-iv	1.338	0.581	0.377	
Constant			-24.500	
Sectioning Point			-0.004	

Table 5.9 Stepwise discriminant analysis results for the best basipalate interlandmark distances including coefficients, centroids and sectioning points.

ILD	Standardised Coefficients	Structure Matrix	Unstandardised Coefficients	Group Centroids
pf_rt-ms_lt	1.073	0.784	0.290	M= 0.827
pf-nc	0.378	0.711	0.066	F= -0.834
ms-anic	-0.745	0.607	-0.161	
poic-iv	0.541	0.632	0.153	
Constant			-26.002	
Sectioning Point			-0.004	

Table 5.10 Comparison of sex estimation accuracies achieved using original and cross-validated basipalate discriminant functions (derived by both direct and stepwise procedures).

	Total N	Males		Females		Average %
		%	N	%	N	
<u>Direct</u>						
Original	227	80.7	92/114	85.0	96/113	82.9
Cross-validated	227	76.3	87/114	80.5	91/113	78.4
<u>Stepwise</u>						
Original	227	78.1	89/114	84.1	95/113	81.1
Cross-validated	227	77.2	88/114	83.2	94/113	80.2

Table 5.11 Individual ILD sex estimation accuracies achieved by logistic regression (LR) and linear discriminant analyses (LDA) and univariate statistics including means, standard deviations (SD), Wilks' lambda and F-ratios for zygomatic landmarks.

ILD	LR	LDA	Male		Female		Wilks' Lambda	F β
			Mean	SD	Mean	SD		
pz_rt-po_lt	79.30	78.41	116.54	4.15	111.26	3.96	0.70	96.43
sz_rt-po_lt	79.30	78.85	119.45	4.22	113.69	3.98	0.67	111.62
sz_rt-ge_lt	79.30	78.41	123.06	4.31	117.46	3.99	0.69	103.42
sz_rt-pz-_lt	77.97	78.41	118.18	4.43	112.28	4.12	0.68	107.90
sz_rt-sz_lt	77.97	77.53	116.38	4.80	110.12	4.36	0.68	105.45
zm_rt-po_lt	77.09	77.53	114.34	4.26	109.23	4.02	0.72	86.70
pz_rt-ge_lt*	77.09	77.09	121.17	4.24	116.00	3.98	0.71	89.77
sz_rt-ar_lt	77.09	77.53	120.40	4.47	114.62	4.01	0.68	105.18
ge_rt-pz_lt*	77.09	77.09	121.17	4.24	116.00	3.98	0.71	89.77
zm_rt-ae_lt	76.65	77.97	116.97	4.31	111.91	4.00	0.73	83.97
pz_rt-ae_lt	75.77	74.89	119.12	4.41	113.83	4.04	0.72	88.86
zm_rt-pz_lt	75.77	76.21	107.18	4.17	102.52	3.88	0.75	75.79
ae_rt-zm_lt	75.33	75.77	111.51	4.34	106.59	3.93	0.74	80.39
ae_rt-po_lt	74.89	74.45	112.93	4.28	108.11	4.00	0.75	76.66
pz_rt-pz_lt*	74.89	73.57	118.34	4.34	112.88	4.17	0.71	93.34
zm-ge*	74.45	74.01	57.65	3.17	53.88	3.04	0.73	83.33
sz_rt-zm_lt*	74.45	74.45	105.46	4.52	100.32	3.98	0.73	82.62
zm_rt-sz_lt*	74.45	74.45	105.46	4.52	100.32	3.98	0.73	82.62
ge_rt-po_lt*	74.01	74.45	111.56	4.31	106.96	4.04	0.77	68.82
po_rt-ge-lt*	74.01	74.45	111.56	4.31	106.96	4.04	0.77	68.82
zm-ae*	74.01	74.01	45.53	2.75	42.16	2.62	0.72	88.98

Table 5.11 (continued) Individual ILD sex estimation accuracies achieved by logistic regression (LR) and linear discriminant analyses (LDA), as well as univariate statistics including means, standard deviations (SD), Wilks' lambda and F-ratios for zygomatic landmarks.

ILD	LR	LDA	Male		Female		Wilks' Lambda	F ^β
			Mean	SD	Mean	SD		
zm-pz*	74.01	74.45	32.98	2.31	30.57	2.29	0.78	62.15
po_rt-po_lt*	73.57	73.13	104.66	4.54	99.92	4.25	0.77	65.95
ge_rt-ge_lt*	73.57	73.57	117.87	4.42	113.42	4.14	0.79	61.16
ae_rt-ge_lt*	73.57	73.57	118.63	4.46	113.90	4.09	0.76	69.31
ge_rt-ae_lt*	73.57	73.57	118.63	4.46	113.90	4.09	0.76	69.31
ae_rt-ae-lt*	73.13	73.13	117.95	4.84	113.00	4.36	0.77	65.51
zm-po*	71.81	71.81	62.25	3.23	58.77	3.04	0.76	69.85
sz-zm	70.93	70.48	29.87	2.91	26.87	2.78	0.78	63.39

^β Significant at p < 0.001

*ILD's not entered into the direct discriminant function due to multicollinearity

Table 5.12 Direct discriminant analysis function coefficients, group centroids and sectioning points for all zygomatic interlandmark distances that achieved discrimination accuracies of 70.0% or above.

ILD	Standardised Coefficients	Structure Matrix	Unstandardised Coefficients	Group Centroids
pz_rt-po_lt	0.168	0.697	0.041	M= 0.931
sz_rt-po_lt	5.050	0.750	1.231	F= -0.939
sz_rt-ge_lt	-5.395	0.722	-1.300	
sz_rt-pz_lt	8.931	0.737	2.085	
sz_rt-sz_lt	-4.477	0.729	-0.976	
zm_rt-po_lt	-4.689	0.661	-1.132	
sz_rt-ar_lt	0.696	0.728	0.164	
zm_rt-ae_lt	4.988	0.650	1.199	
pz_rt-ae_lt	-4.504	0.669	-1.065	
zm_rt-pz_lt	-4.266	0.618	-1.058	
ae_rt-zm_lt	3.833	0.636	0.926	
ae_rt-po_lt	0.018	0.621	0.004	
sz-zm	0.381	0.565	0.134	
Constant			-21.84	
Sectioning Point			-0.004	

Table 5.13 Stepwise discriminant analysis results for the best zygomatic interlandmark distances including coefficients, centroids and sectioning points.

ILD	Standardised Coefficients	Structure Matrix	Unstandardised Coefficients	Group Centroids
sz_rt-po_lt	0.768	0.890	0.187	M= 0.784
sz-zm	0.472	0.671	0.166	F= -0.791
Constant			-26.53	
Sectioning Point			-0.004	

Table 5.14 Comparison of sex estimation accuracies achieved using original and cross-validated zygomatic discriminant functions (derived by both direct and stepwise procedures).

	Total N	Males		Females		Average %
		%	N	%	N	
<u>Direct</u>						
Original	227	85.1	97/114	83.2	94/113	84.1
Cross-validated	227	80.7	92/114	79.6	90/113	80.2
<u>Stepwise</u>						
Original	227	80.7	92/114	84.1	95/113	82.4
Cross-validated	227	80.7	92/114	84.1	95/113	82.4

Table 5.15 Individual ILD sex estimation accuracies achieved by logistic regression (LR) and linear discriminant analyses (LDA) as well as univariate statistics including means, standard deviations (SD), Wilks' lambda and F-ratios for orbital landmarks.

ILD	LR	LDA	Male		Female		Wilks' Lambda	F ^β
			Mean	SD	Mean	SD		
d-d	71.81	71.81	22.17	2.27	19.89	2.05	0.78	62.92
d_rt-fmt_lt	70.04	69.60	63.85	3.03	61.11	2.56	0.81	53.91

^β Significant at p < 0.001

Table 5.16 Direct discriminant analysis function coefficients, group centroids and sectioning points for all orbital interlandmark distances that achieved discrimination accuracies of 70.0% or above.

ILD	Standardised Coefficients	Structure Matrix	Unstandardised Coefficients	Group Centroids
d-d	0.736	0.986	0.340	M= 0.532
d_rt-fmt_lt	0.301	0.913	0.107	F=-0.536
Constant			-13.854	
Sectioning Point			-0.002	

Table 5.17 Stepwise discriminant analysis results for the best orbital interlandmark distances including coefficients, centroids and sectioning points.

ILD	Standardised Coefficients	Structure Matrix	Unstandardised Coefficients	Group Centroids
d-d	1.0	1.0	0.462	M= 0.524 F= -0.529
Constant			-9.720	
Sectioning point			-0.002	

Table 5.18 Comparison of sex estimation accuracies achieved using original and cross-validated orbital functions (derived by both direct and stepwise procedures).

	Total N	Males		Females		Average %
		%	N	%	N	
<u>Direct</u>						
Original	227	67.5	77/114	74.3	84/113	70.9
Cross-validated	227	67.5	77/114	74.3	84/113	70.9
<u>Stepwise</u>						
Original	227	69.3	79/114	74.3	84/113	71.8
Cross-validated	227	69.3	79/114	74.3	84/113	71.8

Table 5.19 Individual ILD sex estimation accuracies achieved by logistic regression (LR) and linear discriminant analyses (LDA), as well as univariate statistics including means, standard deviations (SD.), Wilks' lambda and F-ratios for nasomaxillary landmarks.

ILD	LR	LDA	Male		Female		Wilks' Lambda	F ^β
			Mean	SD	Mean	SD		
na_rt-d_lt	78.86	79.30	48.41	2.40	45.07	2.30	0.66	114.98
d-ins	78.41	78.41	48.32	3.08	44.38	2.79	0.69	102.02
na-d	77.09	77.53	45.25	2.44	42.10	2.36	0.70	97.21
al_rt-d_lt	75.33	75.33	43.69	2.31	40.45	2.24	0.66	114.93
r-zm_rt	74.45	74.45	64.85	3.85	61.22	3.21	0.79	59.40
d_rt-zm_lt	73.57	74.45	70.29	3.36	66.43	3.08	0.73	81.43
al-d	73.56	73.57	37.04	2.34	34.32	2.29	0.74	78.83
al_rt-r	72.69	72.69	32.92	2.74	30.28	2.24	0.78	63.33
d-d	71.81	71.81	22.17	2.27	19.89	2.05	0.78	62.92
ins-n	71.37	71.37	52.38	3.28	49.04	3.21	0.79	59.95
na_rt-r	70.93	71.81	37.93	3.53	35.23	2.71	0.84	41.44
zmo_rt-ins	70.93	70.93	37.99	2.54	35.74	2.24	0.82	50.35
zmo-zm	70.49	70.04	31.69	2.98	28.91	2.79	0.81	52.41

^β Significant at p < 0.001

Table 5.20 Direct discriminant analysis function coefficients, group centroids and sectioning points for all nasomaxillary interlandmark distances that achieved discrimination accuracies of 70.0% or above.

ILD	Standardised Coefficients	Structure Matrix	Unstandardised Coefficients	Group Centroids
na_rt-d_lt	-0.226	0.766	-0.096	M= 0.925
d-ins	1.163	0.722	0.395	F= -0.933
na-d	0.613	0.705	0.255	
al_rt-d_lt	-0.004	0.766	-0.002	
r-zm_rt	-0.060	0.551	-0.017	
d_rt-zm_lt	0.223	0.645	0.069	
al-d	-0.216	0.635	-0.093	
al_rt-r	0.804	0.569	0.321	
d-d	0.472	0.567	0.218	
ins-n	-0.621	0.553	-0.191	
na_rt-r	-0.485	0.460	-0.154	
zmo_rt-ins	-0.400	0.507	-0.167	
zmo-zm	-0.048	0.517	-0.017	
Constant			-17.999	
Sectioning Point			-0.004	

Table 5.21 Stepwise discriminant analysis results for the best nasomaxillary interlandmark distances including coefficients, centroids and sectioning points.

ILD	Standardised Coefficients	Structure Matrix	Unstandardised Coefficients	Group Centroids
d-ins	1.311	0.741	0.446	M= 0.901
al_rt-r	0.407	0.584	0.162	F=-0.909
d-d	0.565	0.582	0.261	
ins-n	-0.596	0.568	-0.184	
zmo_rt-ins	-0.383	0.520	-0.160	
Constant			-16.093	
Sectioning Point			-0.004	

Table 5.22 Comparison of sex estimation accuracies achieved using original and cross-validated nasomaxillary discriminant functions (derived by both direct and stepwise procedures).

	Total N	Males		Females		Average %
		%	N	%	N	
<u>Direct</u>						
Original	227	83.3	95/114	85.8	97/113	84.6
Cross-validated	227	79.8	91/114	81.4	92/113	80.6
<u>Stepwise</u>						
Original	227	84.2	96/114	83.2	94/113	83.7
Cross-validated	227	84.2	96/114	83.2	94/113	83.7

Table 5.23 Individual ILD sex estimation accuracies achieved by logistic regression (LR) and linear discriminant analyses (LDA), as well as univariate statistics including means, standard deviations (SD), Wilks' lambda and F-ratios for all cranial landmarks.

ILD	LR	LDA	Male		Female		Wilks' Lambda	F ^β
			Mean	SD	Mean	SD		
po-g	82.38	82.38	110.07	4.20	103.78	3.70	0.61	143.00
nc-g	79.30	77.53	179.35	6.71	169.10	5.81	0.60	151.26
sz_rt-po_lt	79.30	78.85	119.45	4.22	113.69	3.98	0.67	111.62
d-ins	78.41	78.41	48.32	3.08	44.38	2.79	0.69	102.02
pf_rt-ms_lt	77.09	77.09	91.75	3.70	86.94	3.69	0.70	96.17
ms-ba	73.57	74.01	54.72	2.59	51.81	2.38	0.74	77.42
pf-nc	72.69	73.13	131.95	5.54	125.17	5.93	0.74	79.20
al_rt-r	72.69	72.69	32.92	2.74	30.28	2.24	0.78	63.33
ms-anic	72.25	71.81	110.34	4.30	105.68	4.95	0.80	57.65
d-d	71.81	71.81	22.17	2.27	19.89	2.05	0.78	62.92
ins-n	71.37	71.37	52.38	3.28	49.04	3.21	0.79	59.95
sz-zm	70.93	70.48	29.87	2.91	26.87	2.78	0.78	63.39
zmo_rt-ins	70.93	70.93	37.99	2.54	35.74	2.24	0.82	50.35
poic-iv	70.04	70.04	60.57	3.49	56.85	3.60	0.78	62.49

^β Significant at p < 0.001

Table 5.24 Direct discriminant analysis function coefficients, group centroids and sectioning points for all cranial interlandmark distances that achieved discrimination accuracies of 70.0% or above.

ILD	Standardised Coefficients	Structure Matrix	Unstandardised Coefficients	Group Centroids
po-g	-0.134	0.681	-0.034	M= 1.161
nc-g	0.774	0.700	0.123	F= -1.171
ms-ba	-0.147	0.501	-0.059	
pf_rt-ms_lt	0.595	0.558	0.161	
pf-nc	-0.278	0.507	-0.048	
ms-anic	-0.378	0.432	-0.082	
poic-iv	0.213	0.450	0.060	
sz_rt-po_lt	-0.081	0.602	-0.020	
sz-zm	0.282	0.453	0.099	
d-d	0.300	0.452	0.139	
d-ins	1.002	0.575	0.341	
al_rt-r	0.308	0.453	0.123	
ins-n	-0.664	0.441	-0.204	
zmo_rt-ins	-0.343	0.404	-0.143	
Constant			-22.125	
Sectioning Point			-0.005	

Table 5.25 Stepwise discriminant analysis results for the best cranial interlandmark distances including coefficients, centroids and sectioning points for variables X₁ to X₇ as per equation in Section 5.3.4.3.

Step	Variable name	Standardised Coefficients	Structure Matrix	Unstandardised Coefficients	Group Centroids
nc-g	X ₁	0.535	0.728	0.085	M= 1.116
sz-zm	X ₂	0.338	0.472	0.119	F= -1.126
d-d	X ₃	0.314	0.470	0.145	
d-ins	X ₄	1.052	0.598	0.358	
al_rt-r	X ₅	0.321	0.471	0.128	
ins-n	X ₆	-0.694	0.459	-0.214	
zmo_rt-ins	X ₇	-0.379	0.420	-0.158	
Constant				-25.235	
Sectioning Point				-0.005	

Table 5.26 Comparison of sex estimation accuracies achieved using original and cross-validated cranial discriminant functions (derived by both direct and stepwise procedures).

	Total N	Males		Females		Average %
		%	N	%	N	
<u>Direct</u>						
Original	227	86.8	99/114	89.4	101/113	88.1
Cross-validated	227	84.2	96/114	87.6	99/113	85.9
<u>Stepwise</u>						
Original	227	86.0	98/114	92.0	104/113	89.0
Cross-validated	227	86.0	98/114	90.3	102/113	88.2

CHAPTER SIX

Overall Discussion and Conclusions

6.1 INTRODUCTION

This thesis investigated the intricacies and complexities of human sexual dimorphism (SxD) in white South Africans. Understanding dimorphism, its underlying causes and the effect it has on population variation, is crucial for a number of scientific disciplines including forensic anthropology, evolutionary biology and bioarchaeology. This study focused on the crania of white South Africans because of the paucity of literature on this population relative to black South Africans. The lack of research on the focus group is attributed to the low numbers of dentate specimens currently available for study in South African skeletal collections, which are largely comprised of cadaveric-derived remains. The skull was recently reported to be the single most recovered skeletal element in South African forensic cases, making accurate sexing of the skull all the more important in a South African context of victim identification (46).

White South Africans are originally of Dutch, French, English, Portuguese and other European ancestries. Four centuries of isolation from the founder populations and admixture with African populations have resulted in a number of skeletal attributes that distinguish white South Africans from other white populations of European descent (1,18,193). As a result, population-specific standards are therefore imperative for white South Africans, not only to ensure accurate biological profiles, but also to avoid misclassification of other South African populations.

The aims of this thesis were firstly to quantify the effects of tooth loss in white South African crania, describe its effect on the estimation of sex and ancestry, and to mitigate these effects to allow for the use of all cranial specimens regardless of dental state. The second aim was to use GMM to quantify and describe SxD in white South African cranial morphology both globally and regionally, and to explore the relative contributions of allometric and non-allometric SxD to overall SxD. The final aim was to derive 3-D interlandmark distances (ILDs) and compare them to traditional cranial measurements, with the goal of creating novel, more accurate discriminant functions for sex estimation from the entire cranium and a number of cranial subsets.

6.2 CHAPTER TWO: Assessing the effects of tooth loss on the crania of white South Africans using geometric morphometric

Chapter three aimed to elucidate the effects of tooth loss on various cranial subsets and to interpret its consequences for sex and ancestry estimation. Both fixed and sliding semilandmarks were acquired from the crania of 118 white South African

males and 111 females. Following a partial Procrustes superimposition (PPS), the resulting data were subjected to a number of statistical analyses to test for the effect of tooth loss on the cranium globally, and also on specific subsets including the basicranium, face, maxillae, zygomae, orbits and nasal aperture.

Global results indicated that the loss of teeth leads to a decrease in facial height and prognathism, as a result of superior and posterior recession of the maxilla, an increase in the anterior and inferior flexion of the basicranium relative to the viscerocranium, and an increase in nasal projection and orbit size. When the statistical analyses were repeated on each of the individual subsets, however, only the maxillary alterations proved significant. This more detailed inspection revealed that the anterior third of the alveolus underwent the most dramatic resorption, although bone loss across the maxilla was severe enough to result in increased palatal width. As alveolar prognathism (47) and palate shape (152,168) are qualitative characteristics used when estimating sex and ancestry, a significant decrease in prognathism could result in black individuals being misidentified as white. Conversely, an increase in palate hyperbolism could result in white individuals, who ordinarily have deep, narrow palates, being misidentified as black. Additionally, a number of craniometric measures, including upper facial height and facial length (8,45), rely on measures that incorporate the anterior palate, and hence, excessive resorption will lead to a size reduction of these measures resulting in an increase in sex and ancestry misclassification when identifying edentulous individuals.

Despite a number of orthodontic studies demonstrating the significant effect of tooth loss on the maxilla (91,125,206,207), the effect of tooth loss on other cranial structures and cranial craniometrics has received little focus. Dechow et al. (85) did, however, demonstrate a significant reduction in cortical bone thickness of all regions of edentulous crania, while elastic or sheer moduli and density in the zygomatics were similar or greater. These results support the lack of change observed in the zygomae in the current investigation, suggesting that this structure may be unaffected by tooth loss, at least macroscopically.

6.3 CHAPTER FOUR: Morphological variation in white South African crania: sexual dimorphism and allometry

Following mitigation of the effects of tooth loss, 229 white South African crania were subjected to further analyses. This sample size is nearly double that used in most

studies of white South African crania, even when using a combined dataset collected from the Pretoria Bone Collection and the Dart Collection (1,46,52,193).

To better understand the pattern of dimorphism, rather than simply its magnitude, overall SxD, common allometry (CA) and non-allometric (NASXD) were each investigated in the cranium globally, and in each of the subsets.

Globally, the zygomatics and the nasal aperture displayed the most obvious overall SxD, with male structures being more rugose despite the mitigation of size during PPS. These results are in line with morphological descriptions of the zygomatic bones in males as larger and laterally flared, and nasal bones and the nasal aperture as higher relative to females (43).

All regional subsets under investigation displayed significant overall SxD. In the basicranial region, the female foramen magnum was larger, more elliptical and anteriorly-tilted relative to in males. This is directly opposed to İşcan and Steyn's (1) description of larger and longer foramina magna in males, and to many other metric studies describing larger foramina magna in males (153,154, 200). Few describe its shape, however, making this a possible avenue of future exploration. In the maxilla, females were found to have deeper, "U"-shaped palates compared to shallower, "V"-shaped palates in males. These results are in agreement with morphological descriptions of palatal differences (43). They are contrary to the geometric morphometric study of Bigoni et al. (63), however, that suggested that this characteristic may be specific to white South Africans. Further similarities between the findings of this study and the literature include larger, lateral projection of the male zygomatic (3,40,43), and a longer, narrower nasal aperture in males (40,43,63). When the orbit was analysed in isolation following PPS, very few differences remained between the sexes. This is the only subset for which the results of the current study did not correspond to the literature directly. This may be due to the orbits being analysed only as outlines in the subset analyses, without additional landmarks on the rest of the cranium to provide larger context.

After overall SxD was detailed, the contribution of CA and NASXD were analysed. As with overall SxD, CA was found to be significant in both the global and regional analyses. Specifically, smaller individuals were found to have larger glabellae, supraorbital regions, nasal bones, and more protrusive nuchal crests, while larger individuals had more prominent anterior maxillae.

Finally, after the effects of size on shape (CA) were removed from the dataset, the influence of sex was analysed apart from the size-related trends (NASXD). Despite the fact that most of the differences observed in the analysis of overall SxD appeared enhanced in the global analysis, only the effects on the zygomatics were significant in the regional analyses. These results highlight the importance of considering the effect that size has on shape, especially in GMM investigations in which the two are decoupled.

6.4 CHAPTER FIVE: Traditional cranial measurements versus 3-D derived interlandmark distances for sex estimation in white South Africans.

In Chapter 5, the sex estimation accuracy of 3-D derived ILDs was compared to traditional cranial measurements and these measures were also compared to all possible ILDs. In total, 990 ILDs were derived from the 3-D data described in Chapter Four and their sex estimation accuracy was determined using both linear discriminant analysis (LDA) and logistic regression (LR). Unlike in Chapters Three and Four, size was reintroduced into the dataset in this study after running a PPS to approximate traditionally captured craniometric data. Only fixed landmarks were used for the same reason. The most accurate ILDs were then compared with the cranial measurements most commonly used for both sex and ancestry estimation. Discriminant functions produced using the 3-D ILDs were also directly compared to those commonly used in South Africa when analysing sex in white crania, following İşcan and Steyn (1). Finally, new discriminant functions were produced for the cranium as a whole, and a number of cranial subsets using the most accurate ILDs were produced to estimate sex from partial remains.

The top 17 3-D ILDs derived in this study all achieved sexing accuracies of over 70%, outperforming the top 17 most commonly used traditional measurements by a large margin since less than half of those measures scored over 70%. Four of the traditional measures (i.e. maximum cranial length, bizygomatic breadth, cranial base length and opisthion to glabella) did, however, rank in the top 17. Maximum cranial length at 79.3% was the most accurate traditional measure scoring only 3% below the best novel measure defined in this study: glabella-porion (82.4%). Franklin et al. (194) used a similar method to ascertain the most accurate cranial ILD in Australian populations. A novel measure, glabella-zygion, was found to be the most accurate in their study achieving maximal accuracies of up to 88.0%. Their measurement is quite

similar to that derived in this study suggesting that this oblique ILD between the occiput and the zygomatics represents a novel region in the crania of white individuals that warrants further study. The accuracy of discriminant functions derived using 3-D ILDs mimics the level found by İşcan and Steyn (1) and compares well with the original functions, despite some of the digitised landmarks not corresponding perfectly with their traditional counterparts. On average, the accuracy of the functions derived in the current investigation were only 3.0% less than the originals, but they also had a much lower sex bias (in which one sex classifies correctly at significantly greater rate), which is a favourable outcome as it ensures that the sex distribution of large samples are accurately represented (42)

Finally, discriminant functions were derived for the cranium in its entirety and for the basicranium, basipalate, orbits, zygomatics and nasomaxillae. These subsets are slightly different to those in Chapters 3 and 4, as the landmarks were selected to represent ILDs in each region with sexing accuracies of 70.0% or greater. Global analyses are more accurate, but in many forensic cases, only fragmentary remains are often found. Hence, having a range of functions that span many cranial regions ensures that remains can be sexed independent of where they are damaged or what fragments are found. This was a very important achievement of the current study, as few standards exist for sexing fragmentary cranial remains (4,161,164,172). Sexing accuracies achieved by the global cranial discriminant functions derived in this investigation proved slightly more accurate (88.2%) than the widely used function defined by Steyn and İşcan (1) for white South African crania (86.0%). The current results compare well to those of Franklin et al. (194) who also used 3-D derived ILD to assess cranial dimorphism in western Australians. They achieved 83.5-88.0% accuracy. Franklin and associates (51) also used a similar method to assess sex in black South Africans. That study only achieved 77.0-80.0% accuracy, highlighting the significantly lower levels of dimorphism in black South Africans ancestral groups.

Moderate to high sex estimation accuracies were achieved by individual subset discriminant functions, with the orbit function having the lowest accuracy (71.8%) and the nasomaxillary function the highest (83.7%). The orbit function was based on only a single measurement taken between contralateral dacryons, and compares well with work on other crania of European ancestry (e.g. Bigoni et al. (63) on Central Europeans, which achieved 74.0% sexing accuracy). When compared with black South Africans (69), the current study scored on the lower end of the range, once again

illustrating the difference in the expression of dimorphism between the two South African ancestral groups. The midfacial region (zygomatic and nasomaxillary regions) scored up to 83.7%, the highest sex estimation accuracy in the current study. Despite only a 1.3% higher accuracy achieved using the nasomaxillary function versus the zygomatic function, these results are extremely surprising as numerous authors have found bizygomatic breadth to be the most accurate single sex measure when traditional measurements techniques are used (1,2,5,183,184,188,190). Recent studies of the South African nasal apertures demonstrated only moderate differences in nasal shape (164,172). The McDowell et al.'s (164,172) studies were also GMM-based, but did not reintroduce the effect of size. This may account for the difference in the results. Nonetheless, the current investigation demonstrates the value of re-evaluating commonly measured ILDs such as the nasomaxilla function in the current investigation, which achieved the best accuracies, but consisted largely of mostly non-traditional measurements.

6.5 LIMITATIONS AND FUTURE RESEARCH

Despite achieving favourable results, the current thesis had a number of limitations that could be addressed in future investigations. A major limitation of the investigation is the cross-sectional dataset used. A longitudinal study, including multiple measurements on the same individual over a period of time, would provide a more accurate depiction of the effects of tooth loss on the craniofacial skeleton. Assessing the difference between the effects of pre-canine and post-canine tooth loss would be an important consideration of such a study. Additionally, the progressive nature of alveolar bone loss could be addressed. Finally, a longitudinal dataset would allow the effects of asymmetrical tooth loss to be measured, rather than mitigated, as was done in this investigation. This would allow for a much more accurate, realistic approximation of pre-tooth loss facial morphology using the methods developed in this study.

There were additional limitations in terms of sample composition. As with all studies of white South African crania, this investigation had a disproportionately large number of edentulous crania. Despite the effect of tooth loss being mitigated, future studies using data collected with modern imaging techniques could overcome this limitation by including more dentate individuals. Disproportionately large numbers of

older individuals who donate their bodies to skeletal collections resulted in the average age in the current investigation of 62 years. Additionally, a very low proportion of young individuals were represented. As stated above, this could be remedied using data from CT or MRI scans. Larger sample sizes in general would enhance the significance of all statistical analyses. Errors may be reduced in future studies by first applying dental clay to smooth the irregular surfaces before digitisation and by positioning skulls in such a way that all surfaces are more easily accessed. Finally, studies that explore how anthropologists can mitigate tooth loss in a practical setting would be invaluable.

As with all GMM studies, the use of PPS is plagued by the Pinocchio effect (118,119) in which variation about a single point is averaged out across the dataset. As demonstrated in this thesis, however, these effects are minimised when a large number of well-placed, highly repeatable landmarks are used.

This study did not address possible sources of variation that may have been introduced by secular change. Additionally, it did not attempt to study differences in the degree of expression of SxD between white South Africans and other white populations. Such a studies, chronicling secular trend and the variability of SxD in modern populations would be invaluable in expanding our current understanding of the evolution of SxD. Furthermore, it is unknown whether ante-mortem tooth loss and cranial cortical bone thickness covary with age. Future research investigating possible covariation of these blocks of data would greatly benefit physical, forensic and evolutionary anthropologists. The accuracy of the functions derived in this thesis should be tested, by future studies, on crania from other or unknown ancestral groups, to gauge their practical applicability. Additionally, future investigations should compare the sexing accuracies obtained using the functions derived in this investigation, using 3-D derived distances, to accuracies achieved using traditional means. This would need to be done on the same skulls to validate the 3-D derived discriminant functions outlined in this thesis.

6.6 CONCLUSIONS

After extensive study of the metric and morphological consequences of SxD, as well as the influence of tooth loss on its expression, the following conclusions were draw:

Globally, a number of consequences of tooth loss were demonstrated including severe alveolar resorption, a significant decrease in upper facial height and prognathism, an increase in palatal width, inferior and anterior flexion of the basicranium together with a relative increase in its size, a relative shift of the zygomatics inferiorly coupled with a relative increase in size. A relative increase in orbit and nasal size were also noted.

When anatomical subsets were investigated in isolation, however, the only significant effects of tooth loss were the alveolar resorption, upper facial height resorption and prognathism decrease, and palatal widening (i.e. only the maxillary effects were significant).

Morphological consequences of overall SxD include larger, more elliptical and anteriorly-tilted foramina magna in females. Additionally, females presented with deeper “U”-shaped palates, smaller less projecting zygomatics, and shorter wider nasal apertures, while shape differences between the orbits were minimal.

In terms of the effect of size on shape (CA), all regional and global effects were found to be significant. Specifically, smaller individuals have larger glabellae, supraorbital regions, nasal bones, and more protrusive nuchal crests, whilst larger individuals had more prominent anterior maxillae.

When all size effects were removed (NASXD), only the zygomatics proved significantly affected by sexual dimorphism (i.e. non-allometric effects).

Metric analyses of dimorphism using 3-D derived ILDs proved more accurate than traditional cranial measurements with accuracies ranging between 73.6%-82.4% for individual ILDs as compared to 52.9%-79.3% for traditional measures.

Discriminant functions produced to emulate those derived from the traditional measures in İşcan and Steyn's (1) study compared well to their traditional counterparts. The current investigation achieved only 3% lower sex discrimination accuracies when 3-D ILDs were chosen to mimic traditional cranial measures. Additionally, 3-D ILDs, scored lower overall sex biases.

Individual discriminant functions for the five subsets described in this thesis had moderate to high cross-validated sex estimation accuracies: orbits: 71.8%; basicranium: 74.0%; basipalate: 80.2%; zygomatics: 82.4%; nasomaxillae: 83.7%.

The overall cranial discriminant function derived in this thesis outperformed the commonly used traditional overall cranial function defined by İşcan and Steyn (1) and the validation study of Robinson and Bidmos (209), achieving 88.2% cross-validated sexing accuracy.

REFERENCES

1. Steyn M, İşcan MY. Sexual dimorphism in the crania and mandibles of South African whites. *Forensic Sci Int.* 1998;98(1-2):9–16.
2. Franklin D, Freedman L, Milne N. Sexual dimorphism and discriminant function sexing in indigenous South African crania. *HOMO - J Comp Hum Biol.* 2005;55(3):213–28.
3. Franklin D, Freedman L, Milne N, Oxnard CE. A geometric morphometric study of sexual dimorphism in the crania of indigenous southern Africans. *S Afr J Sci.* 2006;102:229–38.
4. Dayal MR, Spocter MA, Bidmos MA. An assessment of sex using the skull of black South Africans by discriminant function analysis. *HOMO - J Comp Hum Biol.* 2008;59(3):209–21.
5. Robinson MS, Bidmos MA. The skull and humerus in the determination of sex: Reliability of discriminant function equations. *Forensic Sci Int.* 2009;186(1-3):1–5.
6. Bidmos MA, Gibbon V, Štrkalj G. Recent advances in sex identification of human skeletal remains in South Africa. *S Afr J Sci.* 2010;106(11/12):1–7.
7. Barrier ILO, L'Abbé EN. Sex determination from the radius and ulna in a modern South African sample. *Forensic Sci Int.* 2008;179(1):85.e1–85.e7.
8. Krogman W, İşcan MY. *Human Skeleton in Forensic Medicine [Hardcover]*. 2nd ed. Illinois: Charles C Thomas Pub Ltd; 1986.
9. Byers SN. *Introduction to forensic anthropology - a textbook*. 1st ed. Boston.: Pearson Education Inc.; 2002.
10. Rösing FW, Graw M, Marré B, Ritz-Timme S, Rothschild MA, Röttscher K, et al. Recommendations for the forensic diagnosis of sex and age from skeletons. *HOMO - J Comp Hum Biol.* 2007;58(1):75–89.
11. Dawson C, Ross D, Mallett X. Sex Determination. In: *Forensic Anthropology: 2000 to 2010*. 2011. p. 61–94.
12. L'Abbé EN, Loots M, Meiring JH. *The Pretoria Bone Collection: A modern South*

- African skeletal sample. *HOMO - J Comp Hum Biol.* 2005 Aug [cited 2015 Dec 18];56(2):197–205.
13. Dayal MR, Kegley ADT, Štrkalj G, Bidmos MA, Kuykendall KL. The history and composition of the Raymond A. Dart Collection of Human Skeletons at the University of the Witwatersrand, Johannesburg, South Africa. *Am J Phys Anthropol.* 2009;140(2):324–35.
 14. Africa SS. Poverty Trends in South Africa: An examination of absolute poverty between 2006 and 2011. 2014.
 15. Steyn M. Muti murders from South Africa: A case report. *Forensic Sci Int.* 2005;151(2-3):279–87.
 16. Krishan K. Anthropometry in Forensic Medicine and Forensic Science-'Forensic Anthropometry'. *Internet J Forensic Sci.* 2007;2(1).
 17. Ousley S, Jantz R, Freid D. Understanding race and human variation: Why forensic anthropologists are good at identifying race. *Am J Phys Anthropol.* 2009;139(1):68–76. Available from: <http://doi.wiley.com/10.1002/ajpa.21006>
 18. Rooyen C van. Evaluating standard non-metric cranial traits used to determine ancestry on a South African sample. 2010;1–153.
 19. de Villiers H. Sexual dimorphism of the skull of the South African Bantu-speaking Negro. *S Afr J Sci.* 1968;64:118–24.
 20. Rightmire GP. Discriminant Function Sexing of Bushman and South African Negro Crania. *South African Archaeol Bull.* 1971;26(103):132–8.
 21. İşcan MY. Rise of forensic anthropology. *Am J Phys Anthropol.* 1988;31(S9):203–29.
 22. Baab KL, Freidline SE, Wang SL, Hanson T. Relationship of cranial robusticity to cranial form, geography and climate in *Homo sapiens*. *Am J Phys Anthropol.* 2010;141(1):97–115.
 23. Gonzalez PN, Perez SI, Bernal V. Ontogeny of robusticity of craniofacial traits in modern humans: A study of South American populations. *Am J Phys Anthropol.* 2010;142(3):367–79.
 24. O'Higgins P, Johnson DR, Moore WJ, Flinn RM. The variability of patterns of

- sexual dimorphism in the hominoid skull. *Experientia*. 1990;46(7):670–2.
25. Schaefer K, Mitteroecker P, Gunz P, Bernhard M, Bookstein FL. Craniofacial sexual dimorphism patterns and allometry among extant hominids. *Ann Anat*. 2004;186(5-6):471–8.
 26. González-José R, Bortolini MC, Santos FR, Bonatto SL. The peopling of America: craniofacial shape variation on a continental scale and its interpretation from an interdisciplinary view. *Am J Phys Anthropol*. 2008;137(2):175–87.
 27. Bastir M, Godoy P, Rosas A. Common features of sexual dimorphism in the cranial airways of different human populations. *Am J Phys Anthropol*. 2011;146(3):414–22.
 28. Klingenberg CP. Multivariate allometry. *Adv Morphometrics*. 1996;284:23–49.
 29. Leonart J, Salat J, Torres GJ. Removing Allometric Effects of Body Size in Morphological Analysis. *J Theor Biol*. 2000;205:85–93.
 30. Rosas A, Bastir M. Thin-plate spline analysis of allometry and sexual dimorphism in the human craniofacial complex. *Am J Phys Anthropol*. 2002;117(3):236–45.
 31. Gunz P, Mitteroecker P, Bookstein FL. Semilandmarks in Three Dimensions. *Mod Morphometrics Phys Anthropol*. 2005;73–98.
 32. Darwin C. The descent of man and selection in relation to sex, in Charles Darwin, *The origin of species and The descent of man (combined volume)*. *J Anat Physiol*. 1871;5(Pt 2):363–72.
 33. Shine R. Ecological Causes for the Evolution of Sexual Dimorphism : A Review of the Evidence. *Q Rev Biol*. 1989;64(4):419–61.
 34. Rice WR. Sex Chromosomes and the Evolution of Sexual. 1984;38(4):735–42.
 35. Ruff C. Sexual dimorphism in human lower limb bone structure: relationship to subsistence strategy and sexual division of labor. *J Hum Evol*. 1987;16(5):391–416.
 36. Suazo Galdames IC, Zavando Matamala DA, Smith RL. Evaluating Accuracy and Precisión in Morphologic Traits for Sexual Dimorphism in Malnutrition Human Skull: a Comparative Study. *Int J Morphol*. 2008;26(4):877–81.
 37. Nikita E. Age-associated Variation and Sexual Dimorphism in Adult Cranial

- Morphology: Implications in Anthropological Studies. *Int J Osteoarchaeol.* 2012;569(November 2011):557–69.
38. Stini WA. Evolutionary Implications of Changing Nutritional Patterns in Human Populations. *Am Anthropologist.* 1971;73(5):1019–30.
 39. Walker PL. Problems of preservation and sexism in sexing: Some Lessons from the historical collections for palaeodemographers. In: Saunders SR, Herring A, editors. *Grave reflections, portraying the past through cemetery studies.* Toronto: Canadian Scholars' Press; 1995.
 40. Williams BA, Rogers TL. Evaluating the Accuracy and Precision of Cranial Morphological Traits for Sex Determination. *J Forensic Sci.* 2006;51(4):729–35.
 41. Rogers TL. Determining the sex of human remains through cranial morphology. *J Forensic Sci.* 2005;50(3):493–500.
 42. Walker PL. Sexing skulls using discriminant function analysis of visually assessed traits. *Am J Phys Anthropol.* 2008;136(1):39–50.
 43. İşcan MY, Steyn M. *The Human Skeleton in Forensic Medicine.* 3a ed. Charles C Thomas. 2013. 516 p.
 44. Walker PL. Greater sciatic notch morphology: Sex, age, and population differences. *Am J Phys Anthropol.* 2005;127(4):385–91
 45. Buikstra J, Ubelaker J. Standards for data collection from human skeletal remains. *Libr Congr Cat Publ Data.* 1994;
 46. Krüger GC, L'Abbé EN, Stull KE, Kenyhercz MW. Sexual dimorphism in cranial morphology among modern South Africans. *Int J Legal Med.* 2015;129(4):869–75.
 47. L'Abbé EN, van Rooyen C, Nawrocki SP, Becker PPJ. An evaluation of non-metric cranial traits used to estimate ancestry in a South African sample. *Forensic Sci Int.* 2011;209(1-3):195.e1–7.
 48. Lei P-W, Koehly LM. Linear Discriminant Analysis Versus Logistic Regression: A Comparison of Classification Errors in the Two-Group Case. *J Exp Educ.* 2003;72(1):25–49.
 49. Mitteroecker P, Bookstein FL. Linear Discrimination, Ordination, and the

- Visualization of Selection Gradients in Modern Morphometrics. *Evol Biol.* 2011;38(1):100–14.
50. Spicer. Logistic regression and discriminant analysis. *SAGE Res Publ.* 2004;123–52.
 51. Franklin D, Freedman L, Milne N. Three-dimensional technology for linear morphological studies: a re-examination of cranial variation in four southern African indigenous populations. *Homo.* 2005;56(1):17–34.
 52. L'Abbé EN, Kenyhercz M, Stull KE, Keough N, Nawrocki S. Application of fordisc 3.0 to explore differences among crania of north american and south african blacks and whites,. *J Forensic Sci.* 2013;58(6):1579–83.
 53. Loth SR, Henneberg M. Mandibular ramus flexure: A new morphologic indicator of sexual dimorphism in the human skeleton. *Am J Phys Anthropol.* 1996;99(3):473–85.
 54. Franklin D, Freedman L, O'Higgins P, Oxnard CE. A comment on Dayal et al. (2008) assessment of sex using the skull. *HOMO- J Comp Hum Biol.* 2009;60(2):139–42.
 55. Slice DE. Geometric Morphometrics. *Annu Rev Anthropol.* 2007;36(1):261–81
 56. Mitteroecker P, Gunz P. Advances in geometric morphometrics. *Evol Biol.* 2009;36(2):235–47.
 57. Rohlf JF, Marcus LF. A revolution morphometrics. *Trends in Ecology and Evolution.* 1993. p. 129–32.
 58. Adams DC, Rohlf JF, Slice DE. Geometric morphometrics: ten years\nof progress following the “revolution.” *Ital J Zool.* 2004;71:5–16.
 59. Perez SI, Bernal V, Gonzalez PN. Differences between sliding semi-landmark methods in geometric morphometrics, with an application to human craniofacial and dental variation. *J Anat.* 2006;208(6):769–84.
 60. Zelditch ML, Swiderski DL, Sheets HD. *Geometric Morphometrics for Biologists, Second Edition: A Primer [Hardcover].* 2012. 488 p.
 61. Rohlf JF, Slice DE. Extensions of the procrustes method for the optimal superimpositionof landmarks. *Syst Zool.* 1990;39(1):40–59.

62. Ji Y, Qian Z, Dong Y, Zhou H, Fan X. Quantitative morphometry of the orbit in Chinese adults based on a three-dimensional reconstruction method. *J Anat* .
63. Bigoni L, Velemínská J, Brůzek J. Three-dimensional geometric morphometric analysis of cranio-facial sexual dimorphism in a Central European sample of known sex. *HOMO - J Comp Hum Biol*. 2010;61(1):16–32.
64. Green H, Curnoe D. Sexual dimorphism in Southeast Asian crania: A geometric morphometric approach. *HOMO- J Comp Hum Biol*; 2009;60(6):517–34.
65. Franklin D, Oxnard CE, O'Higgins P, Dadour I. Sexual dimorphism in the subadult mandible: Quantification using geometric morphometrics. *J Forensic Sci*. 2007;52(1):6–10.
66. Franklin D, O'Higgins P, Oxnard CE, Dadour I. Discriminant function sexing of the mandible of Indigenous South Africans. *Forensic Sci Int*. 2008;179(1).
67. Steyn M, Pretorius E, Hutten L. Geometric morphometric analysis of the greater sciatic notch in South Africans. *Homo*. 2004;54(3):197–206.
68. Scholtz Y, Steyn M, Pretorius E. A geometric morphometric study into the sexual dimorphism of the human scapula. *HOMO- J Comp Hum Biol*. 2010;61(4):253–70.
69. Pretorius E, Steyn M, Scholtz Y. Investigation into the usability of geometric morphometric analysis in assessment of sexual dimorphism. *Am J Phys Anthropol*. 2006;129(1):64–70.
70. Bookstein FL. *Morphometric tools for landmark data: geometry and biology*. Cambridge University Press. 1991. 435 p.
71. Gonzalez PN, Bernal V, Perez SI. Analysis of sexual dimorphism of craniofacial traits using geometric morphometric techniques. *Int J Osteoarchaeol*. 2011;21(1):82–91.
72. Williams SE, Slice DE. Regional shape change in adult facial bone curvature with age. *Am J Phys Anthropol*. 2010;143(3):437–47.
73. Bodic F, Hamel L, Lerouxel E, Basle MF, Chappard D. Bone loss and teeth. *Jt Bone Spine*. 2005;72(3):215–21.
74. Peltzer K, Hewlett S, Yawson AE, Moynihan P, Preet R, Wu F, et al. Prevalence

- of loss of all teeth (Edentulism) and associated factors in older adults in China, Ghana, India, Mexico, Russia and South Africa. *Int J Environ Res Public Health*. 2014;11(11):11308–24.
75. Kelsey CC. Alveolar bone resorption under complete dentures. *J Prosthet Dent*. 1971;25(2):152–61.
 76. Albert AM, Ricanek Jr K, Patterson E. A review of the literature on the aging adult skull and face: Implications for forensic science research and applications. *Forensic Sci Int*. 2007;172(1):1–9.
 77. Lestrel PE, Kapur K, Chauncey H. A cephalometric study of mandibular cortical bone thickness in dentulous persons and denture wearers. *J Prosthet Dent*. 1980;43:89–94.
 78. Tallgren A. The effect of denture wearing on facial morphology. A 7-year longitudinal study. *Acta Odontol Scand*. 1967;25:563–92.
 79. Bartlett SP, Grossman R, Whitaker LA. Age-related changes in the craniofacial skeleton: An Anthropometric and Histologic analysis. *Plast Reconstr Surg*. 1992;90(4):592–600.
 80. Sveikata K, Balciuniene I, Tutkuvienė J. Factors influencing face aging. Literature review. *Stomatologija*. 2011;13(4):113–6.
 81. Tallgren A. The continuing reduction of the residual alveolar ridges in complete denture wearers: A mixed-longitudinal study covering 25 years. *J Prosthet Dent*. 2003;89(5):427–35.
 82. Mardinger O, Namani-Sadan N, Chaushu G, Schwartz-Arad D. Morphologic changes of the nasopalatine canal related to dental implantation: a radiologic study in different degrees of absorbed maxillae. *J Periodontol*. 2008;79(9):1659–62.
 83. Newton JP, Yemm R, Abel RW, Menhinick S. Changes in human jaw muscles with age and dental state. *Gerodontology*. 1993;10(1):16–22.
 84. Haraldson T, Karlsson U, Carlsson GE. Bite force and oral function in complete denture wearers. *J Oral Rehabil*. 1979;6(1):41–8.
 85. Dechow PC, Wang Q, Peterson J. Edentulation alters material properties of

- cortical bone in the human craniofacial skeleton: functional implications for craniofacial structure in primate evolution. *Anat Rec.* 2010;293(4):618–29.
86. Steyn M, İşcan MY. Osteometric variation in the humerus: Sexual dimorphism in South Africans. *Forensic Sci Int.* 1999;106(2):77–85.
 87. van Wyk PJ, van Wyk C, Wyk P, Wyk C. Oral health in South Africa. *Int Dent J.* 2004;54(6 Suppl 1):373–7
 88. UN Population Division. *World Population Prospects: the 2010 Revision.* *Waste Manag Res.* 2012;27(8):800–12.
 89. Kloss FR, Gassner R. Bone and aging: effects on the maxillofacial skeleton. *Exp Gerontol.* 2006;41(2):123–9.
 90. Heath MR. A cephalometric study of the middle third of the adult human face related to age and the loss of dental tissue. *Arch Oral Biol.* 1966;11(7):677–86.
 91. Crothers AJ. Tooth wear and facial morphology. *J Dent.* 1992;20(6):333–41.
 92. Pietrokovski J, Massler M. Alveolar ridge resorption following tooth extraction. *J Prosthet Dent.* 1967;17(1):21–7.
 93. Greeff JM. Deconstructing Jaco: Genetic heritage of an Afrikaner. *Ann Hum Genet.* 2007;71(5):674–88.
 94. Tipping AJ, Pearson T, Morgan N V, Gibson RA, Kuyt LP, Havenga C, et al. Molecular and genealogical evidence for a founder effect in Fanconi anemia families of the Afrikaner population of South Africa. *Proc Natl Acad Sci U S A.* 2001;98(10):5734–9.
 95. Botha MC, Beighton P. Inherited disorders in the Afrikaner population of southern Africa. Part I. Historical and demographic background, cardiovascular, neurological, metabolic and intestinal conditions. *S AfrMed J.* 1983;64(16):609–12.
 96. von Cramon-Taubadel N. Evolutionary insights into global patterns of human cranial diversity: Population history, climatic and dietary effects. *J Anthropol Sci.* 2013;91:1–36.
 97. Smith HF. Which cranial regions reflect molecular distances reliably in humans? Evidence from three-dimensional morphology. *Am J Hum Biol.* 2009;21(1):36–

- 47.
98. Steen SL. Examining “universal” hide chewing practice among Alaskan Eskimos. In: Lisa Frink KW, editor. *Gender and Hide Production*. AltaMira Press; 2006. p. 123–32.
99. Williams SE. *IS AGING ONLY SKIN DEEP*. 2008.
100. Sheets HD, Kim K, Mitchell CE. A combined landmark and outline-based approach to ontogenetic shape change in the Ordovician trilobite *Triarthrus becki*. *Morphometrics*. 2004;67–82.
101. Gunz P, Mitteroecker P, Bookstein FL, Weber, GW (Vienna Inst for Anthropology, Vienna A. Computer-aided reconstruction of incomplete human crania using statistical and geometrical estimation methods. In: *Enter the Past: Computer Applications and Quantitative Methods in Archaeology*. 2004. p. 92–4.
102. Klingenberg CP, Barluenga M, Meyer A. Shape analysis of symmetric structures: quantifying variation among individuals and asymmetry. *Evolution*. 2002;56(10):1909–20.
103. McManus IC. The distribution of skull asymmetry in man. *Annals of Human Biology*. 1982. p. 167–70.
104. O’Higgins P, Jones N. Tools for statistical shape analysis. 2006 [cited 2013 May 23]. Available from: <http://hyms.fme.googlepages.com/resources>
105. Webster M, Sheets HD. A practical introduction to landmark-based geometric morphometrics (SOM). *Quant Methods Paleobiol*. 2010;SOM.
106. Gunz P. Using semilandmarks in three dimensions to model human neurocranial shape. University of Vienna, Vienna; 2001.
107. Gunz P. Statistical and geometric reconstruction of hominid crania: Reconstructing australopithecine ontogeny. University of Vienna, Vienna; 2005.
108. Le Roux B, Rouanet H. *Geometric Data Analysis: From Correspondence Analysis to Structured Data Analysis*. Dordrecht: KluwerAcademic Publishers; 2004. 180 p.
109. Robert P, Escoufier Y. *A Unifying Tool for Linear Multivariate Statistical Methods:*

- The RV-Coefficient. *Appl Stat.* 1976;25(3):257–65.
110. Klingenberg CP. Morphometric integration and modularity in configurations of landmarks: tools for evaluating a priori hypotheses. *Evol Dev.* 2009;11(4):405–21.
 111. Rohlf JF, Corti M. The Use of Two-block Partial Least-squares to Study Covariation in Shape. *Proefs.* 1999;49(4):1–30.
 112. Maitra S, Yan J. Principle Component Analysis and Partial Least Squares : Not A Pap. 2008;79–90.
 113. Barbeito-Andrés J, Anzelmo M, Ventrice F, Sardi ML. Measurement error of 3D cranial landmarks of an ontogenetic sample using Computed Tomography. *J Oral Biol Craniofacial Res.* 2012;2(2):77–82.
 114. Nishimura I, Hosokawa R, Kaplan ML, Atwood DA. Animal model for evaluating the effect of systemic estrogen deficiency on residual ridge resorption. *J Prosthet Dent.* 1995;73(3):304–10.
 115. Saldanha JB, Casati MZ, Neto FH, Sallum EA, Nociti FH. Smoking May Affect the Alveolar Process Dimensions and Radiographic Bone Density in Maxillary Extraction Sites: A Prospective Study in Humans. *J Oral Maxillofac Surg.* 2006;64(9):1359–65.
 116. Richard MJ, Morris C, Deen BF, Gray L, Woodward J a. Analysis of the anatomic changes of the aging facial skeleton using computer-assisted tomography. *Ophthal Plast Reconstr Surg.* 2009;25(5):382–6.
 117. Stiévenart M, Malevez C. Rehabilitation of totally atrophied maxilla by means of four zygomatic implants and fixed prosthesis: a 6–40-month follow-up. *Int J Oral Maxillofac Surg.* 2010;39(4):358–63.
 118. Chapman RE. Conventional Procrustes Approaches. In: *Proceedings of the Michigan Morphometrics Workshop (Special Publication No 2)*. Ann Arbor: University of Michigan Museum of Zoology; 1990. p. 251–67.
 119. Von Cramon-Taubadel N. The relative efficacy of functional and developmental cranial modules for reconstructing global human population history. *Am J Phys Anthropol.* 2011;146(1):83–93.

120. Ravosa MJ. Interspecific perspective on mechanical and nonmechanical models of primate circumorbital morphology. *Am J Phys Anthropol.* 1991;86(3):369–96.
121. Ravosa MJ, Noble VE, Hylander WL, Johnson KR, Kowalski EM. Masticatory stress, orbital orientation and the evolution of the primate postorbital bar. *J Hum Evol.*
122. Tallgren A. Neurocranial morphology and ageing- a longitudinal roentgen cephalometric study of adult Finnish women. *Am J Phys Anthropol.* 1974;41:285–94.
123. Wulc AE, Sharma P, Czyz CN. Midfacial Rejuvenation. Hartstein ME, Holck DEE WA, editor. Springer; 2012. 15-29 p.
124. Carlsson G, Bergman B, Hedegård B. Changes in contour of the maxillary alveolar process under immediate dentures. A longitudinal clinical and x-ray cephalometric study covering 5 years. *Acta Odontol Scand.* 1967;25(1):45–75.
125. Yüzügüllü B, Gulsahi A, Imirzalioglu P. Radiomorphometric indices and their relation to alveolar bone loss in completely edentulous Turkish patients: a retrospective study. *J Prosthet Dent. The Editorial Council of the Journal of Prosthetic Dentistry;* 2009;101(3):160–5.
126. Stout S, Lueck R. Bone remodeling rates and skeletal maturation in three archaeological skeletal populations. *Am J Physical Anthropol.* 1995;98(2):161–71.
127. Seeman E. From Density to Structure Growing Up and Growing Old on the Surfaces of Bone. *J Bone Miner Res.* 1997;12(4):509–21.
128. Kleerekoper M, Nelson D, Peterson E, Flynn M, Pawluszka A, Jacobsen G, et al. Reference data for bone mass, calciotropic hormones, and biochemical markers of bone remodeling in older (55-75) postmenopausal white and black women. *J Bone Miner Res.* 1994;9(8):1267–76.
129. Christiansen C, Lindsay R. Estrogens, Bone Loss and Preservation. 1990;1:7–13.
130. de Freitas LMA, Pinzan A, Janson G, Freitas KMS, de Freitas MR, Henriques JFC. Facial height comparison in young white and black Brazilian subjects with normal occlusion. *Am J Orthod Dentofacial Orthop.* 2007;131(6):706.e1–6.

131. Işcan M, Steyn M. Craniometric determination of population affinity in South Africans. *Int J Legal Med.* 1999;112(2):91–7.
132. White TD, Black MT, Folkens PA. *Human Osteology.* Human Osteology. Elsevier; 2012. 379-427 p.
133. Pessa JE, Zadoo VP, Yuan C, Ayedelotte J, Cuellar FJ, Cochran CS, et al. Concertina Effect and Facial Aging: Nonlinear Aspects of Youthfulness and Skeletal Remodeling, and Why, Perhaps, Infants Have Jowls. *Plast Reconstr Surg.* 1999;103(2):635–44.
134. Park HK, Chung JW, Kho HS. Use of hand-held laser scanning in the assessment of craniometry. *Forensic Sci Int.* 2006;160(2-3):200–6.
135. Mitteroecker P, Gunz P, Bernhard M, Schaefer K, Bookstein FL. Comparison of cranial ontogenetic trajectories among great apes and humans. *J Hum Evol.* 2004;46(6):679–98.
136. Bastir M, Rosas A. Facial heights: Evolutionary relevance of postnatal ontogeny for facial orientation and skull morphology in humans and chimpanzees. *J Hum Evol.* 2004;47:359–81.
137. Mitteroecker P, Windhager S, Müller GB, Schaefer K. The morphometrics of “masculinity” in human faces. *PLoS One.* 2015;10(2):e0118374.
138. Gonzalez PN, Perez SI, Bernal V. Ontogenetic allometry and cranial shape diversification among human populations from South America. *Anat Rec.* 2011;294(11):1864–74.
139. Klingenberg CP. MorphoJ: an integrated software package for geometric morphometrics. *Mol Ecol Resour.* 2011;11(2):353–7.
140. Burnaby T. Growth-Invariant Discriminant Functions and Generalized Distances. *Biometrics.* 1966;22(1):96–110.
141. Badyaev A V. Growing apart: an ontogenetic perspective on the evolution of sexual size dimorphism. *Trends Ecol Evol.* 2002;17(8):369–78.
142. Perez SI, Diniz-Filho JAF, Bernal V, Gonzalez PN. Alternatives to the partial Mantel test in the study of environmental factors shaping human morphological variation. *J Hum Evol.* 2010;59(6):698–703

143. Lawler RR. Monomorphism, male-male competition, and mechanisms of sexual dimorphism. *J Hum Evol*; 2009;57(3):321–5.
144. Hedrick A V., Temeles EJ. The evolution of sexual dimorphism in animals: Hypothesis and tests. *Trends in Ecology & Evolution*. 1989. p. 136–8.
145. Frayer DW, Wolpoff MH. Sexual Dimorphism. *Annu Rev Anthropol*. 1985;14:429–73.
146. Tarli S, E R. Methodological considerations on the study of sexual dimorphism in past human populations. *Hum Evol*. 1986;1.1(1):51–66.
147. Henneberg M, Van Den Berg ER. Test of socioeconomic causation of secular trend: Stature changes among favored and oppressed South Africans are parallel. *Am J Phys Anthropol*. 1990;83(4):459–65.
148. Holden C, Mace R. Sexual dimorphism in stature and women's work: a phylogenetic cross-cultural analysis. *Am J Phys Anthropol*. 1999;110(1):27–45.
149. Bulygina E, Mitteroecker P, Aiello L. Ontogeny of facial dimorphism and patterns of individual development within one human population. *Am J Phys Anthropol*. 2006;131(3):432–43.
150. Ursi W, Trotman C, McNamara J, Behrents R. Sexual dimorphism in normal craniofacial growth. *Angle Orthod*. 1993;63(1):47–56.
151. Velemínská J, Bigoni L, Krajčovič V, Borský J, Mahelov D, Čagov V, et al. Surface facial modelling and allometry in relation to sexual dimorphism. *HOMO- J Comp Hum Biol*. 2012;63(2):81–93.
152. Suazo Galdames IC, Zavando Matamala DA, Smith RL. Accuracy of Palate Shape as sex Indicator in Human Skull with Maxillary Teeth Loss. *Int J Morphol*. 2008;26(4):989–93.
153. Cock AG. Genetical aspects of metrical growth and form in animals. *Q Rev Biol*. 1966;41(2):131–90.
154. Kimmerle EH, Ross A, Slice D. Sexual dimorphism in America: Geometric morphometric analysis of the craniofacial region. *J Forensic Sci*. 2008;53(1):54–7.
155. Kimbel WH, Rak Y. The cranial base of *Australopithecus afarensis*: new insights

- from the female skull. *Philos Trans R Soc B Biol Sci.* 2010;365(1556):3365–76.
156. Chang H-P, Hsieh S-H, Tseng Y-C, Chou T-M. Cranial-base morphology in children with class III malocclusion. *Kaohsiung J Med Sci*; 2005;21(4):159–65.
 157. Rana T, Khanna R, Tikku T, Sachan K. Relationship of maxilla to cranial base in different facial types—a cephalometric evaluation. *J Oral Biol Craniofacial Res. Craniofacial Research Foundation*; 2012;2(1):30–5.
 158. Doyle WJ, Swarts JD. Eustachian tube-tensor veli palatini muscle-cranial base relationships in children and adults: an osteological study. *Int J Pediatr Otorhinolaryngol*; 2010;74(9):986–90.
 159. Veroni A, Nikitovic D, Schillaci M a. Brief communication: Sexual dimorphism of the juvenile basicranium. *Am J Phys Anthropol.* 2010;141(1):147–51.
 160. Gapert R, Black S, Last J. Sex determination from the foramen magnum: discriminant function analysis in an eighteenth and nineteenth century British sample. *Int J Legal Med.* 2009;123(1):25–33.
 161. Holland TD. Race determination of fragmentary crania by analysis of the cranial base. *Am J Phys Anthropol.* 1986;70(2):203–8
 162. Burdan F, Szumito J, Walocha J, Klepacz L, Madej B, Dworzański W, et al. Morphology of the foramen magnum in young Eastern European adults. *Folia Morphol.* 2012;71(4):205–16.
 163. Lestrel PE, Cesar RM, Takahashi O, Kanazawa E. Sexual dimorphism in the Japanese cranial base: A fourier-wavelet representation. *Am J Phys Anthropol.* 2005;128(December 2003):608–22.
 164. McDowell JL, L'Abbé EN, Kenyhercz MW. Nasal aperture shape evaluation between black and white South Africans. *Forensic Sci Int.* 2012;222(1-3):397.e1–6.
 165. Rosas A, Bastir M, Alarcón JA, Kuroe K. Thin-plate spline analysis of the cranial base in African, Asian and European populations and its relationship with different malocclusions. *Arch Oral Biol.* 2008;53(9):826–34.
 166. Maier C. Palate shape and depth: A shapematching machine learning method for assessment of ancestry from skeletal remains. 2013.

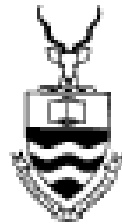
167. Lima LNC, de Oliveira OF, Sassi C, Picapedra A, Francesquini L, Daruge E. Sex determination by linear measurements of palatal bones and skull base. *J Forensic Odontostomatol.* 2012;30(1):37–44.
168. Burris BG, Harris EF. Maxillary arch size and shape in American blacks and whites. *Angle Orthod.* 2000;70(4):297–302.
169. Gill GW. Craniofacial Criteria in the Skeletal Attribution of Race. *Forensic Osteology - Advances in the Identification of Human Remains.* 1998. p. 293–315.
170. Ramsthaler F, Kettner M, Gehl A, Verhoff MA. Digital forensic osteology: Morphological sexing of skeletal remains using volume-rendered cranial CT scans. *Forensic Sci Int.* 2010;195(1-3):148–52.
171. Giles E, Elliot O. Sex Determination by Discriminant Function Analysis of Crania. *Am J Physcial Anthropol.* 1963;21(1):53–68.
172. McDowell JL, Kenyhercz MW, L'Abbé EN. An evaluation of nasal bone and aperture shape among three South African populations. *Forensic Sci Int.* 2015;252:189.e1–189.e7.
173. Pohar M, Blas M, Turk S. Comparison of logistic regression and linear discriminant analysis : A simulation study. *Adv Methodol Stat.* 2004;1(1):143–61.
174. Rafferty KL, Herring SW, Artese F. Three-dimensional loading and growth of the zygomatic arch. *J Exp Biol.* 2000;203(Pt 14):2093–104.
175. Bookstein FL, Slice D, Gunz P, Mitteroecker P. Anthropology takes control of morphometrics. *Coll Antropol.* 2004;28:121–32.
176. Poulsen J, French A. *Discriminant function analysis.* 2012.
177. Fisher RA. The use of multiple measurements in taxonomic problems. *Ann Eugen.* 1936;7(2):179–88.
178. Gualdi-Russo E. Sex determination from the talus and calcaneus measurements. *Forensic Sci Int.* 2007;171(2-3):151–6.
179. Cattaneo C. Forensic anthropology: developments of a classical discipline in the new millennium. *Forensic Sci Int.* 2007;165(2-3):185–93.
180. Dirkmaat DC, Cabo LL, Ousley SD, Symes S a. New perspectives in forensic

- anthropology. *Am J Phys Anthropol.* 2008;Suppl 47:33–52.
181. Peckmann TR, Meek S, Dilkie N, Mussett M. Sex estimation using diagonal diameter measurements of molar teeth in African American populations. *J Forensic Leg Med*; 2015;36:70–80.
 182. Guyomarc'h P, Brůzek J. Accuracy and reliability in sex determination from skulls: A comparison of Fordisc(R) 3.0 and the discriminant function analysis. *Forensic Sci Int.* 2011;208:30–5.
 183. Franklin D, Cardini A, Flavel A, Kuliukas A. Estimation of sex from cranial measurements in a Western Australian population. *Forensic Sci Int*; 2013;229(1-3):158.e1–158.e8.
 184. Mehta M, Saini V, Nath S, Menon SK. CT scan images for sex discrimination – a preliminary study on Gujarati population. *J Forensic Radiol Imaging*; 2015;3(1):43–8
 185. Schlager S. Soft-tissue reconstruction of the human nose Population differences and sexual dimorphism. 2013.
 186. R. Martin KS. *Lehrbuch der Anthropologie.* Stuttgart: Gustav Fischer Verlag; 1957.
 187. Campbell MJ, Swinscow TD V. Chapter 8 The χ^2 tests. In: Campbel M, Swinscow TD V, editors. *Statistics at square one.* 11th ed. Chichester, West Sussex: BMJ Books; 2009. p. 86–101.
 188. Kranioti EF, İşcan MY, Michalodimitrakis M. Craniometric analysis of the modern Cretan population. *Forensic Sci Int.* 2008;180(2-3):1–5.
 189. Mastrangelo P, De Luca S, Sánchez-Mejorada G. Sex assessment from carpals bones: Discriminant function analysis in a contemporary Mexican sample. *Forensic Sci Int.* 2011;209(1-3):196.e1–196.e15
 190. Ogawa Y, Imaizumi K, Miyasaka S, Yoshino M. Discriminant functions for sex estimation of modern Japanese skulls. *J Forensic Leg Med*; 2013;20(4):234–8.
 191. Torimitsu S, Makino Y, Saitoh H, Sakuma A, Ishii N, Yajima D, et al. Morphometric analysis of sex differences in contemporary Japanese pelves using multidetector computed tomography. *Forensic Sci Int*; 2015;17(4):226–31

192. Richard AH, Parks CL, Monson KL. Accuracy of standard craniometric measurements using multiple data formats. *Forensic Sci Int.* 2014;242:177–85
193. Stull KE, Kenyhercz MW, L'Abbé EN. Ancestry estimation in South Africa using craniometrics and geometric morphometrics. *Forensic Sci Int.* 2014;245C:206.e1–206.e7.
194. Franklin D, Cardini A, Flavel A, Kuliukas A. The application of traditional and geometric morphometric analyses for forensic quantification of sexual dimorphism: preliminary investigations in a Western Australian population. *Int J Legal Med.* 2012;126(4):549–58.
195. Press S, Wilson S. Choosing Between Logistic Regression and Discriminant Analysis. *J Am Stat Assoc.* 1978;73(364):699–705.
196. Isaza J, Díaz CA, Bedoya JF, Monsalve T, Botella MC. Assessment of sex from endocranial cavity using volume-rendered CT scans in a sample from Medellín, Colombia. *Forensic Sci Int.* 2014;234:186.e1–186.e10.
197. Ramadan Uysal S, Türkmen N, Dolgun NA, Gökharman D, Menezes RG, Kacar M, et al. Sex determination from measurements of the sternum and fourth rib using multislice computed tomography of the chest. *Forensic Sci Int.* 2010;197(1-3):120.e1–5
198. Dong H, Deng M, Wang W, Zhang J, Mu J, Zhu G. Sexual dimorphism of the mandible in a contemporary Chinese Han population. *Forensic Sci Int;* 2015;255:9–15.
199. Viciano J, D'Anastasio R, Capasso L. Odontometric sex estimation on three populations of the Iron Age from Abruzzo region (central-southern Italy). *Arch Oral Biol.* 2014;60(1):100–15.
200. Shah T, Patel MN, Nath S, Menon SK. Determination of sex using cephalo-facial dimensions by discriminant function and logistic regression equations. *Egypt J Forensic Sci.* Forensic Medicine Authority; 2015;
201. Steyn M, İşcan MY. Sex determination from the femur and tibia in South African whites. *Forensic Sci Int.* 1997;90(1-2):111–9.
202. Patriquin ML, Loth SR, Steyn M. Sexually dimorphic pelvic morphology in South African whites and blacks. *Homo.* 2003;53(3):255–62.

203. Asala SA, Bidmos MA, Dayal MR. Discriminant function sexing of fragmentary femur of South African blacks. *Forensic Sci Int.* 2004;145(1):25–9.
204. Ramamoorthy B, Pai MM, Prabhu L V., Muralimanju B V., Rai R. Assessment of craniometric traits in South Indian dry skulls for sex determination. *J Forensic Leg Med.* 2016;37:8–14.
205. Snow CC, Hartman S, Giles E, Young FA. -Sex and race determination by calipers and computer:test of Giles and Elliot discriminant functions in 52 forensic cases. 1979.
206. Wyatt CC. The effect of prosthodontic treatment on alveolar bone loss: a review of the literature. *J Prosthet Dent.* 1998;80(3):362–6.
207. Berg H, Carlsson GE, Helkimo M. Changes in the shape of the posterior parts of the upper jaws after extraction of teeth and prosthetic treatment. *J Prosthet Dent.* 1989;34(3):262–8.
208. Kamath VG, Asif M, Shetty R, Avadhani R. Binary Logistic Regression Analysis of Foramen Magnum Dimensions for Sex Determination. *Anat Res Int.* 2015;2015:1–9.
209. Robinson MS, Bidmos MA. An assessment of the accuracy of discriminant function equations for sex determination of the femur and tibia from a South African population. *Forensic Sci Int.* 2011;206(1-3):212.e1–5.

APPENDIX A
Ethical Consent Form



Human Research Ethics Committee (Medical)
(formerly Committee for Research on Human Subjects (Medical))

Senate House, Research Office, Room SP10005, 19th floor, Senate House • Telephone: +27 11 717-1234 • Fax: +27 11 359-5799
Private Bag 3, Wits 2050, South Africa

Ref: W-CJ-101109-1

Copy J.

15/05/2013

TO WHOM IT MAY CONCERN:

- Waiver:** This certifies that the following research does not require clearance from the Human Research Ethics Committee (Medical).
- Investigator:** School of Anatomical Sciences (Head: Prof T J M Daly).
- Project title:** Research on cadaveric material.
- Reason:** In terms of Chapter 8, sections 62-64 of the National Health Act No 61 of 2003 donated bodies and their tissues may be used for, among other purposes, health research. Use of such material is subject only to permission from the responsible person in the School of Anatomical Sciences - the Head or person designated by the Head.

Peter Cleaton-Jones



Professor Peter Cleaton-Jones
Chair: Human Research Ethics Committee (Medical)

copy: Anisa Keshav, Research Office, Senate House, Wits

APPENDIX B

Turn-it-in Digital Receipt



Digital Receipt

This receipt acknowledges that **Turnitin** received your paper. Below you will find the receipt information regarding your submission.

The first page of your submissions is displayed below.

Submission author: **Candice Small**
Assignment title: **PhD thesis**
Submission title: **FinalCSmall2016PhDTurnitin.pdf**
File name: **Candice_Small_0717284n_FinalCS...**
File size: **1.27M**
Page count: **173**
Word count: **49,922**
Character count: **263,317**
Submission date: **31-Mar-2016 03:27 PM**
Submission ID: **652428632**

SEXUAL DIMORPHISM IN WHITE SOUTH
AFRICANS

Candice Small



Original content not submitted to Turnitin. University of the
Western Cape, a member of the Council on Higher Education
of South Africa
© 2016 Turnitin, Inc.

ORIGINALITY REPORT

13%

SIMILARITY INDEX

4%

INTERNET SOURCES

11%

PUBLICATIONS

%

STUDENT PAPERS

PRIMARY SOURCES

1	Small, Candice, Desiré Brits, and Jason Hemingway. "Assessing the effects of tooth loss in adult crania using geometric morphometrics", International Journal of Legal Medicine, 2015. Publication	9%
2	www.craniofacial-id.com Internet Source	1%
3	wiredspace.wits.ac.za Internet Source	<1%
4	Hutchinson, Erin F., Mauro Farella, and Beverley Kramer. "Importance of teeth in maintaining the morphology of the adult mandible in humans", European Journal Of Oral Sciences, 2015. Publication	<1%
5	www.nlc-bnc.ca Internet Source	<1%
6	www.aafs.org Internet Source	<1%
7	www.ncbi.nlm.nih.gov	

APPENDIX C

*Assessing the effects of tooth loss in adult crania
using geometric morphometrics Int J Legal Med.*

2015;130(1):233–43

Assessing the effects of tooth loss in adult crania using geometric morphometrics

Candice Small, Desiré Brits & Jason Hemingway

**International Journal of Legal
Medicine**

ISSN 0937-9827

Volume 130

Number 1

Int J Legal Med (2016) 130:233-243

DOI 10.1007/s00414-015-1174-6



Your article is protected by copyright and all rights are held exclusively by Springer-Verlag Berlin Heidelberg. This e-offprint is for personal use only and shall not be self-archived in electronic repositories. If you wish to self-archive your article, please use the accepted manuscript version for posting on your own website. You may further deposit the accepted manuscript version in any repository, provided it is only made publicly available 12 months after official publication or later and provided acknowledgement is given to the original source of publication and a link is inserted to the published article on Springer's website. The link must be accompanied by the following text: "The final publication is available at link.springer.com".

Assessing the effects of tooth loss in adult crania using geometric morphometrics

Candice Small · Desiré Brits · Jason Hemingway

Received: 10 November 2014 / Accepted: 2 March 2015 / Published online: 18 March 2015
© Springer-Verlag Berlin Heidelberg 2015

Abstract With high numbers of unidentified skeletonised remains recovered annually in South Africa and an increased number of edentate individuals being reported, the question arises as to whether tooth loss would result in craniofacial changes which might alter the accuracy of osteological analyses. Forty-five fixed landmarks together with sliding semilandmarks were collected from 229 white South African crania and were used to capture curve data pertaining to the basicranium, alveoli, zygomatic arches, nasal aperture and orbits. Geometric morphometric methods were employed to assess the effects of tooth loss on these structures. Although a number of effects were seen when the skull was analysed in its entirety, only the alveoli proved to be significantly affected when regions were analysed individually. Both upper facial height and palate shape were affected by tooth loss, which may influence various osteometric measurements and qualitative traits that are used during the assessment of ancestry and sex.

Keywords Forensic anthropology · Population variation · Tooth loss · Alveolus/maxilla · Geometric morphometrics · Semilandmarks

Introduction

In South Africa, high rates of interpersonal violence and murder have ignited an increased interest in the field of forensic anthropology as the number of unidentified skeletonised remains uncovered each year continues to climb [1]. A multitude of forensic investigators have set out to derive population-specific standards in order to increase the accuracy of biological profiles and aid in the identification of skeletonised individuals [1–3]. Most of these studies were conducted on individuals socially classified as black South Africans, used traditional morphometrics and none have investigated the effects of tooth loss on the craniofacial structures of South Africans. Unfortunately, information pertaining to edentulism in South Africa is scarce. In 2004, Van Wyk and Van Wyk put forth [4] that the most recent survey that included edentulism was published in 1989. This study, by Du Plessis and associates, showed that 12.6 % of South Africans between the ages of 35 and 44 across the black, white, mixed race or so called “coloured”, and Asian populations were completely edentulous. The incidence of edentulism was found to be highest in the coloured population (51.6 %) and more common in females than males, in all population groups investigated [4].

Despite being of primarily Dutch descent, white South Africans have been isolated from their European ancestors for hundreds of years, allowing admixture and possibly adaptation to the local environment to shape this population into a unique entity worthy of specific population standards [5]. Furthermore, as the life expectancy of South Africans is likely to reach 76 years by 2100 [6], there will inevitably be a large number of skeletonised remains assessed by forensic anthropologists with varying degrees of tooth loss. However, it is difficult to comment on the number of edentulous individuals

C. Small (✉) · D. Brits · J. Hemingway
Faculty of Health Sciences, School of Anatomical Sciences,
University of the Witwatersrand, 7 York Road, Parktown,
Johannesburg 2193, Republic of South Africa
e-mail: candicesmll@gmail.com

D. Brits
e-mail: desire.brits@wits.ac.za

J. Hemingway
e-mail: jason.hemingway@wits.ac.za

which may constitute this sample due to the paucity of research on edentulism in South Africa.

Once teeth are lost due to factors such as poor dental health, periodontal disease, poor diet, bone disease and smoking [7, 8], significant microscopic and macroscopic changes of the maxilla occur. The process of ageing also increases the risk of tooth loss as bone becomes more porous and the number of active osteoblasts versus osteoclasts diminishes. This, together with other histological changes, causes bone loss to double between the ages of 60 and 80 years [9]. It has been shown that 12 months post-extraction, alveolar ridge height decreases by up to 44 % [8] whilst there is up to 500 % reduction in masticatory force, resulting in further resorption of the underlying bone in these inactive areas [10, 11]. Heath [12] evaluated the effects of edentulism on British individuals between the ages of 20 and 84 years and found that although edentulous subjects displayed significant alveolar resorption and a decrease in total facial height, these changes did not extend to the upper face. Facial height decreases were also demonstrated by Tallgren [13], Bartlett et al. [14] and Crothers [15] together with superior-posterior movement of the maxilla [16, 17]. Whilst Heath [12] found no significant changes to the basicranium or the hard palate [12], Pietrokofski and Massler [18] demonstrated that the buccal plate of the maxilla resorbed faster than the palatal plate, resulting in a reduced arch length [18]. It has also been found that edentate individuals display thinner cortical bone in all regions of the face but similar or greater elastic and shear moduli and density in the zygoma and cranial vault [11].

As numerous standard anthropological measurements are taken from the skull for the assignment of sex and ancestry, it may be important to factor in the structural changes associated with the loss of teeth to optimise the accuracy of biological assessments [19].

The aforementioned studies clearly demonstrate that tooth loss has a complex effect on various aspects of the viscerocranium. Despite this, there is a lack of anthropological research which elucidates what effects, if any, these structural changes have on the standard cranial measurements anthropologists take to aid in the estimation of sex and ancestry whilst compiling biological profiles. Furthermore, no research could be found which used geometric morphometric methods to clarify how tooth loss affects specific parts of the viscerocranium and basicranium.

Geometric morphometric methods are steadily gaining favour amongst anthropologists, due to the fact that it uses landmark-based analysis of form as opposed to the analysis of linear measurements [20]. In South Africa, an ever increasing number of anthropologists are using geometric morphometrics to study cranial form in terms of sex and race differences [21–23]. The method allows for greater shape distinguishing power as homologous landmark data maintains the three-

dimensional geometry of the object being analysed, whereas traditional morphometrics collapse form into a number of linear measurements [20]. Hence, the aim of this research was to use geometric morphometric methods to analyse the effects of tooth loss on white South African crania. Analyses were conducted on a global scale as well as on regional subsets by employing both fixed and sliding semilandmarks to investigate fine scale changes to the basicranium, maxilla, zygomatic bones, nasal aperture and orbits.

Materials and methods

A total of 229 crania were randomly selected from the Raymond A. Dart Collection of Human Skeletons, housed in the School of Anatomical Sciences at the University of the Witwatersrand, Johannesburg, South Africa. The sample employed in this investigation consisted of 118 males and 111 females (Table 1) of European descent (white). Most of the white individuals in the collection are from body donations and represent persons who are mainly of Dutch, German, French, British and Portuguese decent [24, 25]. The ages of the samples ranged between 18–95 years to ensure that the skulls assumed an adult configuration and to include a broad spectrum of adult skull morphologies. All of the selected individuals were born between the late nineteenth and twentieth centuries. Crania displaying varying degrees of dental loss were incorporated in the study, including completely edentulous individuals, so that the structural changes that occur in the face as a result of tooth loss could be evaluated. Due to the

Table 1 Age distribution of sample by decade ($n=229$)

Age interval	Male		Female	
	Total sample	Edentate individuals	Total sample	Edentate individuals
18–29	1	1	2	0
30–39	5	1	1	0
40–49	22	10	8	4
50–59	25	16	21	12
60–69	36	26	45	28
70–79	11	9	13	9
80–89	13	12	16	12
90–95	5	4	5	1
Total	118	79	111	66
Interval (years)	28–95	28–95	19–95	45–95
Mean (age in years)	62	68	66	68
SD (age in years) ^a	15	13	14	13

^a Standard deviation

fact that such a large proportion of the white cranial specimens from the collection are edentulous, we decided to include edentate material and hence, the current sample included a total of 145 edentate skulls. When teeth were lost and if the individual wore dentures prior to death were not known. Skulls exhibiting any other signs of damage, pathology or obvious orthodontic rehabilitation were excluded.

Data collection procedure

Clay was used to secure each cranium in a fix position to ensure that all landmarks and curves could be digitised without reorienting the cranium. Fixed landmarks on each cranium were digitised using a Microscribe® 3DX digitizer with a cited accuracy of 0.25 mm (Immersion Corp), interfaced to a desktop computer so that data could be

recorded directly into a Microsoft Excel document. Following this, curve data were captured by tracing the surface of each curve as a continuous stream of points, semilandmarks [26], registered at 1.0 mm intervals between the fixed landmarks. A list defining the landmarks used as well as a figure illustrating the landmarks and curves captured are given in Table 2 and Fig. 1. Landmarks involving the neurocranium were omitted as the skull vault is conventionally removed during dissection and subsequent rearticulation thereof would introduce unwanted error.

Data resampling and reworking

As semilandmarks were taken at a fixed distance from one another and not at bony landmarks, the number of semilandmarks on each curve was standardised using the

Table 2 Definitions and abbreviations for recorded fixed landmarks

Number	Landmark	Definition
1	Nuchal crest (nc)	The most posteriorly projecting point on the superior nuchal crest of the occiput
2	Opisthion (o)	The point on the middle of the posterior curve of foramen magnum
3 and 5	Posterior occipital condyle (poc)	Where the posterior margin of the occipital condyle comes into contact with foramen magnum
4	Basion (ba)	The point in the middle of the anterior aspect of foramen magnum
6	Inferior vomer (iv)	Point of contact between the sphenoid and vomer bones
7	Palatine (p)	Point on the interpalatine suture, laying most posteriorly
8	Posterior incisive canal (poic)	Posterior most point on the incisive canal
9	Anterior incisive canal (anic)	Anterior-most point on the incisive canal
10 and 11	Palatine foramen (pf)	Most anterolateral point on the palatine foramen
12	Intermaxillary (aic)	Most postero-inferior point on the alveolar bone that would normally lie between the central incisors
13 and 20	Mastoidale (ms)	Point situated on the greatest projection of the mastoid
14 and 21	Porion (po)	Point midway on the superior margin of the external acoustic meatus
15 and 22	Glenoidale (ge)	Point directly above the glenoid fossa on the zygoma
16 and 23	Articular eminence (ae)	The most inferolateral point on the articular eminence
17 and 24	Posterior zygotemporale (pz)	Point at the junction between the zygomatic and temporal bones, inferiorly
18 and 25	Zygomaxillare (zm)	Point at the junction between the zygomatic and maxillary bones, inferiorly
19 and 26	Superior zygotemporale (sz)	Point at the junction between the zygomatic and temporal bones, superiorly
27	Glabella (g)	The greatest anterior projection midsagittal aspect of the frontal bone at the level of the supraorbital ridges
28	Nasion (n)	The point between the internasal suture and the nasofrontal suture
29	Rhinion (r)	The most inferior point on the internasal suture
30	Inferior nasal spine (ins)	Tip of the nasal spine on the intermaxillary suture
31	Alveolare (ids)	Most antero-inferior point on the alveolar bone that would normally lie between the central incisors
32 and 37	Frontomalare temporale (fnt)	Point at the junction of the frontal and zygomatic bones, posteriorly
33 and 38	Frontozygomatic orbitale (fo)	Point where the frontal and zygomatic bones meet anteriorly on the orbital margin
34 and 39	Frontotemporale (ft)	Points on the frontal bone across which the bone is narrowest
35 and 40	Dacryon (d)	Point where the sutures of the frontal, maxillary and lachrymal bones meet
36 and 41	Zygomaxillare orbitale (zmo)	Point of junction between the zygomatic and maxillary bones on the orbital margin
42 and 44	Nariale (na)	The most inferior extent of the nasal aperture adjacent to the nasal spine
43 and 45	Alare (al)	The widest point on the nasal lateral margin of the nasal aperture

programme Morphueus (available at <http://www.morphometrics.org>). Points were resampled such that an equal number of semilandmarks represent homologous curves between specimens. The number of landmarks for each curve was chosen so that an average spacing of approximately 7 mm lay between adjacent semilandmarks (determined from 10 randomly selected crania). This ensured that the inherently “deficient” semilandmarks could be treated as homologous anatomical landmarks [7].

Statistical analyses

As the study of asymmetry was beyond the scope of this investigation, the symmetric component of the data was obtained using the statistical programme “MorphoJ” version 2.0 (Available at www.flywings.org.uk) [27] and the regional subsets listed in Table 3 were extracted. Each of the subsets consists of a number of curves defined by means of semilandmarks located between fixed landmarks. The number of semilandmarks employed to define each curve are also given in Table 3.

Following the mitigation of asymmetry, the following set of statistical procedures was conducted by means of programmed algorithms and scripts using the statistical programme “R” version 2.15.1 (www.r-project.org). These procedures were repeated collectively for the viscer- and basicranium during the global analysis as well as on each of

Table 3 Subset breakdown and description of curves and semilandmarks

Subset	Curves	SSL ^a
Basicranium	1. Foramen magnum	16
Alveolus	2. Inner palate	12
	3. Outer palate	14
	4. Inferior zygoma	11
Zygoma	5. Superior zygoma	11
	6. Orbit	18
Nasal aperture	7. Nasal	16

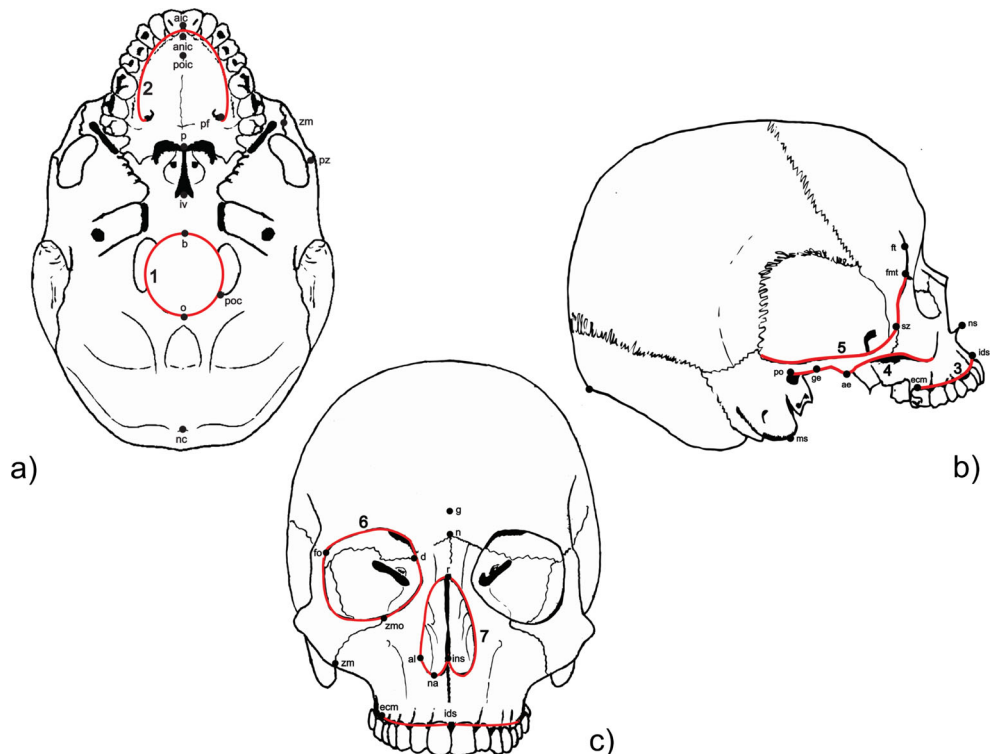
Curve numbers correspond to those in Fig. 1

^a Number of sliding semilandmarks

the subsets listed in Table 3 individually in the regional analysis.

A partial Procrustes superimposition was used to align landmarks by translation, scaling and rotation [28–30], and the resulting data were projected orthogonally to the tangent plane. The thin plate spline algorithm outlined in Gunz [31, 32] was used to allow semilandmarks to slide with each iteration, as opposed to that which minimises the Procrustes distance. Helper landmarks were utilised because sliding semilandmarks are shifted along a tangent to the curve with each iteration during Procrustes superimposition, and not along the curve itself. These helper points were then discarded prior to any statistical analysis. Finally, permutation tests were

Fig. 1 Illustration of the landmarks and curves used in this study. **a** Inferior view. **b** Lateral view. **c** Anterior view. Abbreviation and number index correspond to curve numbers in Table 2



employed to determine whether significant size and age differences exist between the male and female groups.

In this investigation, the analysis of dental loss was categorical, i.e. scoring of absent (0) or present (1). A score of absent was given to teeth lost ante-mortem in which blunting of the alveolar crests was apparent or alveolar resorption was marked. A score of present was given if teeth were either physically present or in cases in which skulls displayed post-mortem tooth loss where well-defined alveoli with minimal blunting of alveolar crests remained. Hence, a 2-block partial least squares (PLS) was employed to assess the effects of dental loss on the morphology of the face and basicranium.

Next, the RV coefficient [33] was used to assess whether a significant amount of covariation exists between the two blocks of data (tooth loss and cranial shape). This coefficient is superficially comparable to the squared Pearson's correlation coefficient in that zero represents no association and one a perfect association (the amount of covariation between X and Y expressed as a fraction of the total variation in blocks X and Y). The significance of the covariation was tested using a permutation test to assess whether the coefficient obtained is significantly greater than that resulting by chance [34]. Where significant covariation existed, this was explored using PLS. PLS is a relatively new dimension-reducing technique that explores *covariation between* a set number of variables or blocks, as opposed to principal component analysis (PCA) which explores *variation within* a block [28, 35]. Due to the fact that the dependant variable, in this case dental loss had been specified, PLS is a better technique than PCA to use [36]. Vector diagrams and colour-coded polygon figures were used to visualise the effects of dental loss on craniofacial morphology.

Results

Global analyses

A significant level of covariation was observed between tooth loss and cranial shape ($RV=0.373$, $p<0.001$), and hence, a two-block PLS analysis was used to elucidate the association between these variables (Fig. 2). In Fig. 2, the x axis variable on each graphs is calculated as a unique linear combination of the dental scores (the presence and absence of each tooth) that is associated with that particular morphological change. The absolute value on the x axis is arbitrary, being centred about 0, 0. The presence and absence for each tooth can be reconstructed for any point along the axis given the loadings calculated for the PLS (i.e. $y=m_1 \times 1 + m_2 \times 2 + m_3 \times 3 \dots$). There is a degree of multicollinearity, which (like other multivariate methods) is accommodated here.

The first PLS vector accounted for 72.01 % of the total covariation seen between dental loss and cranial morphology.

Similarly factors two, three and four account for 4.66, 3.59 and 2.76 % of the covariation in the sample, respectively. All edentulous individuals clustered towards the negative end of the graph for factor one (Fig. 2), independent of skull shape, whereas the remaining vectors only account for a tiny fraction of the covariation and do not align with the order of tooth loss. Vector diagrams and polygon representations were illustrated using R with a colour spectrum representing relative changes of polygon area (Fig. 3). The use of both image types facilitates an understanding of the changes taking place in each structure as the vector diagrams show how and in which direction each structure changes, whilst the polygon images also give an indication as to the localised relative shape changes using a colour gradient.

In the polygon representations of morphological change (Fig. 3), two images are presented, one representing completely edentulous individuals and the other representing dentate individuals. Polygons that experience insignificant change in surface area are green in colour, whereas spectra tending towards red and blue are indicative of increasing and decreasing relative polygon area, respectively. The colour red itself indicates a twofold increase in area, whilst blue represents a halving. It is unsurprising that these images indicate that the greatest change associated with tooth loss is the marked recession of the alveolar bone of the maxilla, which seems somewhat localised in the anterior third of this structure. This severe resorption of bone leads to a marked decrease in facial height and prognathism. There is also a significant decrease in the length of the bony bar that extends from the approximate position of the canine jugum to the infraorbital margin near the zygomaxillare orbitale. This is likely as a result of the decrease in prognathism due to alveolar resorption. As the resorption of bone is not limited to the labial and buccal surfaces of the maxilla but also occurs on the lingual surface, there is a noticeable increase in the width of the palate, making it appear more hyperbolic. There also appears to be less pronounced changes to the interorbital and nasal portions of the facial skeleton, with edentate individuals expressing enlarged regions; however, this may only reflect an artefact from global Procrustes superimposition.

In the vector diagrams (Fig. 3), the two extreme morphologies represented in the data set are superimposed as reference and target images and vectors/arrows are used to show the magnitude and direction of the change that occurs between them. The figures illustrate that the greatest variation is present in the maxilla but specifically highlights the fact that a larger degree of resorption occurs in a posterior medial direction around the labial/buccal surface, whilst a relatively smaller degree of resorption occurs in an anterolateral direction about the lingual/palatal surface.

Additionally, it is apparent that there is an inferior and anterior flexion of the basicranium relative to the viscerocranium such that the external occipital protuberance

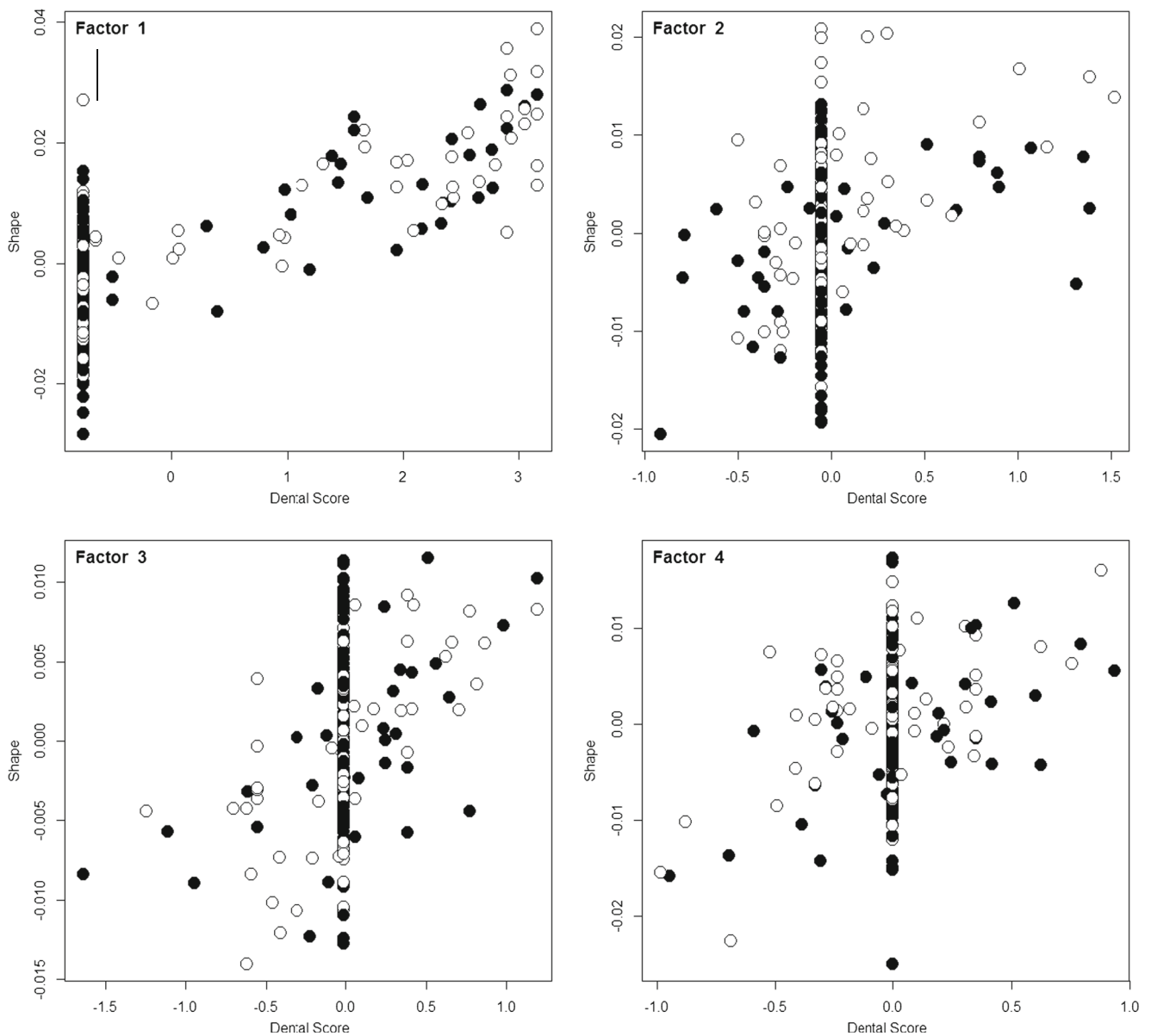


Fig. 2 Results of the two-block partial least squares analyses showing the first four vectors. *Closed circles* indicate female specimens whilst *open circles* represent male specimens. The specimens that are all clustering along a straight line are those that are completely edentulous

comes to lie more inferiorly whilst the mastoid processes appear to move both inferiorly and anteriorly. The relative size of the basicranium also appears marginally larger in the edentate individuals. Based on the vector diagrams, it also becomes apparent that the zygomatic bones shift inferiorly and the bizygomatic breadth becomes relatively larger with tooth loss. Finally, both the protrusion of the nasal bones and the size of the orbits appear to undergo a relative increase in cases of extensive tooth loss. It should be noted, however, that these observations are relative, and it is likely that a decrease in the size of the facial skeleton is responsible for these outcomes rather than an absolute increase in the size of the aforementioned structures.

Individual curve analyses

When each of the subsets including the basicranium, alveolus, zygomatic arch, nasal aperture and orbital rim were analysed individually, the alveolus proved to be the only structure significantly affected by tooth loss. This effect proved to be highly significant ($p < 0.001$). The first vector of the two-block PLS accounts for 82.72 % of the covariation between dental loss and maxillary shape, followed by only 5.56, 2.50 and 2.28 % being accounted for by the next three vectors. The dramatic reduction in the thickness of the alveolar bone is striking (Fig. 4). The anterior third of the maxilla experiences particularly extreme reduction of bone, and it appears as though

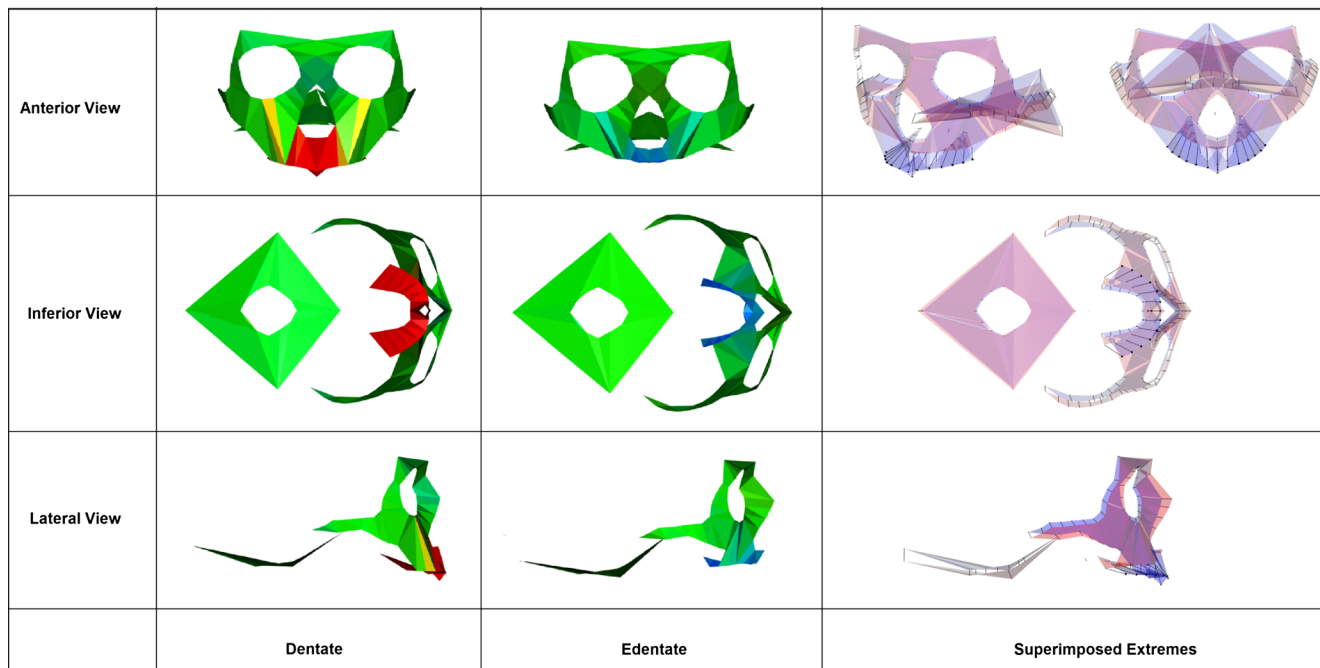


Fig. 3 Anterior, inferior and lateral coloured side by side representations (*left*) and vector diagrams (*right*) illustrating the changes in skull morphology associated with dental loss. In the side by side illustrations, the *image on the far left* represents dentate individuals whilst, on the other extreme, the *image on the right* represents completely edentate individuals. *Green areas* are equivalent; *red* indicates a large increase whilst *blue* shows a large decrease. The gradation of colours between

red and blue, from yellow to turquoise, indicate morphologies that lie between the two extremes. In the vector diagrams on the right, *arrows* indicate the change in a structure from being completely edentate, the red reference form, to being completely dentate, the blue target form. The *size of the arrows* in the figure represents the relative amount of structural change

virtually no bone remains. This severe reduction in bone causes an overall, relative widening of the bony palate which results in a more hyperbolic shape. The vector diagram in Fig. 4 clearly illustrates that the loss of bone associated with edentulism is not limited to the labial/buccal surface but occurs along the lingual surface as well. The depth of the incisive canal, represented by the triangular eminence of bone that appears to extend below the alveolar margin in Fig. 4, is seen to migrate anteriorly and reduce in depth in the images representing the edentate configuration.

Discussion

Due to the fact that the cortical bone of the alveolar ridges of the maxilla is so thin, delicate and labile [8], alveolar resorption following tooth loss is severe, so much so that even a reduction of crown height resulting from tooth wear leads to a decrease in anterior upper facial height [15]. Studies conducted on monkeys showed that the highest rate of resorption occurs within the first few months following extraction and that lack of oestrogen may have a significant effect on continued resorption [37]. This extreme resorption may be further accelerated by smoking, as demonstrated by Saldanha et al. in 2006 [38].

Although a vast number of studies, most of an orthodontic nature, have assessed the effects of edentulism on the mandible and maxilla [8, 12, 13, 17], very few have considered its effects on other bony structures of the cranium and the subsequent effects thereof on the accurate estimation of sex and ancestry. In the current investigation, global analyses of the entire face and basicranium revealed that tooth loss has significant effects on the cranium including severe resorption of the maxillary alveolar bone with a concomitant decrease in alveolar prognathism. A relative increase in both orbit size and projection of the nasal aperture, a relative increase in the width of the zygomatics together with inferior and anterior flexion of the basicranium relative to the viscerocranium was also seen. When each curve was analysed individually, however, only the alveolus of the maxilla proved to be significantly affected. This is surprising since tooth loss was hypothesised to affect the zygoma as the masseter muscle has its origins from the zygomatic bone and arch. This muscle has been shown to atrophy with tooth loss [39], resulting in reduced bite force in edentate individuals [11, 40] and accordingly, this bone should experience a decrease in mechanical loading and hence a degree of attrition, which was not observed. Richard et al. [41] examined the effects of ageing on the craniofacial skeleton, and observed a decrease in the anterior projection of the zygomatics, which may support the idea that this bone should experience some degree of atrophy over

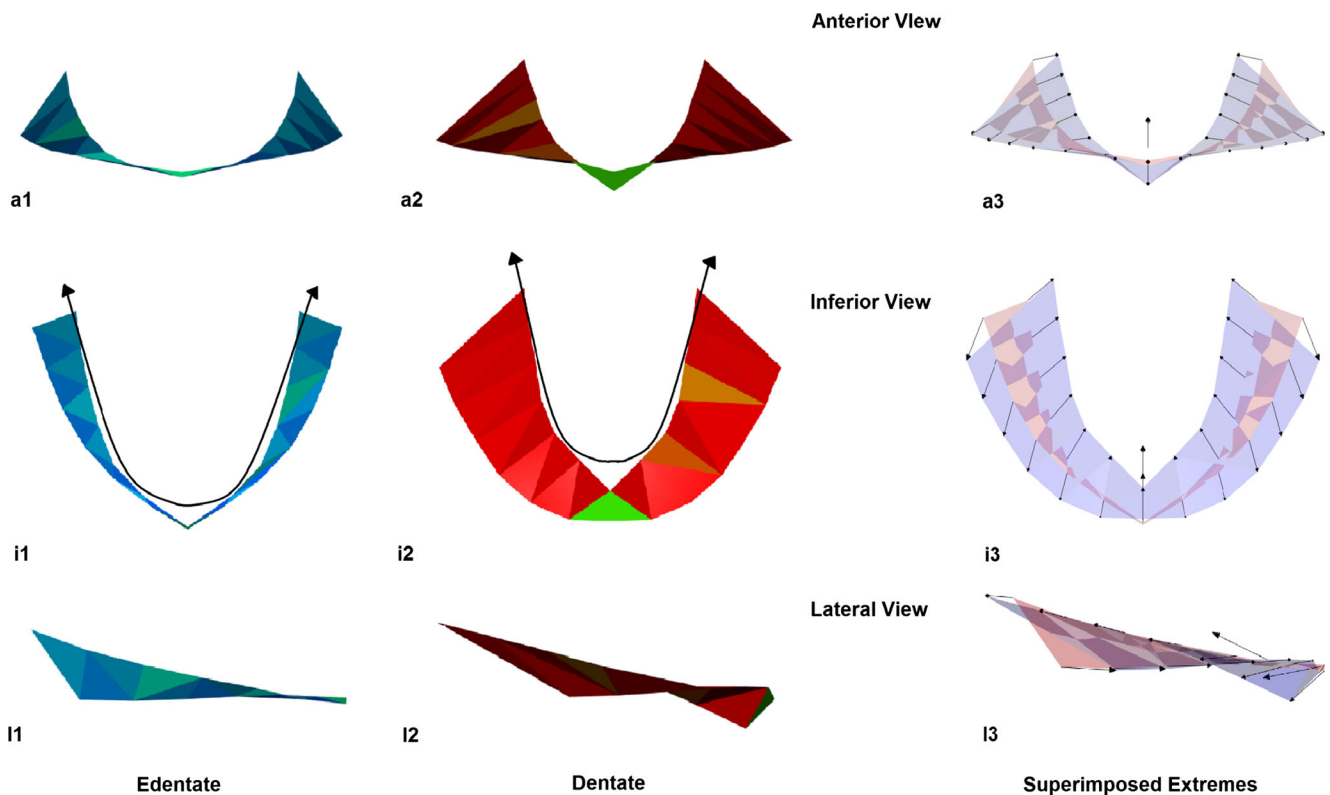


Fig. 4 Anterior, inferior and lateral coloured side by side representations (*left*) and vector diagrams (*right*) of the structural differences in the morphology of the maxilla associated with tooth loss. In the side by side illustrations, *green areas* are equivalent, *red* indicates a large increase, whilst *blue* shows a large decrease. The gradation of colours

between red and blue, from yellow to turquoise, indicate morphologies that lie between the two extremes. In the vector diagrams on the right, *arrows* indicate the change in a structure from edentate, the red reference form, to dentate, the blue target form. The *size of the arrows* in the figure represents the relative amount of structural change

time. Despite this, the cortical bone mass of the zygomatics seems rather stable irrespective of tooth loss which is demonstrated by the fact that severe maxillary alveolar recession can be treated by anchoring fixed dental prostheses by means of four zygomatic implants [42]. The lack of significant changes to this and other regions in the current study suggests that many of the differences observed in the preceding analysis of our work may have resulted on account of the Pinocchio effect. The Pinocchio effect refers to the fact that during Procrustes superimposition, the variance seen at corresponding landmarks is distributed across all landmarks. Hence, if a single landmark shows more variation than the rest, this variation will be distributed such that the variation at that specific location will be minimised but the variation across all other landmarks will show a slight increase [43]. However, the extremely large number of edentate crania in the current sample as well as the sample size itself may also have influenced outcomes. Low masticatory strains along structures located furthest from the chewing apparatus, including the frontal bone as well as the periorbital regions, have been demonstrated by a number of authors [11, 44, 45]. This would suggest that mastication has little effect on these regions and would explain why no alteration to their structure was induced by tooth loss. Conversely, differences in cortical bone thicknesses between

the skulls of dentate and edentate individuals have been demonstrated by Dechow and associates in 2010, with edentulous individuals showing statistically thinner cortical bone even in the frontal and zygomatic bones [11]. This may suggest that despite the lack of gross morphological changes in structures far removed from the masticatory complex, the removal of forces do result in complex histological adaptations.

Regarding the specific modifications of the alveolus, both the labial/buccal and lingual plates of alveolar bone were seen to resorb but the bony tissue of the buccal plate appeared to resorb to a greater extent. Pietrokofski and Massler [18] analysed the effects of unilateral tooth extraction on the degree of alveolar bone loss and also tested the degree of symmetry in edentulous dental arches. Similar to our results, these authors reported that the buccal plate underwent resorption at a greater rate than the palatal plate, resulting in a posterior shift of the anterior-most point of the maxillary alveolar ridge with an associated decrease in total palatal arch length. These findings were supported by Tallgren [46]. Pietrokofski and Massler [18] commented that the total amount of tissue resorption was significantly greater in the molar region as compared to the premolar and incisor region. They additionally found that the absolute amount of tissue lost in the molar region exceeded that of the other regions of the palatal arch.

The severe degree of maxillary bone resorption which was seen in this study results in a dramatic decrease in alveolar prognathism as well as a decrease in upper facial height. Numerous authors have noted a marked shortening of the maxilla in the event of extensive tooth loss [9, 10, 14, 47, 48] although the degree to which the bone is resorbed varies as partially edentulous individuals experience less bone loss than those that are completely edentulous [13]. Additionally, individuals with better fitting dentures experience less resorption [49] whilst females lose bony tissue faster and to a larger degree than do males [50].

The consequence of the decrease in facial height and prognathism seen in this sample can be extrapolated to samples of other populations as there is no fundamental reason to assume the biomechanical process involved in alveolar resorption will be different. The degree of alveolar resorption in response to tooth loss may vary, however, as factors such as nutrition, age [51, 52], population [53] and sexual dimorphism [54] all affect bone turnover rates. As forensic anthropologists rely on various cranial measurements for the estimation of sex [5, 55, 56] and ancestry [21, 57], a decrease in upper facial height will ultimately affect the accuracy of discriminant functions, which make use of these measurements. Furthermore, as the degree of alveolar prognathism is used as a means of discerning black and white crania [58], decreased alveolar prognathism in a black individual due to tooth loss may complicate ancestry estimation, especially for an inexperienced observer.

Additionally, the marked alveolar resorption of both the labial/buccal and lingual plates of the maxilla leads to an increase in the hyperbolic nature of the palate. This is of importance as the shape of the palate may be qualitatively assessed to assist with the estimation of ancestry [59, 60]. Furthermore, in a review of the 17 most commonly used traits to assign sex, palate shape ranked 13th with sexing accuracies of up to 88.8 % being reported [61]. As male palates are generally deeper and narrower, the increased hyperbolic nature of the palate with tooth loss would alter the appearance of male palates such that they take on a more feminine configuration which may decrease, or at the very least complicate, sexing accuracy. Additionally, as palate shape in black individuals is generally more hyperbolic, the increased hyperbolic nature of the palate of edentate white individuals may also result in the incorrect estimation of ancestry.

Finally, this study demonstrated that a decrease in maxillary prognathism leads to a reduction in the length of the bony bar between the canine jugum and the intersection of the zygomatic and maxillary bones at the orbital rim. Earlier work by Pessa and associates [62] support this finding as they noted a similar change in individuals between the ages of 53 and 76. In their study, they found that the elderly and infants display a similar ratio of maxillary height to orbit height whilst this ratio was found to be greater in young individuals. They attributed the reduced ratio in the elderly to a downward expansion of

the orbital shelf with an associated upward migration of the nasal aperture. The authors did not specify whether the elderly individuals used in their investigation were edentate or not, but lack of dentition would also lead to a reduced ratio and would be another point of correspondence between elderly and infant craniofacial skeletal proportions.

Conclusion

This paper not only elucidated the various bony changes that result from maxillary tooth loss, it also demonstrates the importance of considering the effects of tooth loss during the compilation of a biological profile as various structural changes may result in the misclassification of skeletal remains. As demonstrated here, care should be taken when measuring or assessing factors such as upper facial height, prognathism and palatal hyperbolism when compiling biological profiles, especially in cases of severe tooth loss. During the global analyses, tooth loss-related changes were demonstrated in the size of the orbits, the degree of projection of the nasal aperture, bizygomatic breadth and also in the shape and projection of the maxilla. When assessed in isolation, however, only maxillary changes proved significant. Specifically, these changes include severe alveolar bone resorption which resulted in a decrease in both alveolar prognathism and upper facial height. Resorption along both labial/buccal and lingual surfaces was shown to result in an increased palatal hyperbolism. However, it is possible that the extremely skewed number of edentate versus dentate individuals could have influenced the results obtained. Alternatively, partial Procrustes superimposition may have failed to maintain biological relationships between regions, whilst the sliding semilandmarks used to represent curve shape may need to be supplemented with additional surface landmarks. An analysis is restricted by the landmarks used and the structures quantified. Further research using more balanced samples is required to clarify this. Despite this, the current investigation demonstrated the advantage of using geometric morphometric techniques to visualise tooth loss-related changes to the face and maxilla. It also provides the groundwork for future research aimed at improving current standards and deriving new standards for the assessment of partially or fully edentulous cranial material.

Acknowledgments The authors would like to thank Mr Brendon Billings and Mr Diago Shangase for their assistance in the Raymond A. Dart Collection of Human Skeletons. The financial assistance of the National Research Foundation (NRF) towards this research is hereby acknowledged (Grant UID: 79474). Opinions expressed and conclusions arrived at are those of the authors and are not necessarily to be attributed to the NRF.

Conflict of interest The authors declare that they have no conflict of interest.

References

- Barrier ILO, L'Abbé EN (2008) Sex determination from the radius and ulna of a modern South African sample. *Forensic Sci Int* 197: 85.e1–85.e7
- Franklin D, O' Higgins P, Oxnard CE, Dadour I (2008) Discriminant function sexing of the mandible of indigenous South Africans. *Forensic Sci Int* 179:84.e1–84.e5
- Steyn M, İşcan MY (2004) Osteometric variation in the humerus: sexual dimorphism in South Africans. *Forensic Sci Int* 106(1999): 77–85
- Van Wyk PJ, Van Wyk C (2004) Oral health in South Africa. *Int Dental J* 54:373–377
- Steyn M, İşcan MY (1998) Sexual dimorphism in the crania and mandibles of South African whites. *Forensic Sci Int* 98:9–16
- United Nations (2011) World population prospects, the 2010 revision: Prospects and advance tables
- Williams SE, Slice DE (2010) Regional shape change in adult facial bone curvature with age. *Am J Phys Anthropol* 143:437–447
- Bodic F, Hamel L, Lerouxel E, Baslé MF, Chappard D (2005) Bone loss and teeth. *Joint Bone Spine* 72:215–221
- Kloss FR, Gassner F (2006) Bone and aging: effects on the maxillofacial skeleton. *Exp Gerontol* 41:123–129
- Sveikata K, Balciuniene I, Tutkuviene J (2011) Factors influencing face aging. Literature review. *Stomatol Balt Dent Maxillofac J* 13: 113–115
- Dechow PC, Wang Q, Peterson J (2010) Edentulation alters material properties of cortical bone in the human craniofacial skeleton: functional implications for craniofacial structure in primate evolution. *Anat Rec (Hoboken)* 293(4):618–629
- Heath MR (1966) A cephalometric study of the middle third of the adult human face related to aging and the loss of dental tissue. *Arch Oral Biol* 11:677–686
- Tallgren A (1967) The effects of denture wearing on facial morphology. *Acta Odontol Scand* 25(5):563–592. doi:10.3109/00016356709028754
- Bartlett SP, Grossman R (1992) Walker LA (1992) Age related changes of the craniofacial skeleton: an anthropometric and histologic analysis. *Plast Reconstr Surg* 90(4):592–600
- Crothers AJR (1992) Tooth wear and facial morphology. *J Dent* 20: 333–341
- Albert M, Ricanek K, Patterson E (2007) A review of the literature on the aging adult skull and face: implications for forensic science research and applications. *Forensic Sci Int* 172:1–9
- Lestrel P, Kapur K, Chauncey H (1980) A cephalometric study of mandibular cortical bone thickness in dentulous persons and denture wearers. *J Prosthet Dent* 43:89–94
- Pietrokofski J, Massler M (1967) Alveolar ridge resorption following tooth extraction. *J Prosthet Dent* 17(1):22–27
- Buikstra J, Ubelaker D (1994) Standards for data collection from human skeletal remains. *Arkansas Archaeological Survey, Fayetteville*
- Adams DC, Rohlf FJ, Slice DE (2004) Geometric morphometrics: ten years of progress following the revolution. *Ital J Zool* 71:5–16
- Franklin D, Freedman L, Milne N (2005) Three-dimensional technology for linear morphological studies: a re-examination of cranial variation in four southern African indigenous populations. *HOMO* 56:17–34
- Krüger GC, L'Abbé EN, Stull KE, Kenyhercz MW (2014) Sexual dimorphism in cranial morphology among modern South Africans. *Int J Legal Med* DOI. doi:10.1007/s00414-014-1111-0
- Stull KE, Kenyhercz MW, L'Abbé EN (2014) Ancestry estimation in South Africa using craniometrics and geometric morphometrics. *Forensic Sci Int* 245:206.e1–206.e7
- Dayal MR, Kegley ADT, Štrkalj G, Bidmos MA, Kuykendall KL (2009) The history and composition of the Raymond A. Dart Collection of human skeletons at the University of the Witwatersrand, Johannesburg. South Africa. *Am J Phys Anthropol* 140:324–333
- Steyn M, Pretorius E, Hutton L (2004) Geometric morphometric analysis of the greater sciatic notch in South Africans. *HOMO* 54(3):197–206
- Gunz P, Mitteroecker P, Bookstein FL (2005) Semilandmarks in three dimensions. In: Slice DE (ed) *Modern morphometrics in physical anthropology*. Kluwer Academic/Plenum Publishers, New York, pp 73–98
- Klingenberg CP (2011) MORPHOJ: an integrated software package for geometric morphometrics. *Mol Ecol Resour* 11:353–357
- Klingenberg CP, Barluenga M, Meyer A (2002) Shape analysis of symmetric structures: quantifying variation among individuals and asymmetry. *Evolution* 56(10):1909–1920
- Zelditch ML, Swiderski DL, Sheets HD (2012) Ordination methods: principal components analyses, In: *Geometric Morphometrics for Biologists, Second Edition: A Primer*. Academic press, 136–149
- Webster M, Sheets HD (2010) Supplementary online material for a practical introduction to landmark based geometric morphometrics. Available at <http://www.paleosoc.org/shortcourse2010>
- Gunz P (2001) Using semilandmarks in three dimensions to model human neurocranium shape [dissertation]. University of Vienna, Vienna
- Gunz P (2005) Statistical and geometric reconstruction of hominid crania: reconstructing australopithecine ontogeny [dissertation]. University of Vienna, Vienna
- Robert P, Escoufier Y (1976) A unifying tool for linear multivariate statistical methods: The RV-coefficient. *J R Stat Soc* 25(3):257–265
- Klingenberg CP (2009) Morphometric integration and modularity in configurations of landmarks: tools for evaluating a priori hypotheses. *Evol Dev* 11(4):405–421
- Rholf FJ, Corti M (2000) Use of two-block partial least-squares to study covariation in shape. *Syst Biol* 49(4):740–753
- Maitra S, Yan J. Principle Component Analysis and Partial Least Squares: Two Dimension Reduction Techniques for Regression. Accessed 09 October 2011, <http://www.casact.com/pubs>
- Nishimura I, Hosokawa R, Kaplan ML, Atwood DA (1995) Animal model for evaluating the effect of systemic oestrogen deficiency on residual ridge resorption. *J Prosthodont Dent* 73(3):304–310
- Saldanha JB, Casati MZ, Neto FH, Sallum EA, Nociti FH (2006) Smoking may affect the alveolar process dimensions and radiographic bone density in maxillary extraction sites: a prospect study in humans. *J Oral Maxillofac Surg* 64:1359–1365
- Newton JP, Yemm R, Abel RW, Menhinick S (1993) Changes in human jaw muscles with age and dental state. *Gerodontology* 10(1):16–22
- Haraldson T, Karlsson U, Carlsson GE (1979) Bite force and oral function in complete denture wearers. *J Oral Rehabil* 6(1):41–48
- Richard MJ, Morris C, Deen BF, Gray L, Woodward JA (2009) Analysis of the anatomic changes of the aging facial skeleton using computer-assisted tomography. *Ophthal Plast Reconstr Surg* 25(5): 382–386
- Stiévenart M, Malevez C (2010) Rehabilitation of totally atrophied maxilla by means of four zygomatic implants and fixed prosthesis: a 6–40-month follow-up. *Int J Oral Maxillofac Surg* 39:358–363
- von Cramon-Taubadel N, Frazier BC, Lahr MM (2007) The problem of assessing landmark error in geometric morphometrics: theory, methods, and modifications. *Am J Phys Anthropol* 134:24–35
- Narvosa MJ (1991) Interspecific perspective on mechanical and non-mechanical models of primate circumorbital morphology. *Am J Phys Anthropol* 86(3):369–396
- Narvosa MJ, Noble VE, Hylander HL, Johnson KR, Kowalski EM (2000) Masticatory stress, orbital orientation and the evolution of the primate postorbital bar. *J Hum Evol* 38:667–693

46. Tallgren A (1974) Neurocranial morphology and ageing—a longitudinal roentgen cephalometric study of adult Finnish women. *Am J Phys Anthropol* 41:285–294
47. Wulc AE, Sharma P, Cxyz CN (2012) Anatomical basis of facial aging. In: Hartstein, Morris E., Wulc, Allan E., Holck, David EE (eds) *Midfacial Rejuvenation*. Springer, New York, doi:10.1007/978-1-4614-1007-2_2
48. Kelsey CC (1971) Alveolar bone resorption under complete dentures. *J Prosthodont Dent* 25(2):152–161
49. Carlsson G, Bergman R, Hedegard B (1967) Changes in contour of the maxillary alveolar process under immediate dentures: a longitudinal clinical and x-ray cephalometric study covering 5 years. *Acta Odontol Scand* 25:45–75
50. Yüzügülü B, Gulsahi A, Imirzalioglu P (2009) Radiomorphometric indices and their relation to alveolar bone loss in completely edentulous Turkish patients: a retrospective study. *J Prosthodont Dent* 101(3):160–165
51. Stout SD, Lueck R (1995) Bone remodelling rates and skeletal maturation in three archaeological skeletal populations. *Am J Phys Anthropol* 98(2):161–171
52. Seeman E (1997) From density to structure: growing up and growing old on the surfaces of bone. *J Bone Miner Res* 112(4):509–521
53. Kleerekoper M, Nelson DA, Peterson EL, Flynn MJ, Pawluszka AS, Jacobsen G, Wilson P (1994) Reference data for bone mass, calcitropic hormones, and biochemical markers of bone remodelling in older (55–75) postmenopausal white and black women. *J Bone Miner Res* 9(8):1267–1276
54. Christiansen C, Lindsay R (1990) Estrogens, bone loss and preservation. *Osteoporos Int* 1:7–13
55. Robinson MS, Bidmos MA (2009) The skull and humerus in the determination of sex: reliability of discriminant function equations. *Forensic Sci Int* 186:86.e1–86.e5
56. Rightmire GP (1971) Discriminant function sexing of bushman and South African Negro. *Crania S Afr Archaeol Bull* 26(103/104):132–138
57. de Freitas ML, Pinzan A, Janson G, Freitas KM, de Freitas MR, Henriques JFC (2007) Facial height comparison in young white and black Brazilian subjects with normal occlusion. *Am J Orthod Dentofac Orthop* 131:706.e1–706.e6
58. İşcan MY, Steyn M (1999) Craniometric determination of population affinity in South Africans. *Int J Legal Med* 112:91–97
59. Krogman W, İşcan MY (1986) *The human skeleton in forensic medicine*. Charles C Thomas, Illinois
60. White TD, Folken PA (2000) *Human osteology*, 2nd edn. Academic, Florida
61. Galdames IC, Matamala DJZ, Smith RL (2008) Evaluating accuracy and precision in morphologic traits for sexual dimorphism in malnutrition human skull: a comparative study. *Int J Morphol* 26(4):877–881
62. Pessa J, Zadoo V, Yuan C, Ayedelotte J, Cuellar F, Cochran C et al (1999) Concertina effect and facial aging: nonlinear aspects of youthfulness and skeletal remodeling, and why, perhaps, infants have jowls. *Plast Reconstr Surg* 103(2):635–644